UNIVERSITY OF SOUTHAMPTON

SOME INVESTIGATIONS INTO STIMULATED ELECTRONIC RAMAN SCATTERING AND RELATED PROCESSES IN ATOMIC VAPOURS

by

David B. Hearn

A thesis submitted for the degree of
Doctor of Philosophy

Department of Electronics
Faculty of Engineering and Applied Science

April 1982

UNIVERSITY OF SOUTHAMPTON

ABSTRACT

FACULTY OF ENGINEERING AND APPLIED SCIENCE

ELECTRONICS

Doctor of Philosophy

SOME INVESTIGATIONS INTO STIMULATED ELECTRONIC RAMAN SCATTERING AND RELATED PROCESSES IN ATOMIC VAPOURS

by David Brian Hearn

Stimulated electronic Raman scattering, SERS, is a simple method of efficiently generating widely tunable infrared radiation. This work describes techniques by which the tuning capability of this process may be extended. To this end several schemes in Caesium and Barium vapours have been investigated.

In Barium vapour two Raman transitions were studied using fixed frequency lasers. Poor performance of one of these transitions led to the application of biharmonic pumping or 'coherent Raman mixing' to enable generation of infrared light, and was the first observation of this process in an atomic vapour. This technique was subsequently used to generate infrared light from tunable dye laser light, which gave continuous tuning from 1.16 μm to 1.5 μm. The process was found to be limited by atomic saturation. The effect which saturation has on the generation efficiency is considered theoretically, and predicts quite accurately the observed tuning behaviour.

Two methods aimed at reducing molecular absorption effects in SERS in alkali vapours were investigated. The techniques employed either laser excitation and dissociation of the molecules or a reduction in their ground state concentration by superheating of the vapour. Some degree of success was achieved in improving the available tuning from the 6s-7s transition in Caesium. However, the inclusion of the effect of collision broadening of atomic transitions into a calculation of the Raman threshold suggests that little further improvement can be obtained on this transition.

A direct measurement of the Raman threshold power on the $6s\text{-}5d_{5/2}$ transition in Caesium gave excellent agreement with theoretical predictions based on collision broadening of this Raman transition. In addition, this work gave an insight into the role photoionization

plays in increasing the threshold under certain circumstances. The analysis suggests that laser pulse duration and vapour column length are important in determining whether Raman threshold can be exceeded.

CONTENTS PAGE

CHAPTER 1

Introduction

The infrared region of the electromagnetic spectrum has long been recognized as important in physical, chemical and biological studies. However, the development of tunable laser sources in this region has lagged behind that of visible lasers. The organic dye laser has provided an excellent tool for such studies in the visible and near infrared. In the infrared only fortuitous coincidences between fixed frequency infrared lasers and molecular transitions were available in the past. Techniques developed using the dye laser, cry out to be used in the infrared and have led to a tremendous urge to create novel tunable sources. The infrared tunability required from such a source for a particular experiment may be in general quite small. Despite this it is of great advantage to develop sources having wide tuning ranges. Having one laser source which covers a wide range of wavelengths allows many different experiments to be performed while at the same time maintaining good economy and utilization of laboratory space.

Molecular vibrational and rotational resonance can be excited by infrared light. Tunable sources allow the selective excitation of specific chemical species and allow isotope separation (Bloembergen and Yablonovitch (1979), Zare (1979)). Allied to these are molecular multiphoton ionization and dissociation studies. The results obtained can be enhanced by a suitable choice of laser wavelength. Important information on molecular dynamics can be gleaned from studies of the fluorescent decay of molecules and the rate of energy transfer within and between molecules (Kaiser and Lauberau (1979)). The use of such techniques is not restricted to simple molecules but can also be applied to biological investigations. Infrared lasers are also finding increasing use in the field of remote pollution detection and monitoring (Hinkley (1976)).

Many techniques have been employed to generate the required tunable infrared light. These have been in two main areas; namely the development of new tunable infrared lasers, and nonlinear optical methods for shifting visible and near visible lasers into the infrared. Quasi-continuous tuning has been achieved with various high pressure gas lasers such as CO_2 lasers (Carman and Dyer (1979)), where the normal line structure is smeared out by pressure broadening. Alkali halide crystals containing colour centres have been shown to 'lase' over ranges of the infrared. For example, the $(F_2^+)_A$ centre in Li:KI, optically pumped with an Er:YLF laser, can be tuned over the range 2.59 μm to 3.65 μm (Schneider et al (1982)).

Recently, interest in phonon terminated lasers has been reawakened by the results obtained with Alexandrite (Walling et al (1980)). Although this material operates in the 700-800 nm range, similar materials (such as Ni^{2+} or Co^{2+} in MgF_2, MnF_2, $KMgF_3$, $KZnF_3$) which lase in the infrared may soon become sufficiently developed for routine use. Good results in these materials have already been achieved in both the CW and pulsed modes (Moulton and Mouradian (1979)).

The use of nonlinear optical methods is now well established. Parametric generation by optically mixing two lasers in a nonlinear crystal, such as two dye lasers or a dye laser with a strong fixed frequency laser (see review by Byer and Herbst (1977)), have proved to be very effective. Associated with these is the optical parametric oscillator (OPO). Two tunable infrared beams are generated from one fixed frequency beam within a nonlinear crystal. Frequency selection is obtained by a combination of an optical cavity, which can be tuned as with a dye laser, and the photon energy and momentum matching (phasematching) requirements of the process. These devices are capable of multi-millijoule outputs of high spectral purity ($\sim$0.1 cm^{-1}). For picosecond applications, parametric fluorescence from the same crystals can be tuned over a wide range simply by using the angular phasematching requirement (Rabson et al (1972)). At present the parametric oscillator and fluorescent sources offer the most widely tunable and energetic infrared sources. For example, a Lithium Niobate OPO pumped by a 100 mJ Nd:YAG laser can produce a total of up to 10 mJ in the two outputs; these being typically

tunable from 1.5 -2.1 μm and 2.1 - 3.5 μm (Wyatt, Turner and Smith (1977)).

The main disadvantage of such devices is their use of crystalline materials. These must be of the highest optical quality and are therefore necessarily expensive to produce. In order to observe nonlinear effects in these materials, high laser intensities must be used and this carries with it the possibility of irreparable optical damage to the crystals. The outputs which can be produced must lie within the transparency regions of the crystal. In most cases this limits the generated wavelengths. For example, no output beyond 4.2 μm can be produced by a $LiNbO_3$ parametric oscillator.

Stimulated Raman scattering in high pressure molecular media such as N_2, CH_4 and H_2 has been employed to convert visible light into the infrared. Frey and Pradere (1976) used the Stokes lines of high power dye lasers as a source of infrared light, but for the longer wavelengths more than one Raman shift is required, (the largest molecular shift is that of H_2, i.e. 4155 cm^{-1}) and the efficiency of higher order Stokes production becomes progressively lower. The use of gaseous media does have the distinct advantage that the nonlinear medium cannot suffer irreparable damage.

Larger Raman shifts (>10000 cm^{-1}) are available from stimulated electronic Raman scattering in atomic vapours. This process was first demonstrated in potassium vapour by Sorokin et al (1967) and Rokni and Yatsiv (1967). The effect that the comparatively low atomic number density of these materials has on the Raman gain is offset by the ability to use intermediate resonance with single photon transitions of the atomic species. Highly efficient conversion of dye laser light into the infrared can be achieved over a wide tuning range (Cotter and Hanna (1976)). A major drawback of this process is atomic saturation, which limits the total energy which can be extracted from a particular volume (see Section 2.6 and Cotter and Hanna (1976)). In this respect, the low working number density is a distinct disadvantage.

The long wavelength cut-off of SERS is due to limitations of the process such as a reduction in the gain for long wavelength

production, and diffraction loss of the generated light. Vapours of alkalis and alkaline earth materials, as used in the experiments described in this thesis, are generally transparent in the infrared. However, alkali molecules present in alkali metal vapours curtail long wavelength production by absorbing the visible pump laser light.

In this work several techniques have been used in an attempt to overcome these limitations in Caesium vapour. It is believed that the presence of dimer molecules stops efficient infrared generation beyond 3.5 μm on the 6s-7s Raman transition. They do so by absorbing the blue dye laser pump light as well as by being photoionized by the high intensities involved. To reduce their concentration, superheating the vapour has been tried, and to reduce their absorption, a bleaching method has been used. Some degree of success has been achieved in improving the tuning limit. This work is described in Chapter 6.

The use of the Caesium 6s-7s Raman transition requires a blue dye laser. The energy efficiency in generating 3 μm radiation will not be very great, as each Stokes photon will carry an order of magnitude less energy than the pump photon. The energy difference is just the Raman shift of the medium. Attention has recently turned to the possible use of the 6s-5d transition in Caesium (Hodgson (1979), Wyatt and Cotter (1980)). This scheme involves the smallest Raman shift of all the alkalis, namely 14596 cm^{-1}. To produce 3 μm radiation, an orange dye laser would be used offering a definite advantage in efficiency. Constructive interference of the enhancement from the 6s-6p and 6s-7p transitions in this wavelength region makes the Raman gain remain roughly constant. Using picosecond laser pulses Wyatt and Cotter (1981) have observed wide Stokes tuning between 3.3 μm and 8.4 μm on this transition, but with nanosecond pulses such tuning has not been achieved. This can be explained partially by the vastly greater intensity and hence Raman gain obtained in the short pulse work. However, other effects may prevent Raman scattering in regions where naive application of normal Raman calculations suggest threshold should easily be exceeded. In this work the problems arising from the use of long (22 ns) pulses have given clues to the reasons for dramatically increased thresholds (see Chapter 6).

Barium vapour has been used as a Raman shifting medium for excimer lasers (Djeu and Burnham (1977), Cotter and Zapka (1978)) as well as for near infrared dye lasers (Carlsten and Dunn (1975), Tuttlebee (1977)). The absence of absorbing dimer molecules in Barium vapour is a very attractive feature. In the alkalis these molecules have been blamed for the discrepancies between theory and experiments. In this present work an attempt has been made to use a different intermediate resonant state, the $6s6p\ ^1P_o$ with no success. However, the first application of biharmonic pumping in an atomic medium to this transition allowed efficient infrared generation over the range 1.16 μm to 1.59 μm (Hearn et al (1980)). Biharmonic pumping is a form of non-degenerate four wave mixing and has been described by Venkin et al (1975). The efficiencies obtained in the experiments described here of up to ∿1% represent an order of magnitude improvement over previous results in atomic vapours (Tyler et al (1975), Karkkainen (1977)). These efficiencies are substantially lower than predicted by the theoretical analysis of four wave mixing by Yuratich (private communication (1979)) and can be explained in terms of atomic saturation of the medium. An outline of the theory of biharmonic pumping is given in Chapter 3 and experiments performed using this process are discussed in Chapter 5.

CHAPTER 2

Stimulated Electronic Raman Scattering in Atomic Vapours

This chapter is devoted to outlining the principal characteristics and limitations of stimulated electronic Raman scattering (SERS) in atomic vapours. Emphasis will be placed on particular schemes in Caesium and Barium, although the conclusions drawn can easily be extended to other materials. The ideas presented are directed toward the device potential of SERS, and so the prediction of whether or not a chosen wavelength can be produced in this way plays an important role. If the wavelength can be produced, guidelines are presented to enable optimization of the output energy or tuning range.

2.1 Small Signal Gain

In SERS the growth of the Stokes wave in the presence of a pump wave is described by a Raman gain per unit length G_R. If diffraction is ignored by assuming uniform plane waves, the small signal growth of the Stokes intensity with distance z is given by

$$I_s(z) = I_{so}\exp(G_R z) \qquad 2.1$$

where I_{so} is a starting 'noise' intensity due to spontaneous Raman scattering. This is found to be of the order of 10^{-8} to 10^{-6} W cm^{-2} (see, for example, Section 3.5 of Hanna et al (1979)).

For this 'noise' to grow to a readily detectable power of $\sim$1 W, an intensity gain of around exp(30) is required. This, in conjunction with Equation 2.1, allows a threshold condition $G_R \ell = 30$ to be imposed. ℓ here is the length of the nonlinear medium. A knowledge of G_R for a particular SERS scheme is required in order to determine whether or not this detector threshold will be exceeded.

The Raman gain per unit length can be expressed as the product of a gain coefficient and pump laser intensity: $G_R = g_R I_p$. The gain coefficient can be written in terms of the Raman polarizability α_R as

$$g_R = \frac{N\omega_s}{\varepsilon_o c\hbar\Gamma_R} |\alpha_R|^2 \qquad (2.2)$$

where N is the number density of the nonlinear medium. General formulae for the evaluation of α_R and g_R are given by Hanna et al (1979); here they will be restricted to certain cases applicable to SERS in Caesium and Barium. In Chapter 3, where consideration is given to the related process of biharmonic pumping, explicit formulae for α_R will be given.

In the Caesium experiments described in this thesis, two Raman transitions were used: the 6s-7s and the 6s-$5d_{5/2}$. With the pump and Stokes waves taken as linearly polarized in the same direction†, the gain coefficient for the 6s-7s transition is:

$$g_R = \frac{N\omega_s e^4}{18\varepsilon_o^2 c^2 \hbar^3 \Gamma_R} \left| \sum_n \langle 7s|r|np\rangle \langle np|r|6s\rangle \left(\frac{2}{3\Delta_n(3/2)} + \frac{1}{3\Delta_n(1/2)} \right)^2 \right|^2 \qquad (2.3)$$

while for the 6s-$5d_{5/2}$ it is:

$$g_R = \frac{2N\omega_s e^4}{75\varepsilon_o c^2 \hbar^2 \Gamma_R^3} \left| \sum_n \frac{\langle 5d|r|np\rangle \langle np|r|6s\rangle}{\Delta_n(3/2)} \right|^2 \qquad (2.4)$$

These equations recognize the splitting of the atomic p doublets; the denominators $\Delta_n(3/2)$ and $\Delta_n(1/2)$ are the detunings of the laser

---

† This assumption of parallel polarizations is, in fact, only correct when the pump laser is tuned to a frequency which lies outside an atomic p doublet. Cotter et al (1976) confirmed the prediction of Yuratich and Hanna (1976) that between the doublets there is a frequency region in which the Raman gain on the 6s-7s transition is higher for a Stokes wave polarized perpendicularly to the pump wave.

frequency from the $np_{3/2}$ and $np_{1/2}$ levels respectively, and are in angular frequency units. The absence of a $\Delta_n(1/2)$ denominator in the gain for the $6s\text{-}5d_{5/2}$ Raman transition is a direct consequence of the selection rule on the magnetic quantum number m; $\Delta m = 0, \pm 1$. The initial state has $m = 1/2$ and the final state has $n = 5/2$. This implies that the only intermediate states to be considered are the $np_{3/2}$ states.

The summations over n are over all allowed p states $|np\rangle$ of the atom. In practice these summations converge rapidly, especially for 6s-7p transitions where close resonance to the 6s-7p transition is used to enhance the gain. In this case, and any other in which close intermediate resonance is used, the summations can be replaced by a single dominant term.

In order to calculate the Raman gain coefficients the tabulated radial matrix elements of, for example, Eicher (1975) can be used. These are given in atomic units and must therefore be multiplied by a factor a_o, the Bohr radius (5.292×10^{-11} m), before being inserted into Equations 2.3 or 2.4.

The most convenient source of data for Barium are the tables of Miles and Wiese (1969), in which transition oscillator strengths are given. Although these can be converted to radial dipole matrix elements, it is convenient to use a gain formula which utilizes oscillator strengths. The Raman transitions in Barium considered later in this thesis are between the $J_g = 0$ ground state and a $J_f = 2$ final state, and involve only one dominant intermediate level. The Raman gain coefficient for linearly polarized light is given by†:

$$g_R = \frac{4\pi^2 r_e^2 c^2 N\omega_s}{\hbar\Gamma_R} \cdot \frac{f_{fi} f_{ig}}{\Omega_{if}\Omega_{ig}} \cdot \frac{1}{(\Omega_{ig} - \omega_p)^2} \qquad (2.5)$$

(r_e is the classical electron radius 2.818×10^{-15} m)

---

† It is important to observe the ordering of labels on the oscillator strengths. If we take g_f to be the degeneracy of the final state, then $g_f f_{fi} = g_i f_{ig}$, thus allowing either f_{fi} or f_{if} to be used.

The parameter Γ_R is the spontaneous Raman transition linewidth. Collisional dephasing and broadening play a significant role in determining the magnitude of Γ_R. Choosing values applicable to Barium and Caesium is the subject of Section 2.3; typically $\Gamma_R = 0.03\ cm^{-1}$ for Barium and $\Gamma_R = 0.2\ cm^{-1}$ for Caesium.

2.2 Limitations Imposed by Pump Absorption

Up to this point depletion of the pump laser by single photon absorption has been ignored. This absorption can arise in two ways: from the atoms in which SERS is being performed or from the presence of dimer molecules. Both cause the Raman threshold to be increased.

In order to make use of the available enhancement to SERS afforded by intermediate resonance, the pump laser frequency often lies near to an allowed atomic single photon transition. If a Lorentzian lineshape is assumed, then the absorption coefficient per unit length in the wings of the absorption ($|\Delta| >> \Gamma_i$) will be

$$\beta = \frac{N\omega_p}{\varepsilon_o c\hbar} \mu_{ig}^2 \frac{\Gamma_i}{\Delta^2} \tag{2.6a}$$

Here μ_{ig} is the electric dipole moment matrix element for the single photon transition, and is related to the radial matrix element and the Bohr radius a_o, by $\mu_{ig} = ea_o \langle i|r|g\rangle$. In terms of the transition oscillator strength f_{gi}, the absorption coefficient is

$$\beta \simeq 2\pi r_e c N f_{gi} \frac{\Gamma_i}{\Delta^2} \tag{2.6b}$$

where the symbols have their usual meanings.

The largest contribution to the absorption linewidth, Γ_i, is from collision broadening. For the principal line absorptions this is realized by a resonance broadened linewidth (HWHM) of

$$\Gamma_i = 2\pi r_e c^2 k_{gi} \left(\frac{2J_g + 1}{2J_i + 1}\right)^{\frac{1}{2}} \frac{f_{gi}}{\Omega_{ig}} N \tag{2.7}$$

The factor k_{gi} is close to unity (Hindmarsh (1974)) and can be taken as unity. The bracketed term is the ratio of the ground and intermediate state multiplicities and is given in terms of their total angular momenta, J_g and J_i. For metal vapour pressures of a few torr this linewidth is typically around a few hundredths of a wavenumber and leads to absorption coefficients which are large, even when the detuning from the intermediate level is large. For example, the linewidth of the $6s-7p_{3/2}$ absorption at 10 torr is given by Equation 2.7 as 0.015 cm^{-1}. For a transmission of 50% through a vapour column of 30 cm, the laser frequency must be tuned away from the $7p_{3/2}$ level by 31 cm^{-1}. Atomic absorption is seen not to be negligible even at large detunings.

Another absorption present in Caesium (but not Barium) is that due to dimer molecules. These constitute up to 5% of the vapour and have absorption bands which extend over large portions of the visible and infrared regions of the spectrum. These bands have been studied by Lapp and Harris (1966), Benedict et al (1977) and Gupta et al (1978). Typical absorption cross-sections for the dimer molecules lie between $\sigma = 10^{-18}$ cm^2 and 10^{-15} cm^2, giving rise to values of β in the range 5×10^{-3} to 5 cm^{-1}. For a 30 cm vapour column at a pressure of a few torr, these correspond to transmissions of 85% and 10^{-5}% respectively. Some of the absorption bands will be considered in more detail in Chapter 4.

The effect of absorption on the Raman gain can easily be shown to correspond to a replacement of the column length by an effective length ℓ_{eff}, where

$$\ell_{eff} = \frac{1}{\beta}(1 - e^{-\beta\ell}) \qquad (2.8)$$

which is seen to tend to ℓ, the real column length, for small values of β. On the other hand, large values of β make the effective column length equal to the extinction length of the light; namely β^{-1}. The growth of the Stokes is as though it were curtailed at this length, with $I_s = I_{so} \exp(G_R/\beta)$, as may be expected.

Based upon this, a new threshold criterion is apparent - the Stokes growth in the length ℓ_{eff} must exceed exp(30), and so the threshold pump intensity is given by $g_R I_{pth} \ell_{eff} = 30$. This condition can, however, be somewhat relaxed when dimer absorption is considered, as the number density of the absorbing dimers is significantly less than that of the atomic species. By suitable focusing, the number of absorbers illuminated can be minimized. If there are many more pump photons than molecules in this region, the dimers can be bleached, i.e. promoted to a long lived excited state by the early part of the pump pulse. The latter part of the pulse then sees a reduced absorption coefficient and thus an increased effective length.

The criterion for threshold is, therefore, a function of the dimer number density, the pump laser pulse energy and the focusing of the laser. The threshold pump intensity should however, lie between the limits set on it by $g_R I_{pth} \ell_{eff} = 30$ and $g_R I_{pth} \ell = 30$.

2.3 Collision Broadening of the Raman Linewidth†

In this section the contribution which collision broadening makes to the Raman transition linewidth is considered. The effect of this is seen to be 'saturation' of the Raman gain as the atomic number density is increased. This leads to a departure from the normal prediction of the gain increasing with number density.

For two photon resonant processes such as stimulated Raman scattering, a 'Raman linewidth' Γ_R is introduced into the nonlinear susceptibility. This parameter makes allowance for damping mechanisms, such as atomic motion, which lead to decay of the oscillating material excitation in the medium. It can thus be related to the dephasing time T_2, by $T_2 = \Gamma_R^{-1}$, and gives a measure of the response time of the medium to changes in the pump laser field. The material excitation will be considered in more detail in Chapter 3.

In the absence of collisions, atomic motion will give rise to a linewidth characterized by the Doppler broadened width of

---

† For simplicity, linewidths are HWHM throughout.

the Raman transition. For atoms of mass m at temperature T, the Doppler width Γ_D (HWHM) for forward Raman scattering is

$$\Gamma_D = \Omega_{fg} \left(2\ln 2 \frac{kT}{mc^2}\right)^{\frac{1}{2}} \tag{2.9}$$

where Ω_{fg} is the Stokes shift. Typically Γ_D is around 0.015 cm^{-1} on the 6s-7s transition in Caesium at 400°C. This can be compared with the natural width of the transition which is 5×10^{-5} cm^{-1} and can thus be neglected. This natural width arises from spontaneous decay on the 7s-6p transition.

The Raman linewidth will be further broadened by collisions between atoms. The interaction between the atoms will lead to a transient change in the transition frequency. Equivalently this can be viewed as a change in phase of the contribution to the material excitation from these atoms. This gives rise to a further decrease of the excitation due to dephasing, this time characterized by the collisionally broadened linewidth. Considered separately, collision broadening gives rise in the impact approximation to a Lorentzian profile centred on the natural transition frequency. This approximation is typically valid within a few wavenumbers of the transition frequency (Hindmarsh (1974)). The collisional linewidth Γ_c is proportional to the atomic number density. In terms of a broadening coefficient, γ_c, the linewidth is $\Gamma_c = \gamma_c N$.

Collisional self broadening has been studied on several single photon transitions in Caesium. In particular Sayer and co-workers (1971) gave values of the collisional broadening coefficients for the 6s-5d quadrupole transition, which will be taken as applicable to 6s-$5d_{5/2}$ SERS. Their value of γ_c is, in terms of wavenumbers, in the range 0.6 to 1×10^{-18} cm^3 per cm^{-1}. Caesium pressures of between 10 and 100 torr lead to collisional widths between 0.13 and 1.3 cm^{-1} and so at pressures typically used in SERS experiments, Γ_c is of the order of 10 to 100 times larger than the Doppler width of the two photon transition and thus makes the dominant contribution to the Raman linewidth. Similar behaviour is expected on the 6s-7s transition where measured Raman thresholds

(Cotter (1976), Wyatt (1976)) are not consistent with the Doppler width but rather with a width of one to two orders of magnitude larger.

In order to see the effect of the linewidth changing from Doppler to collision broadened, the two profiles can be convoluted into a Voigt profile. The linewidth of a Voigt profile Γ_V is given approximately in terms of Γ_D and Γ_c, by

$$\Gamma_V \simeq (\Gamma_D^2 + \Gamma_c^2)^{\frac{1}{2}} = (\Gamma_D^2 + (\gamma_c N)^2)^{\frac{1}{2}} \qquad (2.10)$$

Substituting this into the equation for the Raman gain (Equation 2.2),

$$g_R = \frac{N\omega_s}{\varepsilon_o c\hbar(\Gamma_D^2 + (\gamma_c N)^2)^{\frac{1}{2}}} \cdot |\alpha_R|^2 \qquad (2.11)$$

is obtained. For small N ($\gamma_c N << \Gamma_D$), this tends to the normal gain equation with $\Gamma_R = \Gamma_D$. However, for $\gamma_c N >> \Gamma_D$ as will be the case for p > 1 torr, the Raman gain becomes essentially independent of the atomic number density. The limiting value of the gain is that obtained by substituting γ_c^{-1} for N/Γ_R in the gain equation. The effect of this saturation of the gain on SERS threshold is immediately apparent; for sufficiently high atomic pressure there is no further decrease in Raman threshold to be achieved by increasing the pressure. The steady state threshold for $6s\text{-}5d_{5/2}$ SERS is plotted in Figure 2.1 for two values of γ_c, corresponding to the limits placed on it by Sayer et al (1971), namely 6×10^{-19} and 1×10^{-18} cm^3 per wavenumber. Although collision broadening of this type has not previously been suggested for SERS in atomic vapours, this effect was considered by Vrehen and Hikspoors (1977) in their work on stimulated hyper-Raman scattering in Caesium. Collision broadening of the vibrational Raman linewidth in high pressure Hydrogen gas has been noted by many authors (see for example Trutna, Park and Byer (1979)).

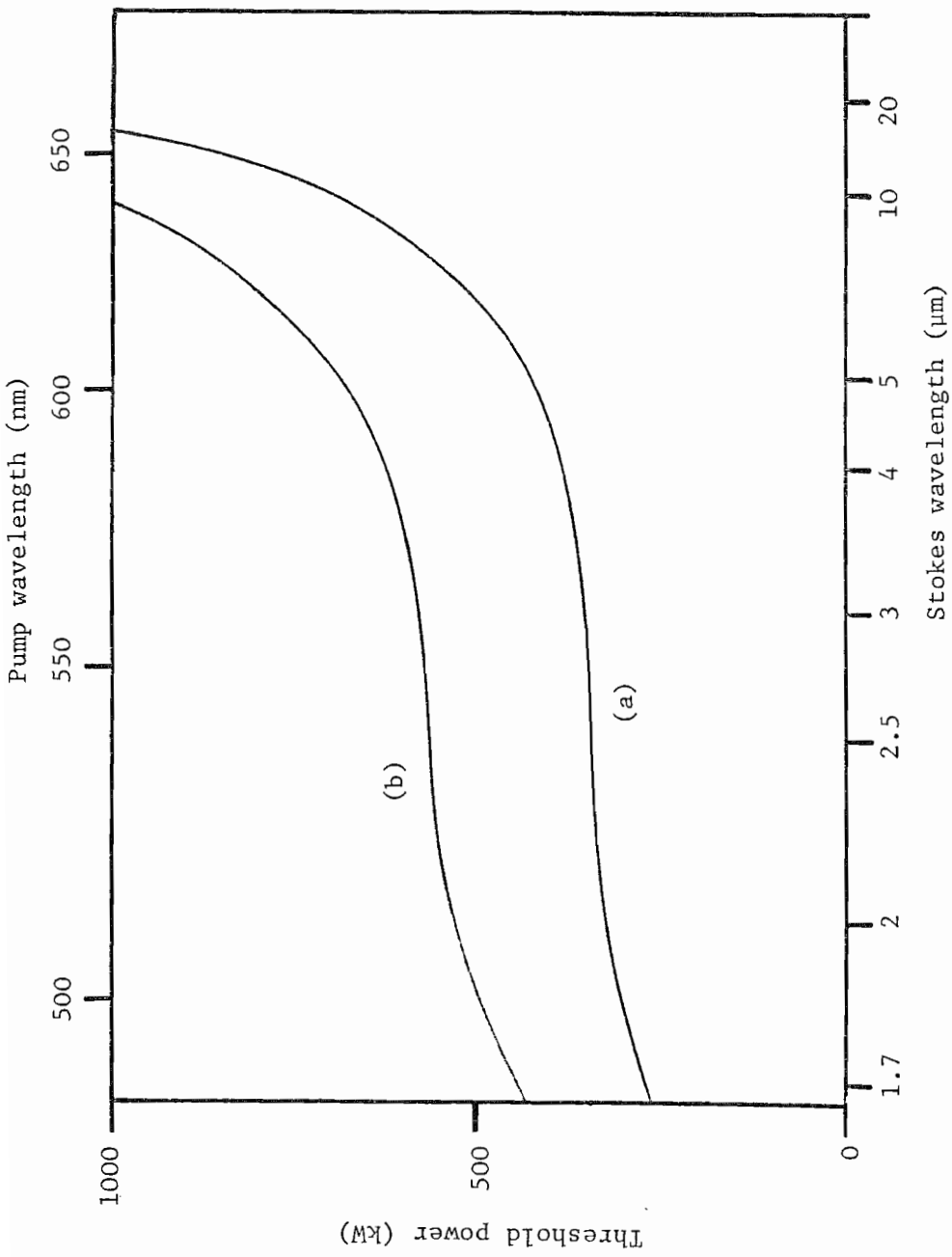

Figure 2.1 Calculated Raman threshold power for the Caesium $6s-5d_{5/2}$ transition

(a) $\gamma_c = 6 \times 10^{-19}$ cm^3 cm^{-1}

(b) $\gamma_c = 10^{-18}$ cm^3 cm^{-1}

2.4 The Effect of Laser Linewidth on Raman Threshold

In the previous section, the effect that collision broadening has on the Raman gain was discussed. A 'steady state' threshold was considered with no regard to pump laser linewidth. An attempt will now be made to redress the balance by considering the effect of the laser linewidth on the Raman threshold. First, however, the importance of the relative magnitudes of the two linewidths will be examined.

The relationship between the two linewidths falls naturally into three obvious regimes: either the laser linewidth is much less than, much greater than or approximately equal to the Raman transition linewidth. The response of the medium will depend upon which regime is appropriate. The realm of transient Raman scattering is not dealt with as it is beyond the scope of this thesis (see for example Penzkofer et al (1979)).

If the laser linewidth is much less than the transition linewidth, the response time $T_2(\Gamma_R^{-1})$ of the medium is much shorter than the characteristic time scale of fluctuations in the pump laser intensity, τ_c. (This, of course, is related to the laser linewidth Γ_L by $\tau_c \simeq \Gamma_L^{-1}$.) In this limit the material can follow the intensity variations of the pump laser instantaneously and can thus respond to any high intensity 'spikes' on the laser pulse. If any of these peaks are above Raman threshold then generation of a Stokes output will ensue. The experimentally determined threshold will, therefore, be critically dependent on the exact pulse structure. The only reliable threshold measurements under these conditions will be made with a laser operating on a single longitudinal cavity mode. If more than one mode is present, uncertainties in the relative phases of the modes will lead to considerable fluctuation of the peak intensity. Although in principle it is possible to monitor the pulse shape, these peaks may have a duration which is too short to allow direct experimental measurement of the intensity on a single shot basis.

At the other extreme, where $\Gamma_L >> \Gamma_R$, the response of the medium is too slow to follow the fast fluctuations in the laser

intensity. The medium will, to a large extent, smooth out the overall pulse shape and respond only to the average intensity (Akhmanov et al (1974)). The measured threshold will, therefore, be consistent with that calculated for a single mode laser of the same averaged power.

The third case, $\Gamma_L \simeq \Gamma_R$, is somewhat more difficult. The medium can neither precisely follow the laser fluctuations nor smooth them out. No general analytical solutions for the behaviour of SERS in this regime have yet been found. However, if Γ_R and Γ_L are significantly broader than the linewidth of the laser operating on a single longitudinal mode (here $\sim$0.005 cm^{-1}) the experimental threshold will be lower than that obtained under single mode conditions. The medium can follow the progress of the pulse as its intensity variations take it above the average; it is therefore possible to exceed threshold even though the single mode pulse could not.

It can be seen that careful consideration must be given to the relative linewidths of the Raman transition and the laser light when predictions or measurements concerning threshold are made. In Chapter 6, measurements of SERS threshold on the 6s-5d transition in Caesium are presented which serve to illustrate this point.

2.5 Diffraction and Gain Focusing of the Stokes Wave

The plane wave theory of SERS describes the growth of a Stokes wave in the presence of a pump wave having uniform intensity and infinite transverse extent. In this section allowance is made for the (typically) Gaussian transverse distribution and for the focusing of the pump laser beam. An alternative to the plane-wave threshold condition is presented for confocal focusing.

In practice, focused laser beams are used to generate infra-red Stokes waves. The transverse extent of the pump laser beam is limited to a focal spot radius of around 200 μm. Some account, therefore, must be made of the diffraction of the Stokes wave out

of the illuminated region. In addition, as the transverse distribution of the pump laser light is typically Gaussian rather than uniform, the Raman gain will vary across the beam, being largest on the axis of the beam. The higher rate of growth of the Stokes wave on this axis will therefore appear as gain focusing of the Stokes light.

The effect of diffraction and gain focusing on the threshold behaviour of SERS was studied in detail by Cotter, Hanna and Wyatt (1975). Starting from the wave equation describing the growth of the Stokes wave, they showed that two thresholds could be defined. Firstly there is a gain threshold below which the loss due to the diffraction spread of the Stokes wave out of the illuminated region exceeds the gain which the wave receives from the scattering process. Secondly, there is a detector threshold analogous to the $g_R I_p \ell = 30$ of the plane wave treatment. By solving the wave equation in the case of a focused pump beam, with the requirement that the small signal growth of the Stokes wave from a noise power P_{so} gives a detectable power P_s, they found that a threshold pump power of

$$P_{th} = \frac{\pi c}{2\kappa\omega_p g_R}\left[1 + \left[1 + \frac{\kappa \ln(P_s/P_{so})}{\tan^{-1}(\ell/b)}\right]^{\frac{1}{2}}\right]^2 \qquad (2.12)$$

is needed. The Stokes frequency enters in the factor $\kappa = \omega_s/\omega_p$ and the effect of focusing of the pump beam over the nonlinear medium is described by the $\tan^{-1}(\ell/b)$ term. The confocal parameter b of the pump beam is related to the focal spotsize w_o by

$$b = \frac{2\pi w_o^2}{\lambda_p} \qquad (2.13)$$

For loose focusing, b is large and $\tan^{-1}(\ell/b)$ is small and dependent on ℓ, the length of the medium. However, tight focusing (with $b < \ell$) causes this term to tend to $\frac{1}{2}\pi$. Focusing any tighter than confocally ($b = \ell$) gives diminishing returns; there is only a factor

of two to be gained from the $\tan^{-1}$ term, and competing processes such as multiphoton ionization will become increasingly important.

For the experiments described in this thesis the lasers were focused such that the confocal parameter of the beam was approximately equal to the metal vapour column length (i.e. $\ell \simeq b$). In this case, Equation 2.12 can be re-expressed in terms of a new effective gain-length product required for threshold with a focused pump beam as:

$$(g_R I_p \ell_{th}) = \frac{\pi}{4\kappa}\left[1 + \left[1 + \frac{4\kappa}{\pi}\ln(P_s/P_{so})\right]^{\frac{1}{2}}\right]^2 \qquad (2.14)$$

This can be used as a refined threshold condition. Acknowledging that a typical power gain of around exp(30) is needed for the Stokes wave to reach a detectable level, $\ln(P_s/P_{so})$ can be replaced by 30. The gain-length product at which threshold will be exceeded is shown as a function of ($\kappa = \omega_s/\omega_p$) in Figure 2.2.

Fortunately, for SERS on the 6s-7s and 6s-5d transitions in Caesium and on the $6s^2$-6s5d in Barium, κ is large and lies between 0.1 and 1. The Raman threshold for these processes is therefore expected to exceed the calculated plane-wave threshold by only a factor of 2-3. However, generation of Stokes waves on transitions with larger Stokes shifts will be subject to dramatically increased thresholds.

No attempt has been made to solve the wave equation with the inclusion of pump absorption. Physically, small absorption ($\beta\ell \ll 1$) will leave the threshold condition relatively unscathed, but this will not be true in the case of strong absorption. The pump wave effectively only gives gain to the Stokes wave for a distance equal to the pump light extinction length, β^{-1}. After this distance the Stokes light propagates without substantial gain focusing. Approximate use can be made, therefore, of the threshold condition, but with the cell length replaced by the effective length, ℓ_{eff}, defined by Equation 2.8. This length is substituted for ℓ in the $\tan^{-1}(\ell/b)$ term.

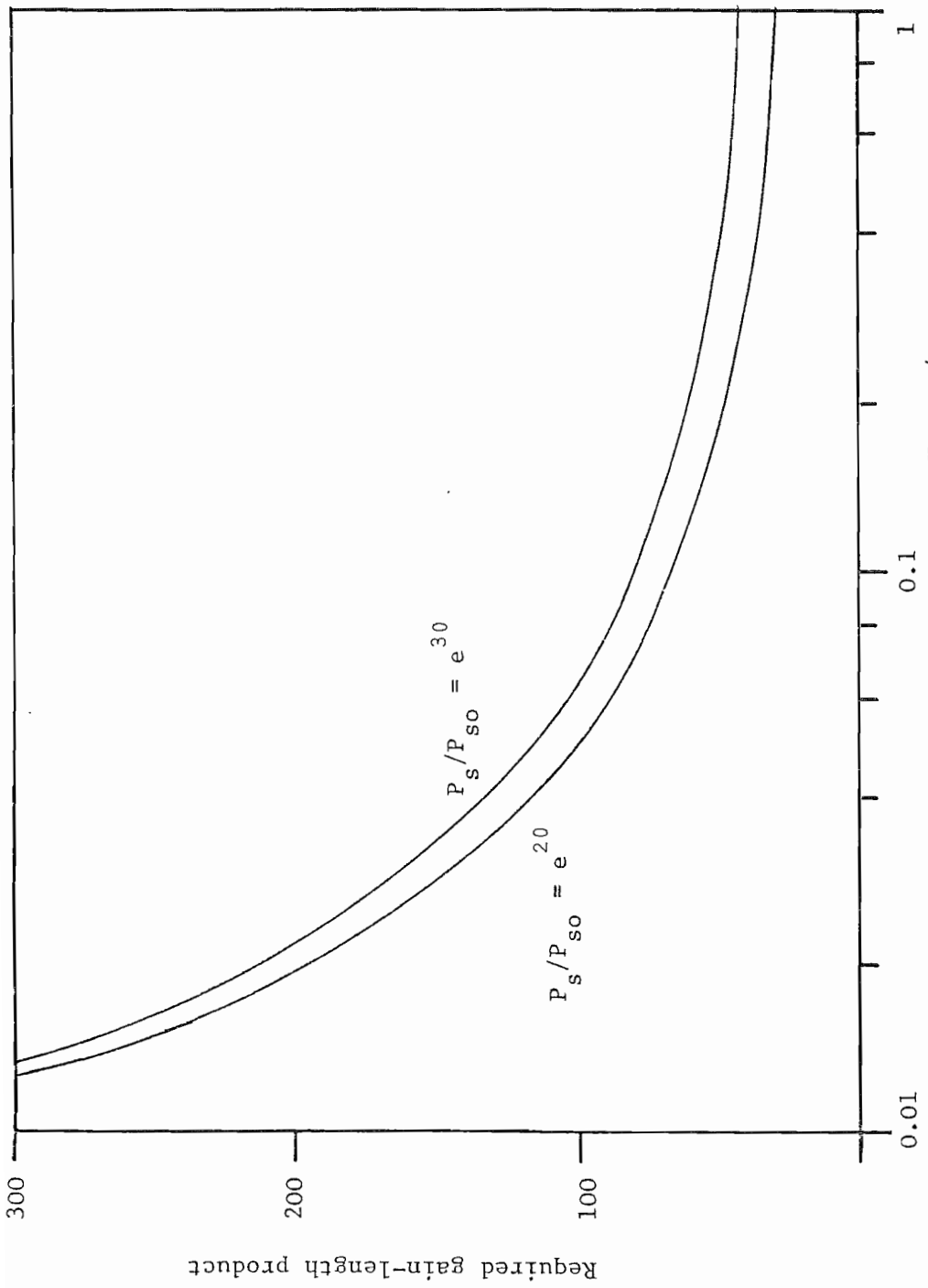

Figure 2.2 Threshold gain-length product required by the diffraction and gain focusing theory of Cotter, Hanna and Wyatt (1975)

In conclusion, the effects of diffraction and gain focusing cause the Raman threshold to be higher than that expected from plane wave considerations. Absorption of the pump laser light by the nonlinear medium increases the threshold further. Some allowance can be made for this by using an effective length of the vapour column rather than the real length in the evaluation of the gain-length product of Equation 2.14.

2.6 Large Signal Growth of SERS

The analysis of the previous section dealt with the small signal exponential growth of the Stokes wave. This growth cannot, of course, continue indefinitely. Two mechanisms play a significant role in limiting the Stokes output.

If the photon flux of the Stokes wave becomes large, depletion of the pump wave will occur, since the total photon flux in the two waves must be conserved in the absence of single photon absorption. This leads to a reduction in the Raman gain per unit length ($G_R = g_R I_p$) as the pump intensity I_p falls off. This is termed pump saturation. In addition, if the number of Stokes photons generated per unit volume approaches the atomic number density, the available number density will decrease. This occurs because production of a Stokes photon leaves an atom in the final (excited) Raman level. In general this excited atom will only decay back to the ground state slowly. This will be due either to the final level being metastable, as in Barium, or to rapid decay of the excited state to a radiation trapped lower state, as will be the case in Caesium. The reduction in available ground state atoms will lead to a reduction in g_R. This effect is termed atomic saturation.

The large signal behaviour of SERS under the conditions of atomic and pump saturation was considered by Cotter and Hanna (1978). A particularly interesting point arising from this study is that the total output Stokes energy is dependent on the small signal gain of the Stokes wave. How this arises is now considered. In order to simplify the discussion to just the effect of pump and atomic

depletion, and thus ignore dynamic effects, the pump laser pulse will be considered as being much smaller in length ($c\tau_p$) than the nonlinear medium. The generated Stokes pulse is assumed to remain with the pump pulse as it travels through the medium.

The growth of the Stokes wave in the first part of the cell takes place in the small signal regime and will not be subject to any saturation. However, this will cease to be true at some distance ℓ_{th}, into the cell. This distance will be the distance at which the process reaches the 'threshold' condition $G_R \ell_{th} = 30$. At this point atomic saturation begins to set in; the Stokes wave now tends to grow linearly with distance as, for every two atoms which are within the illuminated region, a maximum of one Stokes photon can be produced. In the absence of depletion of the pump laser, the Stokes output energy will be proportional to the length of cell remaining after this threshold length ℓ_{th}, and will therefore be dependent on the small signal gain. The maximum energy that can be obtained at the Stokes wavelength will be limited by atomic depletion to a total equivalent to one photon for every two ground state atoms illuminated by the pump laser. Typically, on the 6s-7s Caesium transition, a total latent Stokes energy of around 90 μJ is available from a 30 cm length of vapour at 10 torr. Of course a calculation of the threshold length and hence the saturated length is needed to give a better estimate of the energy expected in the atomic depletion limit.

The output energy cannot, however, exceed the limit set by the available number of pump laser photons. In terms of the input pump energy E_p, the pump saturation limited Stokes output energy is

$$E_s = \frac{\omega_s}{\omega_p} E_p \qquad (2.15)$$

and for SERS will be less than E_p. In view of the presence of pump absorption and other higher order competing processes, the 100% conversion limit implied by Equation 2.15 cannot in general be realised. Despite this, efficiencies in excess of 50% have been reported on the 6s-7s transition in Caesium (Cotter and Hanna (1978))

and of over 80% in Barium on the $6s^2$-6s5d transition (Djeu and Burnham (1977)). Taking again the example of 6s-7s scattering in Caesium, a maximum Stokes energy of 15 μJ can be obtained from a pump laser of 120 μJ in the limit set by Equation 2.15. From a pump laser of, say 3 mJ, this increases to 450 μJ which is above the limit set at 90 μJ by atomic saturation.

As can be seen, two mechanisms play significant roles in determining the energy produced by SERS. Consideration of the pump and atomic saturation limited output energies allow an estimate of the expected Stokes energy to be made.

2.7 Optimization of the Raman Output

In the previous sections the evaluation of the small signal gain for SERS was discussed. Reference was made to the effects of single photon absorption and collision broadening. Attention is now given to optimizing the conditions under which SERS takes place so as to maximize either the output energy at a particular wavelength, or the available tuning range. Maximizing the tuning range is equivalent to optimizing the output energy at the ends of the tuning range.

The Stokes energy produced by SERS is dependent on the small signal Raman gain. The smaller the threshold length, the more energy will be produced and so to obtain the largest infrared output, the Raman gain must be maximized. When there is no pump absorption, this can be satisfied by having a high number density of the nonlinear material. Pump attenuation is usually present, however, due to either atomic or molecular absorption. These will be considered separately.

In alkali metal vapours, the presence of dimer molecules can give rise to significant absorption. The number density of these absorbers in a saturated vapour rises more rapidly with increasing temperature than that of the atomic species. At sufficiently low pressures, the absorption will be negligible, and the Raman gain will increase approximately linearly with pressure. As the pressure

is further increased, collision broadening of the Raman transition will cause the gain to saturate. At higher pressures, the molecular absorption starts to reduce the effective length defined by Equation 2.8. As $\beta\ell$ becomes large ($\beta\ell > 1$) the effective length tends to β^{-1}, and is thus inversely proportional to the number density of dimers, N_D. In this limit the effective gain G_R/β decreases rapidly with increasing atomic (and hence molecular) number density.

For wavelengths at which the absorption cross-section of the molecules is large, gain reduction due to the shrinking effective length may occur before saturation of the gain by collisional broadening has become apparent. Neglecting bleaching of the molecular absorption by the pump laser pulse, the maximum obtainable Raman gain is less than its broadening limited value. Figure 2.3 shows curves of the effective Raman gain coefficient against atomic number density for both large and small values of the absorption cross-section. In both cases the optimum conditions will occur in the pressure region where the effect of the reduction in effective length is just starting to dominate. For high absorption, this corresponds simply to the peak of the gain, but for low absorption this will lie at the high pressure end of the collision affected gain plateau. Although no increase in gain can be achieved by working here, the higher number density will help to minimize the effects of atomic saturation.

In order to judge the correct operating pressure for optimum production of a particular Stokes wavelength, a criterion based on the effective length can be used. Choosing this length to correspond to half the real cell length, the pump laser attenuation required by Equation 2.14 results in a value of $\beta\ell = 1.6$. As a guide to the best operating pressure for a particular pump laser wavelength, the cell length should be around one and a half optical extinction lengths.

In Caesium, the dimer absorption cross-section increases with increasing wavelength in the neighbourhood of the atomic 7p doublet (see Figure 4.8). The generation of long wavelength Stokes radiation is hampered by the resulting strong dimer absorption

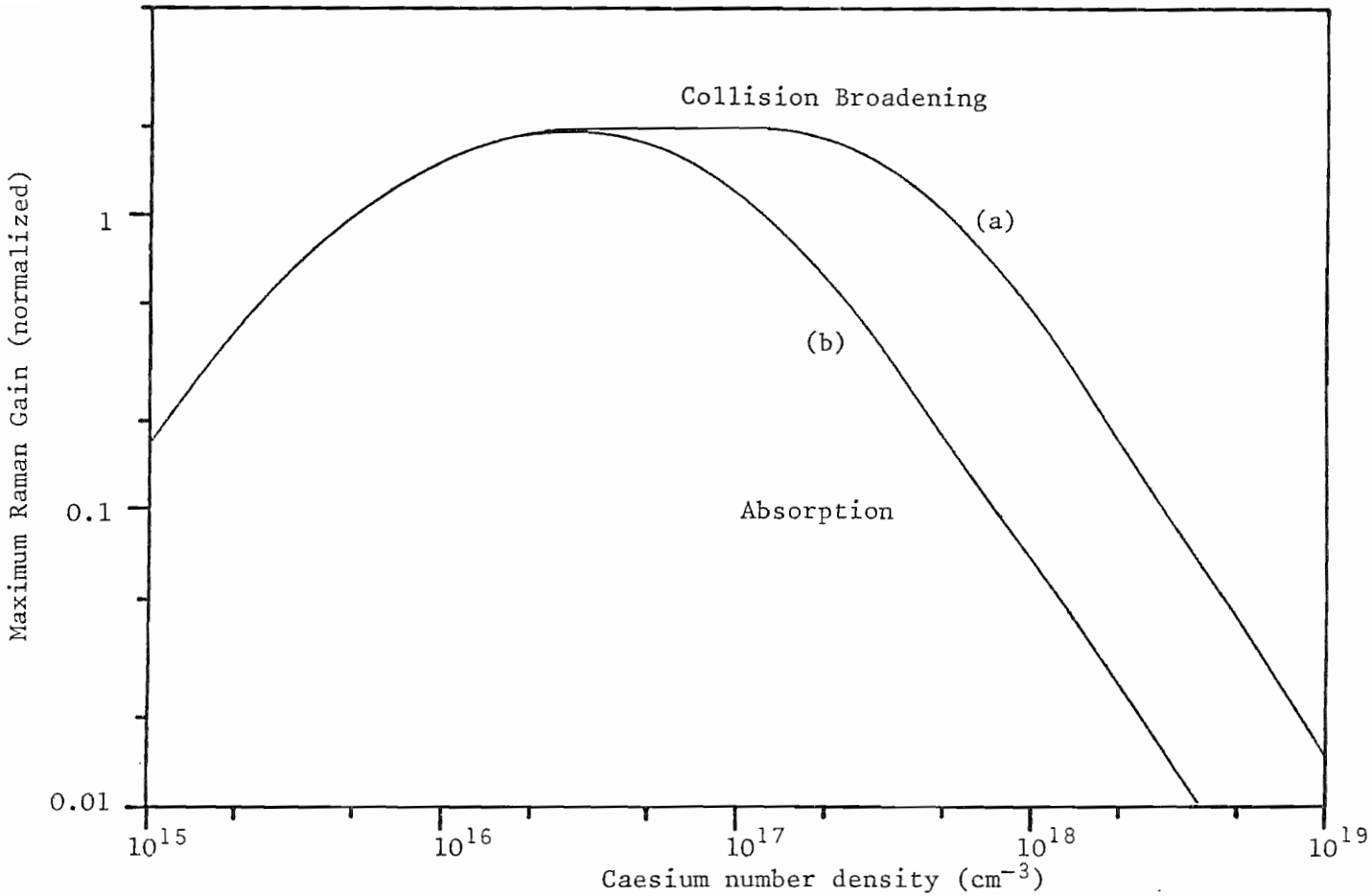

Figure 2.3 Effect of collision broadening and dimer absorption on the Raman gain (see text).

(a) $\sigma_D = 10^{-17}$ cm^2

(b) $\sigma_D = 5 \times 10^{-17}$ cm^2

of the pump laser. The above discussion would seem to preclude the generation of Stokes light at these wavelengths, where the Raman gain is low and the dimer absorption cross-section at the pump wavelength is high. This is not necessarily true; bleaching of the absorption can occur raising the Raman gain to a value approaching the broadening limited one. The amount of bleaching will depend on the relative number of dimer molecules in the volume illuminated by the pump laser and the total number of photons in the pump laser pulse. If there are many more photons than molecules then these will be bleached and the gain will be broadening limited†. If, on the other hand, there are many more molecules than pump photons, the Raman gain will be absorption limited. To be able to bleach the absorption and still have sufficient pump photons left to perform SERS, the condition that the total number of dimers should be at most 10% of the number of pump photons, should be satisfied.

The number of dimers illuminated can, of course, be minimized for a given atomic number density. This can be achieved by reducing the column length of the vapour while still maintaining the same ratio of confocal parameter to vapour length. The penalties which are incurred in doing so are two fold; the total number of the atoms illuminated is also reduced, which results in the onset of severe atomic saturation at a lower output energy, and perhaps more importantly the focusing over the shorter cell is necessarily tighter. Competing processes, such as multiphoton ionization, which depend on the local intensity of the laser will then become more effective and can inhibit the generation of a Stokes output. For SERS, on the other hand, the total Stokes gain depends on an intensity x length product. The reduction in Raman gain due to multiphoton ionization will be discussed in Chapter 6.

So far, attention has been restricted to the effect of dimer absorption. Near to the principal resonance lines of an atom, the absorption due to these will overshadow the molecular contribution.

---

† For this discussion molecular ionization is neglected. However, the importance of photo-ionization will be discussed in Chapter 6.

Now, however, the absorption is solely dependent on the atomic number density and cannot be bleached without reducing the ground state population for SERS as well. In addition, the absorption coefficient increases with increasing number density. When the pump laser is tuned close to resonance, the absorption is strong ($\beta\ell > 1$) and so the effective length defined by Equation 2.8 tends to β^{-1} and the gain length product tends to $G_R\beta^{-1}$.

In the impact approximation, the resonance broadened absorption lineshape will be Lorentzian with a linewidth given by Equation 2.7; this width is dependent on the atomic number density. For large detunings ($\Delta >> \Gamma$), the effect of this Lorentzian profile is to make the gain-length product $G_R\beta^{-1}$ independent of the detuning Δ, both G_R and β being inversely proportional to Δ^2. The product $G_R\beta^{-1}$ represents the highest obtainable gain on a particular resonant Raman transition, and places an upper limit on the value of $g_R I_p \ell$ which can be used in the threshold condition. If $G_R\beta^{-1}$ is less than the value required by Equation 2.14, the process cannot exceed Raman threshold. This independence of gain from detuning will be invalid when $\beta\ell$ becomes less than two. The effect of the exponential term in Equation 2.8 will then make the effective length exceed β^{-1}. However, the absorption due to dimers may also be comparable to the atomic absorption and so both factors must be taken into account.

For low atomic pressures the absorption and Raman linewidths will not be purely Lorentzian, as they will contain comparable contributions from Doppler and collision broadening. The effect of this on the Raman gain was discussed in Section 2.3. For SERS on the 6s-7s transition in Caesium the Raman gain will stop increasing when the atomic vapour pressure exceeds $\sim$3 torr. At around the same pressure, the collisional broadening of the 6s-7p transitions will start causing the absorption linewidth to significantly exceed the Doppler width. The effect of single photon absorption on the small signal Raman growth and therefore the output energy, will have an increasing effect above this pressure. In order to optimize the output Stokes energy with the pump laser tuned very near to single photon resonance, a low atomic vapour pressure must be chosen (<3 torr for 6s-7s scattering in Cs).

In considering the achievement of the maximum tuning range from a particular SERS scheme, two limiting cases are apparent. These are illustrated by the two wavelength limits of 6s-7s SERS in Caesium. Neglecting other competing effects, the process is curtailed by either insufficient Raman gain or by absorption of the pump laser light by dimer molecules. In the first case the gain for a given pump power can be maximized by increasing the atomic number density to a point at which collision broadening of the Raman transition is dominant. No further gain or tuning can be obtained by increasing the number density further. However, the output energy will be increased over the tuning range as, in a high number density vapour, atomic saturation will not take place so readily. This will be applicable to the short wavelength limit of 6s-7s Stokes generation.

At the long wavelength limit dimer absorption is strong. As the number density is increased, the pump laser attenuation will also become greater. As the atomic density is increased, the dimer density increases more rapidly and so the maximum integrated Raman gain ($G_R\beta^{-1}$) will be reduced. Unlike the case above, there is no advantage in using higher atomic number densities than necessary. The optimum output tuning is likely to occur when collision broadening of the Raman transition just dominates over Doppler broadening. In this way the energy produced near the tuning limit is maximized. For 6s-7s SERS in Caesium, this corresponds to an atomic pressure of around 10 torr. The work of Cotter (1976) has shown that this pressure is, in fact, optimum. Using lower pressures the tuning is curtailed; using higher pressures the output energy is reduced.

CHAPTER 3

Two Photon Resonant Four Wave Mixing

In this chapter, the principles of two photon resonant four wave mixing are presented for the particular case of biharmonic pumping. This process, which consists of two coupled Raman processes, is seen to allow Stokes generation from a pump laser normally incapable of exceeding Raman threshold. It can, therefore, be used as a method of Raman shifting weak tunable lasers into the infrared. Limitations arising from atomic saturation of the non-linear medium and absorption of the weak laser are also described.

Stimulated Raman scattering and biharmonic pumping are related processes. The latter is shown schematically in Figure 3.1 and appears as two coupled Raman processes. The waves at frequencies ω_1 and ω_{1s} and those at ω_2 and ω_{2s} form Raman resonant pairs both sharing the same final Raman level $|f\rangle$. This level, as with SRS, can be an electronically, vibrationally or rotationally excited state.

In the classical description of SRS (see for example Yariv (1975), Section 18.4), the applied pump laser field sees the atomic polarizability modulated at the transition frequency Ω_{fg}. This has the effect of modulating the dielectric constant, thereby phase modulating the pump laser and producing a sideband at $\omega_p - \Omega_{fg}$. This is, of course, at the Stokes frequency. The growth of the Stokes wave from the induced polarization thus set up is exponential with distance as described by Equation 2.1. These ideas can easily be extended to the case of biharmonic pumping. Modulation of the polarizability by one pair of waves affects the other pair. Phase modulation of the second pump wave leads to the generation of its Stokes frequency. Unlike SRS, however, the generation of this Stokes component takes place without the second pump laser necessarily exceeding Raman threshold.

A complete description of the biharmonic pumping process requires the effect of both wave pairs on the polarizability to be

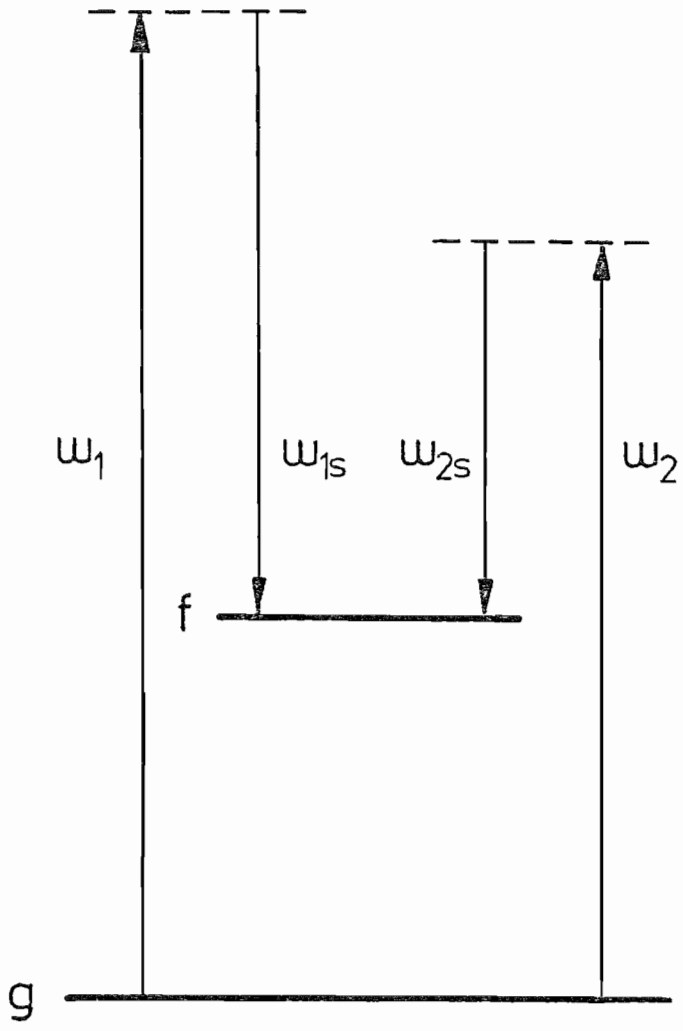

Figure 3.1 Biharmonic pumping-schematic

taken into account; the next section deals with this. The small signal and large signal growth regimes will be discussed.

3.1 Material Excitation

In the introduction to this chapter the nonlinear interaction of four waves was described in terms of a modulated polarizability or 'excitation' set up in the medium. Attention is now focused on the description of this excitation and the role it plays in SRS and biharmonic pumping.

In the classical description of stimulated vibrational Raman scattering, the macroscopic polarization which gives rise to Stokes radiation is given in terms of the applied pump field by

$$P_s = N\alpha_R Q^* E_p \tag{3.1}$$

where N is the number density of the nonlinear medium and α_R is the Raman polarizability (Hanna et al (1979)). For molecules, Q represents the displacement of the constituent atoms from their equilibrium positions. Equation 3.1 expresses the idea of a laser field E_p interacting with an excitation Q, oscillating at the Raman transition frequency Ω_{fg}, to produce a polarization at the Stokes frequency of the laser field $\omega_s = \omega_p - \Omega_{fg}$. In stimulated electronic Raman scattering in atomic media, the above interpretation of Q is no longer applicable, but the ideas embodied in Equation 3.1 can still be used to describe SERS.

The excitation per atom, Q, can be written for steady state SERS in terms of the interacting pump and Stokes fields as

$$Q = \frac{\alpha_R E_s^* E_p}{4\hbar\Gamma_R} \tag{3.2}$$

where exact Raman resonance has been assumed. Γ_R is the normal Raman linewidth discussed in Section 2.3, and relates to the time

dependent behaviour of Q (Hanna et al (1979); Section 2.7.3). In the absence of pump or Stokes fields any excitation present in the medium decays with a time constant $\tau \simeq \Gamma_R^{-1}$.

Combining Equations 3.1 and 3.2, the usual expression for the polarization induced during SERS is obtained

$$P_s = \frac{N|\alpha_R|^2}{4\hbar\Gamma_R} |E_p|^2 E_s \qquad (3.3)$$

As the polarization at the Stokes frequency is proportional to the Stokes field already present, this equation leads to exponential growth of the Stokes wave. By substituting Equation 3.3 into the wave equation for E_s, the value of the Raman gain at frequency ω_s can be derived.

To find the polarization induced in biharmonic pumping, the definition of Q must be extended to cover both Raman resonant pairs of waves present in the medium. As may be anticipated, the total excitation is just the sum of contributions from the two wave pairs

$$Q = \frac{1}{4\hbar\Gamma_R} \{\alpha_{fg}(-\omega_{1s}; \omega_1)E^*_{1s}E_1 + \alpha_{fg}(-\omega_{2s}; \omega_2)E^*_{2s}E_2\} \qquad (3.4)$$

where the labelling scheme of Figure 3.1 has been used. The Raman polarizability α_R is critically dependent on the interacting frequencies. To distinguish the two values of α_R occurring in biharmonic pumping, they are also labelled by their corresponding frequencies. Similarly, the frequency arguments of the polarizability used in Equation 3.1 must also correspond to the wave pair under consideration.

3.1.1 The Small Signal Behaviour of Biharmonic Pumping

Central to the theory of two photon resonant nonlinear optics is the two photon transition polarizability α_R. As can be seen from Equations 3.1 and 3.2, this parameter plays two roles. It is

a coupling coefficient for the generation of the excitation Q by the oscillating fields present, as well as for the polarization present at the Stokes frequency from the interaction of the pump field with this excitation.

The polarizability applicable to SERS and biharmonic pumping in atomic media is given, for linearly polarized fields at frequencies ω_p and ω_s, by

$$\alpha_{fg}(-\omega_s;\ \omega_p) = \frac{1}{\hbar}\sum_i \mu_{fi}\mu_{ig}\left(\frac{1}{\Omega_{ig} - \omega_p} + \frac{1}{\Omega_{ig} + \omega_s}\right) \qquad (3.5)$$

The μ's are dipole matrix elements for transitions $g \to i$ and $i \to f$. The summation is over all states i which are connected to both the ground and final states by single photon transitions. Some simplifying approximations can be made to Equation 3.5. Firstly the second denominator term $\Omega_{ig} + \omega_s$ will, in general, be large in comparison to the first term $\Omega_{ig} - \omega_p$ and so the term containing $\Omega_{ig} + \omega_s$ can usually be neglected. Secondly, in the experiments which will be described in Chapter 5, the pump laser is near resonance with one particular single photon transition starting from the ground state. One term in the summation will therefore dominate in this case, as it has a small resonant denominator.

These simplifications are of immense use when nonlinear optics for example in Barium is considered. The available data for the alkaline earths (for example Friedrich and Trefftz (1968), Miles and Wiese (1970)) are restricted to oscillator strengths of the transitions, rather than dipole matrix elements. Although dipole matrix elements and oscillator strengths are related, upon transforming the latter into dipole matrix elements an indeterminacy of sign arises. For near resonant processes this is of little concern, but for nonresonant calculations, large uncertainties in the value of α_{fg} appear due to a lack of knowledge of the sign of terms in the summation of Equation 3.5.

For processes having a dominant intermediate level $|i\rangle$ the

summation collapses to

$$\alpha_{fg}(-\omega_s;\ \omega_p) = \frac{2\pi\varepsilon_o r_e c^2}{\Omega_{ig} - \omega_p}\left[\frac{f_{fi}f_{ig}}{\Omega_{if}\Omega_{ig}}\right]^{\frac{1}{2}} \tag{3.6}$$

for an upper Raman level with $J_f = 0$. This must be multiplied by $\sqrt{2}$ for an upper level with $J_f = 2$ (e.g. a $^3D_2$ state in the alkaline earths).

The growth of a wave at frequency ω_{2s} is determined by the polarization present at that frequency. As the electric fields of the waves are running waves, the substitution

$$E_\omega(z) = E_\omega \exp(ik_\omega z) \tag{3.7}$$

can be made in Equations 3.1 and 3.2. E_ω is the field envelope; propagation has been taken to be in the z direction. The polarization at ω_{2s} is a function of the position along the length of the medium, and is given by

$$P_{2s} = \frac{N\alpha_{fg}(-\omega_{2s};\ \omega_2)}{4\hbar\Gamma_R}\left[\alpha_{fg}(-\omega_{1s};\ \omega_1)E_{1s}E_1^*E_2 e^{i\Delta kz} + \alpha_{fg}(-\omega_{2s};\ \omega_2)|E_2|^2 E_{2s}\right] e^{ik_{2s}z} \tag{3.8}$$

where the phase mismatch Δk has been introduced. For biharmonic pumping Δk is given by

$$\Delta k = k_2 - k_{2s} - k_1 + k_{1s} \tag{3.9}$$

Calculation of the phase mismatch will be considered in Section 3.4. Equations similar to 3.8 can be written for all the interacting waves.

The equation describing the growth of a wave from its generating polarization is obtained by substituting the nonlinear

polarization into the wave equation. The envelope functions of the waves are slowly varying and so the wave equation can be well approximated by

$$\frac{dE_{2s}}{dz} = \frac{i\omega_{2s}P_{2s}}{2\varepsilon_o c\eta_{2s}} e^{-ik_{2s}z} \qquad (3.10)$$

η_{2s} is the refractive index of the nonlinear medium at ω_{2s}, which for an atomic vapour is generally close to unity.

The procedure which led to Equation 3.10 can be repeated for all the interacting waves and gives four coupled wave equations. The solutions of these have been described by Venkin et al (1975) and Yuratich (Private communication (1979); see also Hanna, Yuratich and Cotter (1979) Sections 3.4.1 and 3.4.2). The equations can be simplified by normalizing the electric fields to have the dimensions of $(\text{Intensity})^{\frac{1}{2}}$. It is natural to also introduce the Raman gain coefficients

$$g_1 = \frac{N\omega_{1s}}{2\varepsilon_o^2 c^2 \hbar \Gamma_R} \left|\alpha_{fg}(-\omega_{1s};\ \omega_1)\right|^2 \qquad (3.11a)$$

and

$$g_2 = \frac{N\omega_{2s}}{2\varepsilon_o^2 c^2 \hbar \Gamma_R} \left|\alpha_{fg}(-\omega_{2s};\ \omega_2)\right|^2 \qquad (3.11b)$$

The resulting equations are shown in Figure 3.2

As an example of the solution of these equations, a case relevant to biharmonic pumping in Barium is now considered. In Barium, a 532 nm laser of up to 10 mJ pulse energy is found to be incapable of exceeding Raman threshold. On the other hand, a laser operating at 355 nm can exceed threshold easily. From this consideration, the SERS terms can be dropped from the equations governing E_2 and E_{2s}. Similarly the SERS term is likely to dominate in the equations relevant to E_1 and E_{1s}. The Raman driven parametric approximation of Venkin et al (1975) ignores the smaller term in each equation, effectively divorcing the effects of four wave mixing on the growth of E_{1s}, and imposing only parametric growth on E_{2s}.

$$\frac{dE_1}{dz} = -\frac{g_1}{2}\frac{\omega_1}{\omega_{1s}}\left[\left|\frac{\alpha_2}{\alpha_1}\right| E_{1s}E_{2s}E_2\, e^{i\Delta kz} + |E_1|^2 E_{1s}\right]$$

$$\frac{dE_{1s}}{dz} = \frac{g_1}{2}\left[\left|\frac{\alpha_2}{\alpha_1}\right| E_1E_{2s}E_2\, e^{-i\Delta kz} + |E_1|^2 E_{1s}\right]$$

$$\frac{dE_2}{dz} = -\frac{g_2}{2}\frac{\omega_2}{\omega_{2s}}\left[\left|\frac{\alpha_1}{\alpha_2}\right| E_{2s}E_{1s}E_1 e^{-i\Delta kz} + |E_2|E_{2s}\right]$$

$$\frac{dE_{2s}}{dz} = \frac{g_2}{2}\left[\left|\frac{\alpha_1}{\alpha_2}\right| E_2E_{1s}E_1 e^{i\Delta kz} + |E_2|E_{2s}\right]$$

Figure 3.2 The normalized coupled wave equations of biharmonic pumping (see text). The electric fields have been taken as real and

$\alpha_1 = \alpha_{fg}(-\omega_{1s};\ \omega_1)$, $\alpha_2 = \alpha_{fg}(-\omega_{2s};\ \omega_2)$

The growth of E_{1s} in the small signal regime is easily seen to be exponential with distance into the medium. When the form of the growth of E_{1s} is substituted into the other equations, the growth of E_{2s} is also seen to grow exponentially and with the same gain coefficient G_1. In other words the growth of E_{1s} is impressed upon E_{2s}.

In the small signal region of the medium, where the fields E_1 and E_2 have not been severely depleted by the four wave mixing process, the growth of the Stokes wave at ω_{2s} is exponential with distance and is given by

$$I_{2s} = \frac{\omega_{2s}}{\omega_{1s}} \Lambda R^2 I_{1so} \exp(g_1 I_1 z) \tag{3.12}$$

i.e. of the form of Equation 2.1 but with a gain per unit length of $g_1 I_1$. This solution is valid for $\Delta k = 0$. Two parameters relevant to biharmonic pumping have been introduced into this solution. The parameter R expresses the relative coupling of the wave pairs to the material excitation, and is given by

$$R = \left(\frac{\omega_{2s}\omega_2}{\omega_{1s}\omega_1}\right)^{\frac{1}{2}} \frac{\alpha_{fg}(-\omega_{2s};\ \omega_2)}{\alpha_{fg}(-\omega_{1s};\ \omega_1)} \tag{3.13}$$

Λ is the ratio of the photon fluxes in the two input waves:

$$\Lambda = \frac{\omega_1 I_{2o}}{\omega_2 I_{1o}} \tag{3.14}$$

Equation 3.12 describes small signal growth in biharmonic pumping and will not hold if atomic saturation is present or either of the pump waves suffer depletion. In Equation 3.12, an effective starting noise $(\omega_{2s}/\omega_{1s})\Lambda R^2 I_{1so}$ appears naturally from the analysis as an equivalent for I_{1so}.

3.2 Large Signal Behaviour of Biharmonic Pumping

The exponential growth described by Equation 3.15 will give way to a more complex behaviour if either of the pump waves become

depleted. The approximate solution of the coupled wave equations in Figure 3.2 now breaks down. The equations have been solved by Yuratich (private communication (1979)) for the case of an infinite length of nonlinear medium. The pump wave at ω_1 would, in the absence of the wave at ω_2, be entirely converted to its Stokes wave at ω_{1s}. There would then be an excitation Q set up in the medium which varies with distance. As the pump wave is converted to its Stokes wave, the excitation will peak up around the distance at which the product of the two fields is a maximum. Of course, Q will be much smaller at short and large distances into the medium.

Allowing a weak pump wave to enter the medium as well causes an interaction between this wave and the excitation present†. The Stokes wave of this pump will be radiated in the medium and will exhibit relative growth similar to that of the strong Stokes wave. Again the growth of the field E_{1s} is impressed upon E_{2s}. However, if the second pump wave has an intensity comparable to that of the strong pump, the situation is somewhat different. The growth of the Stokes field E_{2s} in conjunction with the pump wave at ω_2 will set up an excitation of their own. Venkin and Yuratich both found that, in the growth of E_{2s} by four wave mixing, the phase of this Stokes wave is such that this extra excitation tends to interfere destructively with the original excitation. The growth of both Stokes waves will now be lessened. The wave at E_{2s} will grow until the excitation has been entirely cancelled. The steady state (infinite distance) photon conversion efficiency from ω_2 to ω_{2s} is now given by

$$\eta = \sin^2\left(\frac{R\pi}{2}\right) \tag{3.15}$$

where R is the material ratio given by Equation 3.13. This equation is relevant to infinite length nonlinear media, but, for R < 1,

---

† The term 'weak' will be used to denote the pair of waves which can be considered to be driven by excitation (namely E_2 and E_{2s}). Similarly, the 'strong' pair (E_1 and E_{1s}) can be thought of as driving the excitation.

represents a limiting value of the conversion efficiency for finite media. In addition, the inclusion of the effects of phase mismatch in the analysis contributes a further reduction to η. The conversion efficiency with phase mismatch Δk is given in terms of the $\Delta k = 0$ value by (Yuratich, private communication (1979)).

$$\eta(\Delta k) = \eta(\Delta k = 0)\ \mathrm{sech}^2\left(\frac{\pi \Delta k}{G_R}\right) \tag{3.16}$$

G_R here is the sum of the Raman gains per unit length for the two Stokes waves. For a second pump wave which is weak or lacks the advantages of near resonance, this can be well approximated by $G_R = G_1$, the Raman gain per unit length for the Stokes wave at ω_{1s}.

The effect of nonzero Δk on the conversion efficiency given by Equation 3.16 differs from the more usual

$$\eta(\Delta k) = \eta(\Delta k = 0)\left[1 + \left(\frac{2\Delta k}{G_R}\right)^2\right]^{-1} \tag{3.17}$$

as given, for example by Byer and Herbst (1977). This result is obtained by neglecting pump depletion and only admitting terms describing SERS growth of ω_{1s}, and parametric growth of ω_{2s}, into the analysis. The equations of Figure 3.2 are then readily soluble as for the case of the Raman driven parametric approximation, but now with the inclusion of the phasemismatch. For small $\Delta k/G_R$, both Equations 3.16 and 3.17 tend to the phasematched efficiency.

Under the conditions of small Δk or large G_R, together with $R = 1$, the photon conversion efficiency tends to unity; under these circumstances total conversion of the second pump to its Stokes is possible. In atomic media other processes will prevent this being achieved. The most important of these are absorption of the second pump wave and atomic saturation. These topics will now be discussed.

3.3 The Effect of Atomic Saturation on the Conversion Efficiency

Up to this point, the growth of the generated waves has been assumed to be limited only by pump saturation, in which a large proportion of the available pump photons are converted into Stokes photons. In the conversion process, a ground state atom becomes excited to the final Raman level for every Stokes photon produced. If the time taken for that atom to return to its ground state is long compared with the laser pulse duration, the atom will no longer take part in the nonlinear process. The growth of the generated waves will be severely affected if a significant fraction of the available atoms are lost in this way. The effect which this atomic saturation has upon SERS was discussed in Section 2.6. The same restriction on growth appears in four wave mixing and leads to a large divergence from the photon conversion efficiency predicted by Equation 3.16.

From Equation 3.1, the polarization induced at ω_{2s} is dependent on the number density of atoms available for the four wave mixing process. If atomic saturation occurs, this polarization will be greatly reduced over the saturated region. In the extreme case, where the medium is highly saturated, the polarization will vanish. In such a limit, generation of the Stokes wave from the weak pump wave would not occur everywhere; the entire growth of this wave would take place in the unsaturated part of the medium.

To judge the effect on the growth of this Stokes wave, the distance into the medium at which saturation of the strong Stokes wave occurs needs to be found. By equating the number of Stokes photons generated per unit volume at a distance z into the medium to the number density of the medium, it can easily be shown that the onset of saturation takes place at the normal threshold length ℓ_{th}, where $G_1 \ell_{th} \simeq 30$. After this distance the Stokes wave can only grow linearly with distance. The growth of the weak Stokes wave can only take place in the region up to this point. This growth occurs, therefore, entirely within the small signal regime. Equation 3.15 for the exponential growth of I_{2s}, can be used

together with the restricted length ℓ_{th} obtained above, to give the generated weak Stokes intensity:

$$I_{2s} = \frac{\omega_{2s}}{\omega_{1s}} I_{1so} \Lambda R^2 \exp(3Q) \tag{3.18}$$

In order to find the photon conversion efficiency, Λ can be re-expressed in terms of the two pump intensities with the result that

$$\eta = \frac{\omega_1 I_{1so}}{\omega_{1s} I_1} R^2 \exp(3Q) \tag{3.19}$$

and is independent of the input pump intensity at ω_2. In addition, as I_1 is increased, the value of η is reduced. This is because the length over which I_{2s} grows is curtailed.

3.3.1 Inclusion of Pump Absorption and its Effect on Efficiency

In the previous section, it was shown that atomic saturation caused by the growth of the strong Stokes wave implies that the simple results of the small signal analysis are sufficient to describe four wave mixing in atomic media. Hence, use can be made of the Raman driven parametric approximation to describe this process. This analysis can be readily extended to include the effects of absorption of the weak pump wave. This is of great importance when use is made of close intermediate resonance, as this will also lead to a depletion of the weak pump light by single photon absorption.

If the weak pump wave experiences an attenuation described by an absorption coefficient β, the intensity of this wave will vary as

$$I_2(z) = I_{2o} \exp(-\beta z) \tag{3.20}$$

where I_{2o} is the intensity incident upon the medium. This functional dependence on distance can be inserted into the growth equation for the wave at ω_{2s}. The resulting equation is readily soluble:

$$\frac{dE_{2s}}{dz} = \frac{g_2}{2} \left|\frac{\alpha_1}{\alpha_2}\right| E_{1o} E_{2o} E_{1so} \exp (G_1 - \beta) \frac{z}{2} \qquad (3.21)$$

Except for a term which is small when $G > \beta$; the result is of the same form as Equation 3.12. Now, however the growth with distance is no longer governed by G_1 alone, as the gain per unit length seen by the Stokes wave is reduced to $G_1 - \beta$. The generated intensity is now dependent on the difference of G_1 and β and will be maximized by having a large value of G_1. This is to be expected as the growth of E_{2s} will occur faster the larger the field E_2 is. If G_1 is large, the growth takes place in a region in which the weak pump intensity has not been attenuated to any large extent. If the strong pump intensity is reduced, the weak pump may undergo substantial absorption in the threshold length ℓ_{th} and therefore be incapable of undergoing significant conversion to its Stokes wave.

The effect of pump absorption has been seen to cause a reduction in the generated Stokes light. The analysis can be easily extended to cover the case of imperfect phasematching by replacing G by $G_1 - \beta$ in the expression governing the effect of Δk on the conversion efficiency (Equations 3.15 and 3.18). The results of this section will be used in Chapter 5 to explain the qualitative behaviour of four wave mixing in Barium when a tunable dye laser is shifted into the infrared. In this work the dye laser was tuned close to a single photon transition of the medium and therefore suffered absorption by the medium.

3.4 Calculation of the Phase Mismatch Δk

In Section 3.12 the running nature of the interacting fields led to the wave equation being dependent on a phase mismatch Δk.

This is a measure of the distance over which the travelling weak Stokes wave becomes out of phase with its generating polarization. The wavevector of this polarization depends on the wavevectors of the three waves which are interacting to produce it. If these are taken as k_1, k_2 and k_{1s}, for the strong and weak pump and strong Stokes respectively, the wavevector of the polarization is

$$k_p = k_2 - k_1 + k_{1s} \tag{3.22}$$

for the particular case of biharmonic pumping. The difference between k_p and the wavevector of the generated weak Stokes is the phase mismatch Δk

$$\Delta k = k_2 - k_{2s} - k_1 + k_{1s} \tag{3.23}$$

In order to calculate this parameter the individual wavevectors must be found.

For a wave at frequency ω, the wavevector can be found in terms of the wavenumber, $\bar{\omega} = (2\pi c_{cgs})^{-1}\omega$, as

$$k_\omega = 2\pi\eta_\omega\bar{\omega} \tag{3.24}$$

where η_ω is the refractive index of the medium at the frequency ω. This refractive index can be found using the standard Sellmeier equation. In terms of the atomic transition oscillator strengths f_{ig}

$$\eta_\omega = 1 + \frac{Nr_e}{2\pi} \sum_i \frac{f_{ig}}{\bar{\Omega}_{ig}^2 - \bar{\omega}_p^2} \tag{3.25}$$

The sum over i takes account of all single photon transitions starting from the ground state; these have transition wavenumbers $\bar{\Omega}_{ig}$. In practice, the summation can be truncated as the higher lying states generally have smaller values of f_{ig} and the denominators become large.

When Equations 3.25 and 3.26 are substituted into 3.24, four terms cancel. These constitute $2\pi(\bar{\omega}_2 - \bar{\omega}_{2s} - \bar{\omega}_1 + \bar{\omega}_{2s})$ and vanish as they are a restatement of the frequency condition placed upon the four photon process. They arise from the first term of Equation 3.26 and are large in comparison with their counterparts from the second term. If left in the evaluation of Δk they would dominate. It is therefore sensible to remove them from the calculation of the separate wavevectors, and use the related quantities

$$k'_\omega = 2\pi(\eta_\omega - 1)\bar{\omega} \tag{3.26}$$

These are simply the difference between the vacuum wavevector and the wavevector in the medium. The result for the phase mismatch in terms of these quantities is just

$$\Delta k = k'_2 - k'_{2s} - k'_1 + k'_{1s} \tag{3.27}$$

and is the most simple method of calculating Δk.

CHAPTER 4

Dye Lasers, Heat-pipe Ovens and Metal Vapours

During the work described in this thesis, various tunable lasers and atomic vapour cells were required. Several laser pumped dye laser systems were constructed. In essence these differed only in their output wavelength although two different methods of frequency selection were employed. In addition heat-pipe ovens were used to contain the atomic nonlinear media, namely Caesium and Barium. Details of the construction and operation of these ovens will be described in this chapter, as will the properties of the atomic vapours.

4.1 Tunable Dye Laser Systems

For the Caesium work described in Chapter 6, a blue dye laser was needed. For this a Coumarin dye laser was constructed using either 7D4MC (7 Diethylamino 4 Methyl Coumarin) or Coumarin 102, the choice of which depended upon the exact wavelength range of interest. These were pumped by up to 40 mJ of 351 nm light from an XeF excimer laser, and produced up to 3 mJ of blue light. For the Barium experiments of Chapter 5 a blue green Coumarin 522 dye laser was pumped by 355 nm third harmonic light from a Nd:YAG laser. Up to 40 μJ were generated from a portion of the 3 mJ harmonic beam. Although higher efficiencies are attainable from such dye lasers, preference was given to good beam quality.

All the dye lasers were transversely pumped with the focused pump laser light (see Figure 4.1). Cylindrical silica lenses were used to focus the incoming light into a 1 cm long streak in the 1 cm dye cell. The dyes were dissolved in Ethanol and were stirred to minimize thermal distortion effects. The waist size of the incoming light and the dye concentration (and hence absorption depth) were chosen to make the pumped region extend over approximately one Fresnel zone of the dye laser cavity. In this way single transverse

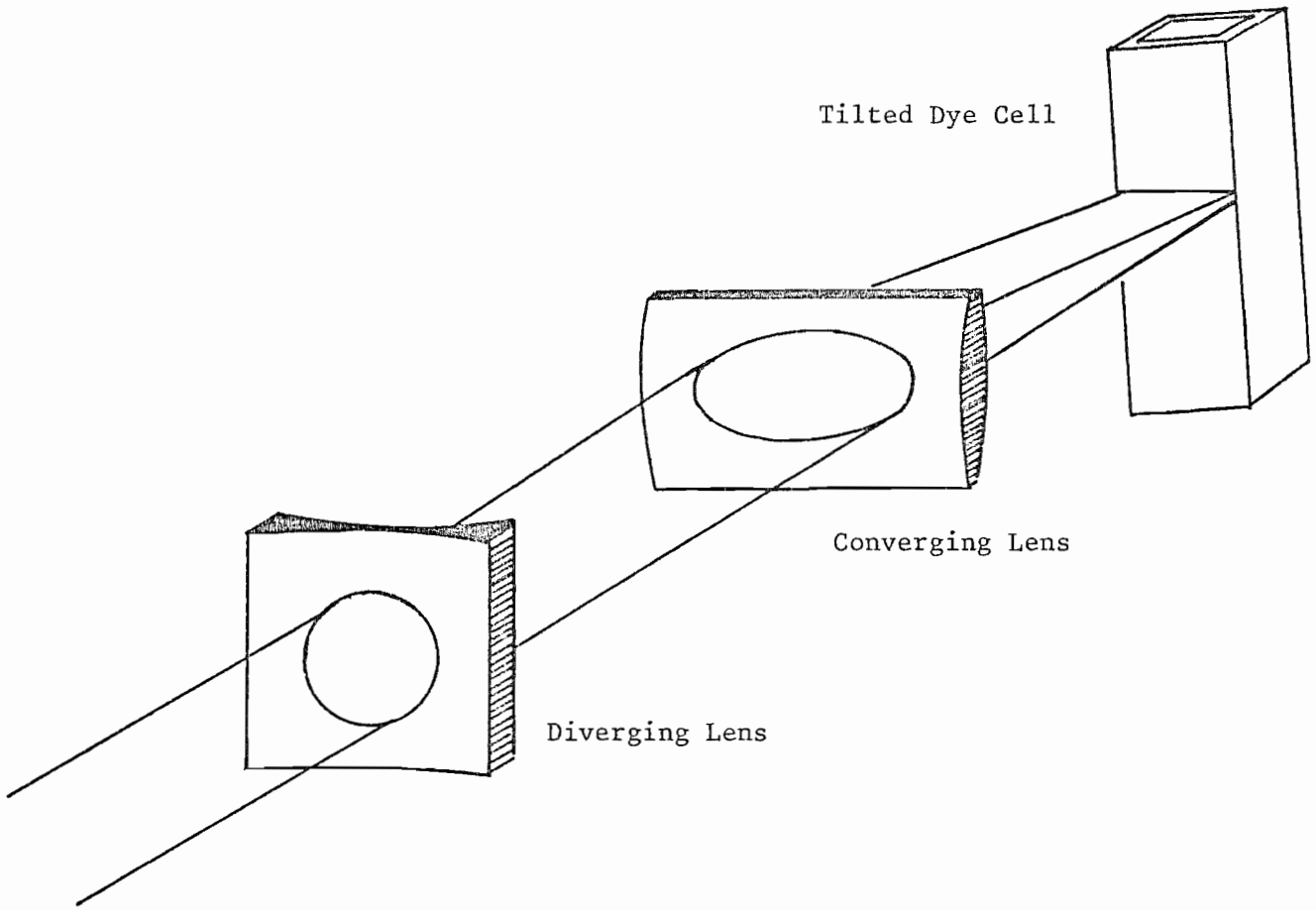

Figure 4.1 Dye laser pumping arrangements
(For excimer laser pumping, diverging lens was not used as the pump beam was already a streak)

mode operation was selected. A laser cavity consisting of a frequency selecting element at one end and a silica flat at the other, provided sufficient feedback for lasing to occur.

Two techniques of frequency selection and restriction were employed. Both use diffraction gratings to disperse the light falling on them and it is only the bundle of rays returning through the optically pumped dye region which is amplified. To alter the wavelength it suffices to alter the narrow range of frequencies which can pass back through this region. The difference between the two methods lies in the way in which the range of retro-reflected frequencies is reduced.

For the work in Caesium a four prism beam expander, of the type described by Laycock (1979), spread the light entering it into a streak across the diffraction grating thereby greatly enhancing the selectivity of the grating. In the Littrow arrangement a narrow band of wavelengths is reflected back along the incident path by the grating. It is only these wavelengths which are subject to feedback and amplification. In passing back through the prisms the angular spread of these wavelengths is multiplied by the magnification of the beam expander (see Figure 4.2a). A significantly reduced bandwidth (of the order of 0.1 cm^{-1}) is therefore obtained from the dye laser.

In the Barium experiments a dye laser using a grazing incidence grating was employed. This type of laser has been described by Shoshan et al (1977) and Littman and Metcalf (1978). Rather than expand the beam with prisms, the light falls obliquely onto the grating making an angle of around 86-88 degrees with the grating normal. A silvered mirror, placed close to the grating surface, reflects light which has been diffracted into a specific grating order back onto the grating (see Figure 4.2b). Only a narrow range of wavelengths is then returned back along the axis of the pumped region. Again, as in the case of the prism beam expander, frequency selectivity is increased by the resonant light being streaked across the grating. In both cases the combination of a highly dispersive element and a small amplifying region give narrowband operation. Unlike the original descriptions of these types of

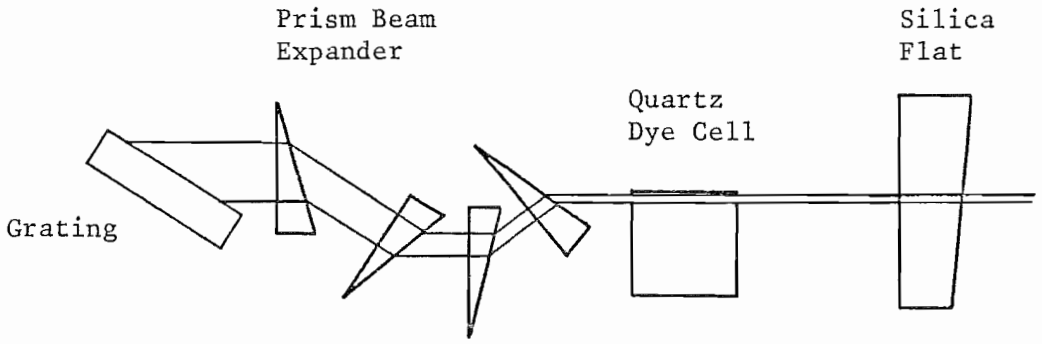

Figure 4.2a Dye laser with prism beam expander

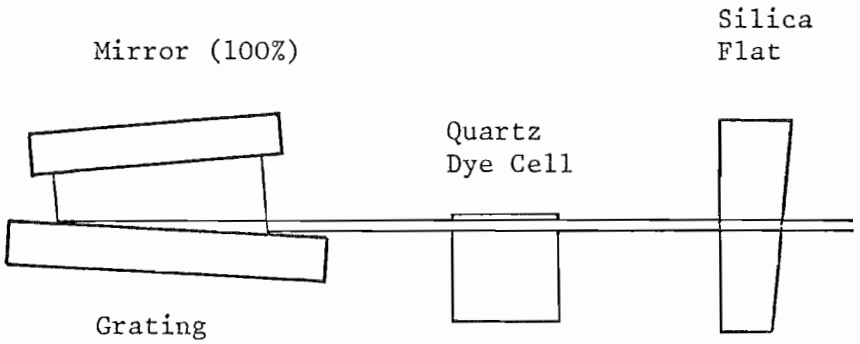

Figure 4.2b Dye laser with grazing incidence grating

laser the output was taken through an uncoated silica plate. In the original designs the position of this plate was occupied by a 100% reflecting mirror and the output was taken from the frequency selecting element. By using a silica plate, the amount of amplified spontaneous emission present in the output light at the ends of the dye tuning range was reduced.

To increase the output energy obtained from this type of laser (typically 100 μJ/pulse) a dye amplifier was employed in the Caesium work. For this work, 2 cm long Quartz dye cells were used. The optically pumped region of the cell was arranged to match the size and direction of the beam entering the cell from the dye laser oscillator. The dye concentration was adjusted to give optimum performance measured in terms of output beam quality and pulse energy. Inevitably some compromise has to be made and usually high beam quality took preference.

The quality of the beam leaving a laser can be determined by comparing the far field diffraction spread of the beam to that expected from diffraction theory. If a Gaussian beam is focused by a lens and its focal spot-size (w_o) measured, the far field diffraction limited spread of the beam will be $\lambda/\pi w_o$. A high quality beam will have a divergence close to this. In the case of the high energy blue dye laser, the beam spread was typically 1.2 and 1.4 times the diffraction limited value in the vertical and horizontal directions respectively. When such a high quality beam is focused into a vapour cell, the spatial variation of intensity along the cell is known quite accurately; for beams which are not diffraction limited, this knowledge cannot be assumed.

4.2 Metal Vapour Containment - Operation of Heat-pipe Ovens

In this work, metal vapour columns with lengths of about 30 to 100 cm were required. The simplest method of achieving this is to use a 'heat-pipe' oven of the type described by Vidal and Cooper (1969). This kind of oven has been widely used in the laser and nonlinear optics fields as a method of obtaining long vapour columns

of high homogeneity and optical quality. The ovens used in this work will be described in later sections.

The principle of operation is simple. A typical heat-pipe oven (see Figure 4.3) consists of a stainless steel tube of length 60 cm and internal diameter of around 3 cm. A stainless steel mesh forms a wick in contact with the inside wall of the tube and is soaked in the metal required as a vapour. Optical windows suited to the particular wavelength regions to be studied are mounted with O-ring seals on flanges at both ends of the tube. These are kept cool by cooling coils or fins mounted near the flanges.

In operation, the system is first evacuated, flushed with inert gas and then filled with inert gas to a pressure of a few torr. The choice of fill pressure will be discussed shortly. Power is supplied to a heater mounted centrally around the pipe and this causes metal in the heated region of the wick to melt and finally evaporate. Vapour moving toward the windows does so until it is cooled sufficiently by the inert buffer gas to condense on the walls of the tube. Still molten the metal returns to the heated central region of the wick by capillary action. With sufficient heat input a steady column of length nearly equal to the distance between the cooling coils can be set up. The question of minimum power required for such an oven to function is the subject of the work of Melton and Wine (1980).

To calculate the required inert gas 'cold fill' pressure for a given hot vapour pressure, the ideal gas laws can be invoked. After turning on the heater, a vapour column of volume V_{vc} pushes the buffer gas into the rest of the system; the entire system has volume V_s. As the temperature of the buffer gas remains essentially constant over most of its volume, Boyle's Law gives

$$\frac{p_H}{p_C} = \frac{V_s + V_{vc}}{V_s} = 1 + \frac{V_{vc}}{V_s} \qquad (4.1)$$

where p_C and p_H are the cold and heated pipe buffer gas pressures. Of course, the ends of the metal vapour have the same pressure as the buffer gas and so this equation gives the pressure of metal

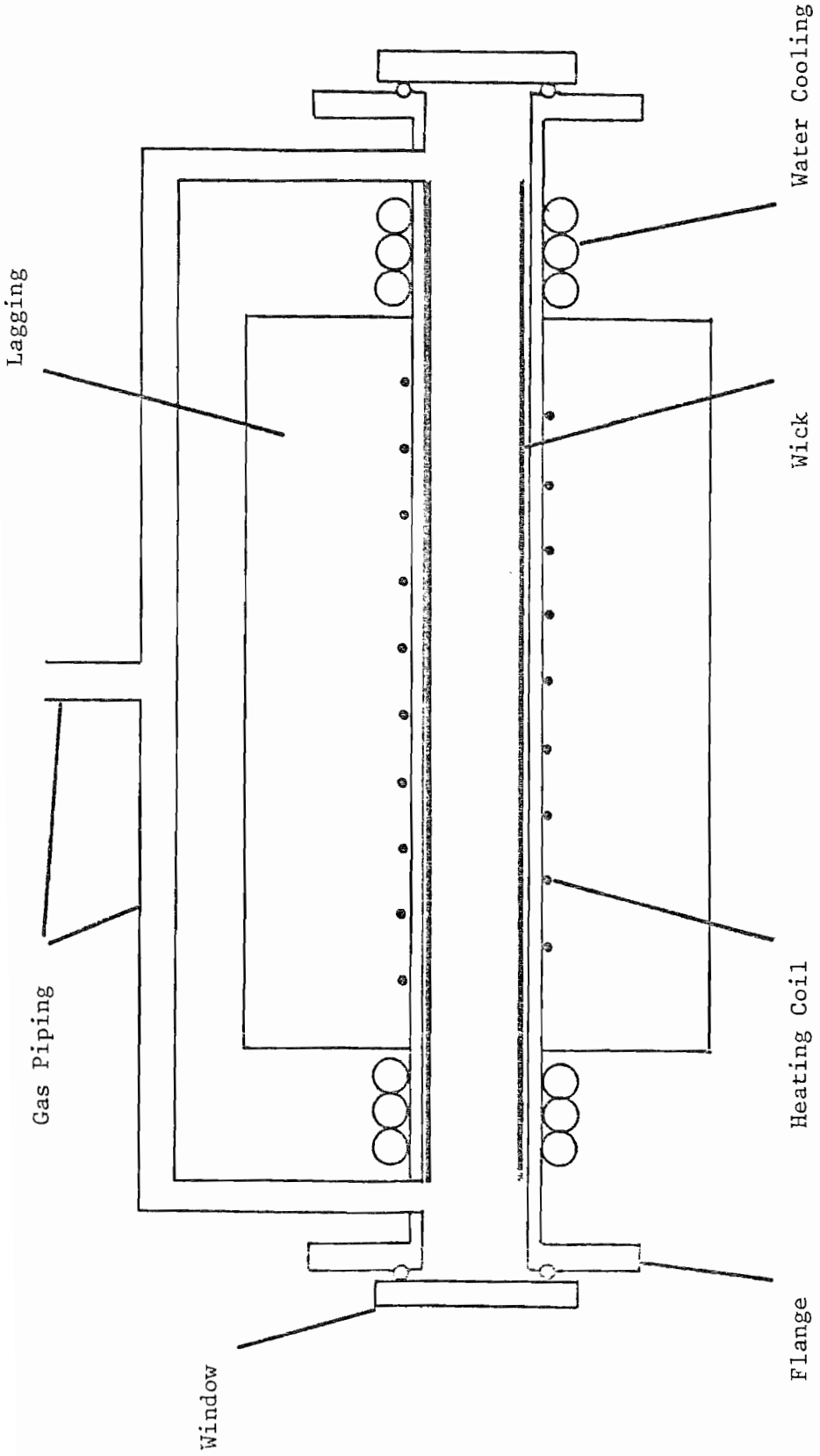

Figure 4.3 Schematic of heat-pipe vapour cell

vapour expected from an ideally operating heat-pipe. (The pressure of the metal vapour in the heated region will be slightly higher to offset the capillary action.)

The choice of buffer gas is limited to gases which have a large thermal conductivity, which allows them to efficiently stop the metal vapour reaching the windows. They must also be inert up to the temperatures typically used in experiments (1100^{o} C). These criteria are satisfied by the noble gases - Helium and Argon being the best and least expensive - and some other gases such as Nitrogen†. However, Helium is not recommended with Caesium heat-pipes as Equation 4.1 is not always satisfied when this gas is used. In fact, after prolonged use of Helium, heated pressures of over five times that predicted have been observed. This makes setting a particular pressure somewhat difficult and unrepeatable. A possible explanation for this phenomenon is that Helium atoms can, in a rigid spheres model, occupy interstitial sites in Caesium; when heated the Helium will be liberated and cause a rise in pressure. However, no data have been found on the solubility of Helium in solid Caesium. Argon, therefore, was used in the experiment described in this thesis. Even this gas is not free from problems. As also noted by Hodgson (1979) Argon, when used as a buffer gas with Caesium, causes particulate dust clouds to form in the cooling regions. This does not have too serious an effect, however, unless excessive power is supplied to the heaters In this case heavily swirling dust clouds appear and particulate Caesium is deposited into the cold regions. These dust clouds scatter light and reduce the transmission of the heat-pipe.

4.3 The Properties of Caesium and Caesium Vapour Cells

The Caesium atom has one valence electron. This gives rise to a relatively simple energy level structure. A term diagram

---

† Although the noble gases were used almost exclusively in this work, Nitrogen was found to give very similar results for SERS in Caesium on the 6s-7s transition. This gas, when admixed with Caesium would quench any atoms in the 6p state and could be used to advantage in some experiments.

for Caesium showing the low lying s, p and d levels is given in Figure 4.4. In addition, the physical properties of Caesium are summarized in Table 4.1. It is a heavy alkali metal with a low melting point, is readily available and relatively cheap in quantities required for the operation of vapour cells (typically a few grams). Being highly reactive, due care must be taken in the choice of material for the cells; for this work grade 306 stainless steel was used for both the heat-pipe tube and the mesh wick.

The Caesium used was supplied in 5 gram ampoules. These were loaded individually into the cell under a continuous flow of Argon gas, the ampoules were then broken using stainless steel rods and the cell was sealed. With a few torr of Argon present, the cells were heated to $\sim 300^{\circ}$ C; the Caesium then distilled out of the ampoule into the wick. Shining a torchlight through the vapour allowed this process to be monitored. Caesium vapour has a characteristic green colour due to its molecular content (see Section 4.4) and gives a good indication that the metal is leaving the ampoule. In addition, the ampoule becomes transparent when empty. When the cell has cooled, the ampoule can be removed under a flow of Argon. For larger cells this filling process may be repeated to ensure the presence of a sufficient quantity of Caesium to completely wet the wick. A rough estimate of the minimum amount of Caesium metal needed can be obtained by multiplying the wick area by its thickness. Making use of the density of Caesium, i.e. 1.87 g cm^{-3} the required weight may be found.

To ensure correct heat-pipe operation in a normal cell, the Caesium must be heated such that its vapour pressure exceeds the buffer gas pressure; the expected heated pressure can be obtained using Equation 4.1 and the cell wall temperature required may be found using the approximate law

$$T = \frac{a}{d - \ln p_H} \qquad (4.2)$$

where p_H is the heated pressure in torr. The values of a and d are given for Caesium in Table 4.1. Heating the exterior of the cell to a temperature slightly in excess of this will increase the Caesium transport rate and the inside wall will become stabilized to the

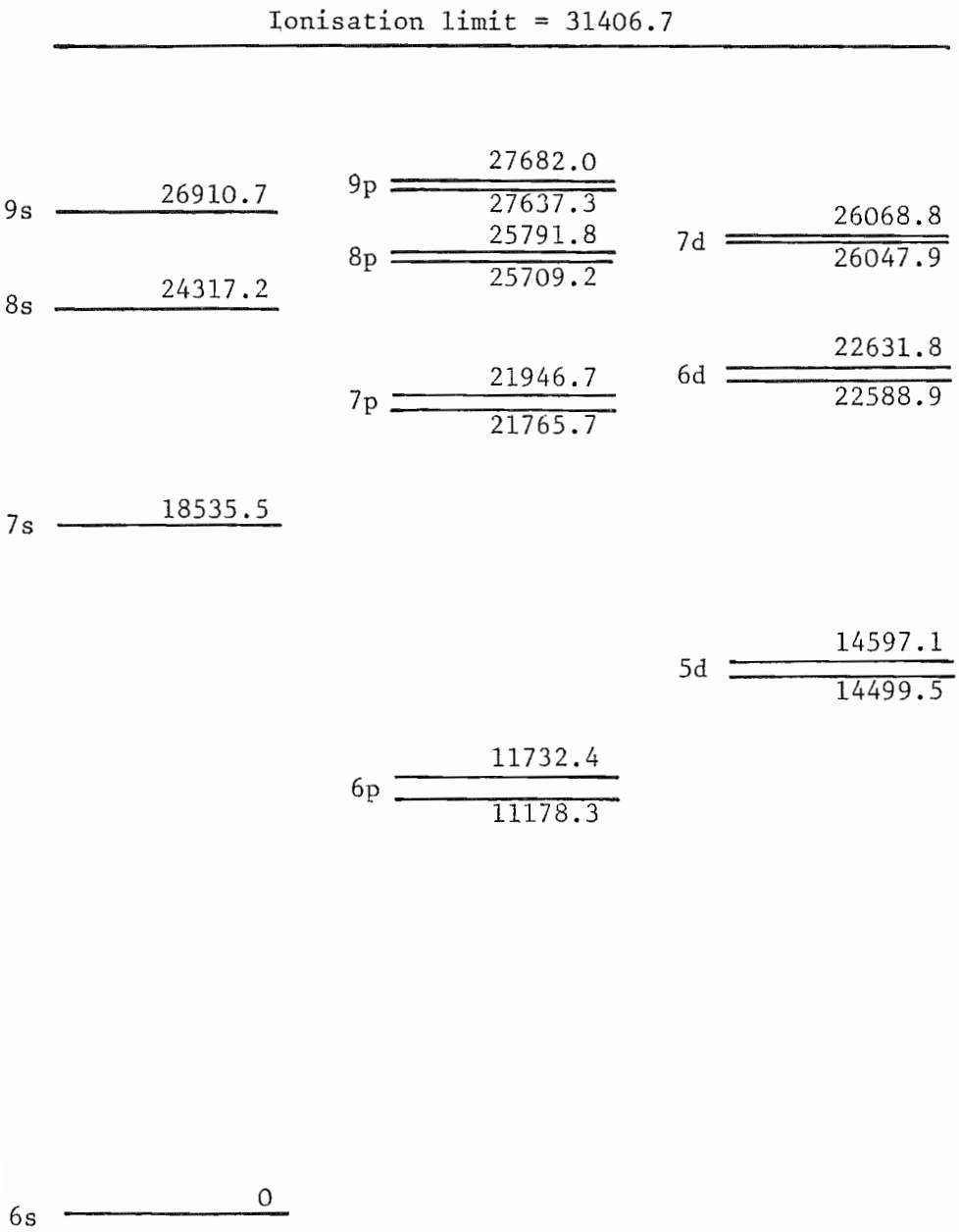

Figure 4.4 Partial term diagram for the Caesium atom (energy in cm^{-1}).

		Caesium	Barium
Atomic Weight		133	137
Ground State		$6s\ ^2S_{\frac{1}{2}}$	$6s^2\ ^1S_o$
Ionization Limit		31407 cm^{-1}	42032 cm^{-1}
Melting Point		28° C	729° C
Vapour Pressure Constants	a	8827 K	21414 K
	d	16.0	16.8
Temperature for 10 torr		373° C	1203° C
Oscillator strength data		Warner (1968)	Miles and Wiese (1969) Friedrich and Trefftz (1966)
Radial matrix element data		Eicher (1975)	-
Energy level data		Moore (1958)	Moore (1958) Friedrich and Trefftz (1966)

Table 4.1

required temperature. The saturated number density (cm^{-3}) of Caesium is given in terms of p_H as

$$N = 9.66 \times 10 \quad \frac{p_H}{T} \tag{4.3}$$

and is shown as a function of temperature in Figure 4.5.
Figure 4.5 shows the saturated number density law for Caesium dimer molecules. These are always present in Caesium vapour, as up to ∿5% of the vapour, and give rise to its green colouration in transmission. As will be seen in Chapter 6, their presence is detrimental to nonlinear optical processes in Caesium vapour.

In this work three cells were used. Two of these operated in the normal heat-pipe mode described in Section 4.2 and had heated lengths of 30 cm and 100 cm†. In an attempt to alleviate the problems arising from high dimer concentration, a third superheated cell was constructed from high temperature stainless steel type 310. The central 90 cm of the cell lacked a wick and so no liquid Caesium was present. Short wicks near the ends of the lagged region contained the metal. When heated, Caesium circulated in these two regions and diffused into the centre becoming heated to around 900° C. This cell is shown in Figure 4.6. The power input required for correct operation of this cell has been calculated by Smith (1982) and lies between 2 kW and 4 kW.

Heating of the cell was performed, unlike for the other heat-pipes, by direct resistive heating of the cell wall. Tight fitting stainless steel contacts were clamped around the stainless steel tube near the water cooling coils. A good electrical connection between these contacts and the cell tube was ensured by cleaning the touching surfaces with emery cloth and then sandwiching a piece of Copper foil between the tube and the contacts. At elevated temperatures the more rapid expansion of Copper led to an improvement in the electrical contact. Earlier attempts using brass clamps without foil failed as the contact resistance increased with increasing temperature, leading to a large fraction of the power being dissipated into the contacts. This thermal runaway was not present in the final design.

---

† For the 30cm cell air cooling fins were used in place of water cooling coils.

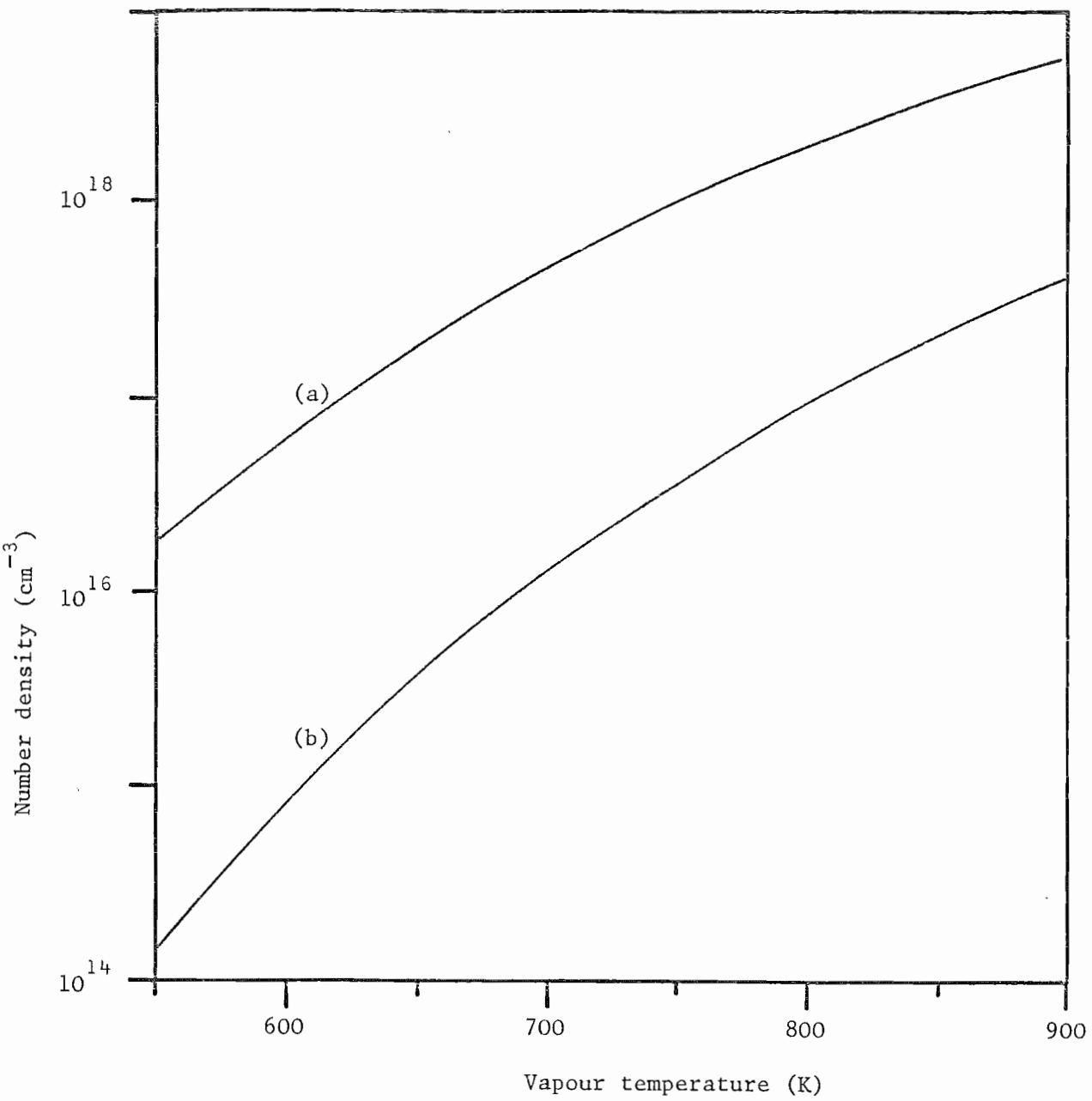

Figure 4.5 Saturated number density of Caesium and Caesium molecules

(a) Cs (b) Cs_2

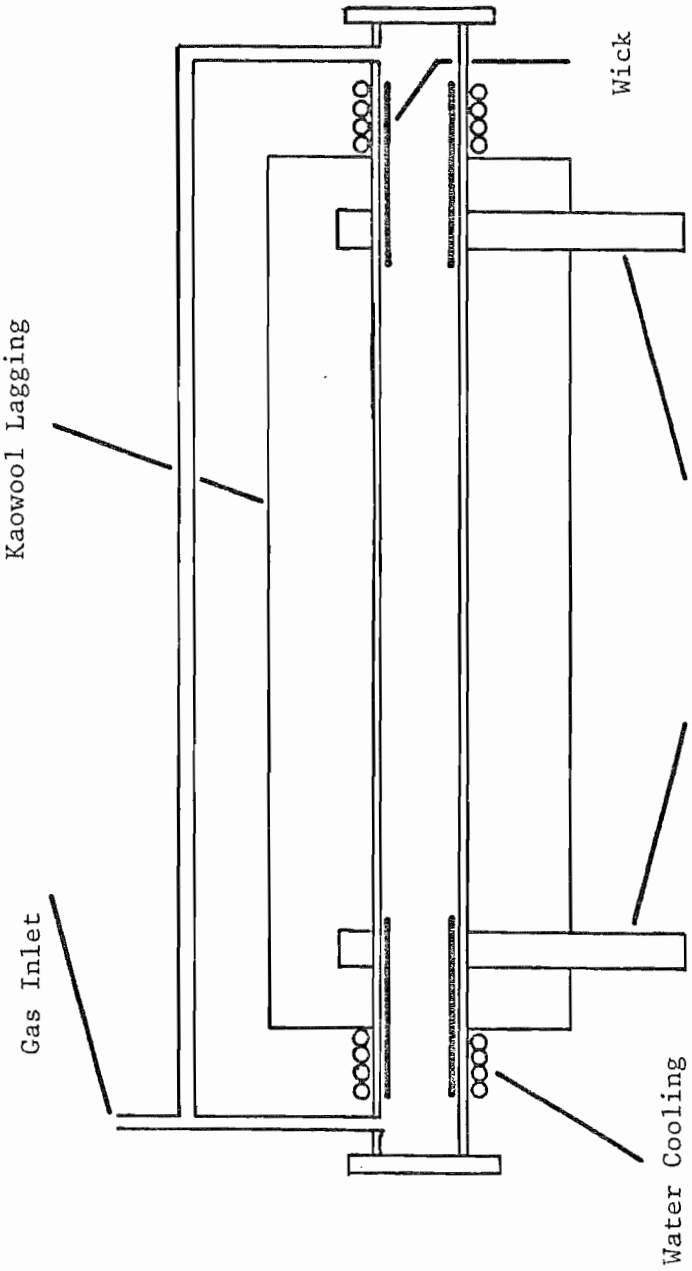

Figure 4.6 Schematic of superheated split-wick vapour cell

Figure 4.7 shows $N_D\ p_v^{-2}$, where N_D is the dimer number density (cm^{-3}) and p_v is the total vapour pressure in torr. For increasing temperature the dimer density decreases for a given Caesium pressure. A reduction in dimer density in the centre of the superheated cell is therefore obtained. However, this is also accompanied by a reduction in the number density of atomic Caesium in this region. By considering the ideal gas law it is easily seen that (for temperatures above the boiling point) the atomic Caesium number density will be inversely proportional to the absolute temperature of this central region. The choice of materials for this vapour cell are described by Smith (1982), who has also performed a detailed numerical analysis of its operation.

4.4 Caesium Dimer Properties

In this last section, the presence of a significant number density of dimer molecules in Caesium vapour was mentioned. Their importance arises from the absorption bands they exhibit throughout the visible and near-infrared and the detrimental effects these have on SERS processes.

Figure 4.8 shows the variation of the absorption cross-section over the wavelength ranges of interest in this work. Several bands are of particular importance. On the 6s-7s Raman transition, long wavelength production is hindered by absorption to the $E\ ^2\Pi_u$ excited molecular state. For SERS on the 6s-5d transition, absorption by the bands lying to either side of 530 nm will cause pump depletion. In addition, the longer wavelength band is dissociative and excitation of the molecule in this band results in the production of a ground state and an excited state (5d) atom. The 6s-5d Raman experiments detailed in Chapter 6 neglect the presence of dimer molecules as the absorption of 532 nm light is very small. In extending this work to longer wavelengths, account will have to be taken of the increasing attenuation and other competing effects arising from dimer absorption.

In the laser bleaching studies of Section 6.2, a Nd:YAG laser was used to excite the molecular species. For reference,

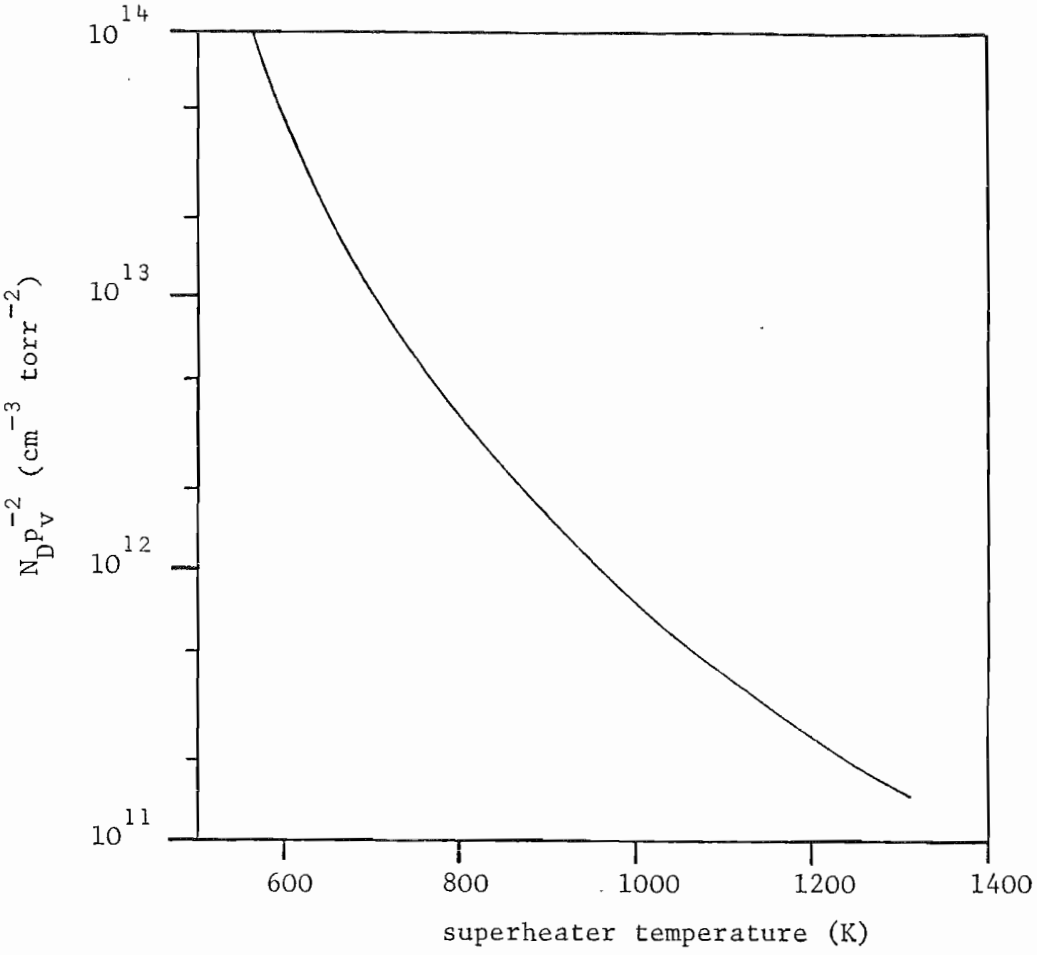

Figure 4.7 The dependence of Caesium dimer number density upon superheating temperature.

To obtain number density multiply $N_D p_v^{-2}$ by the square of the vapour pressure.

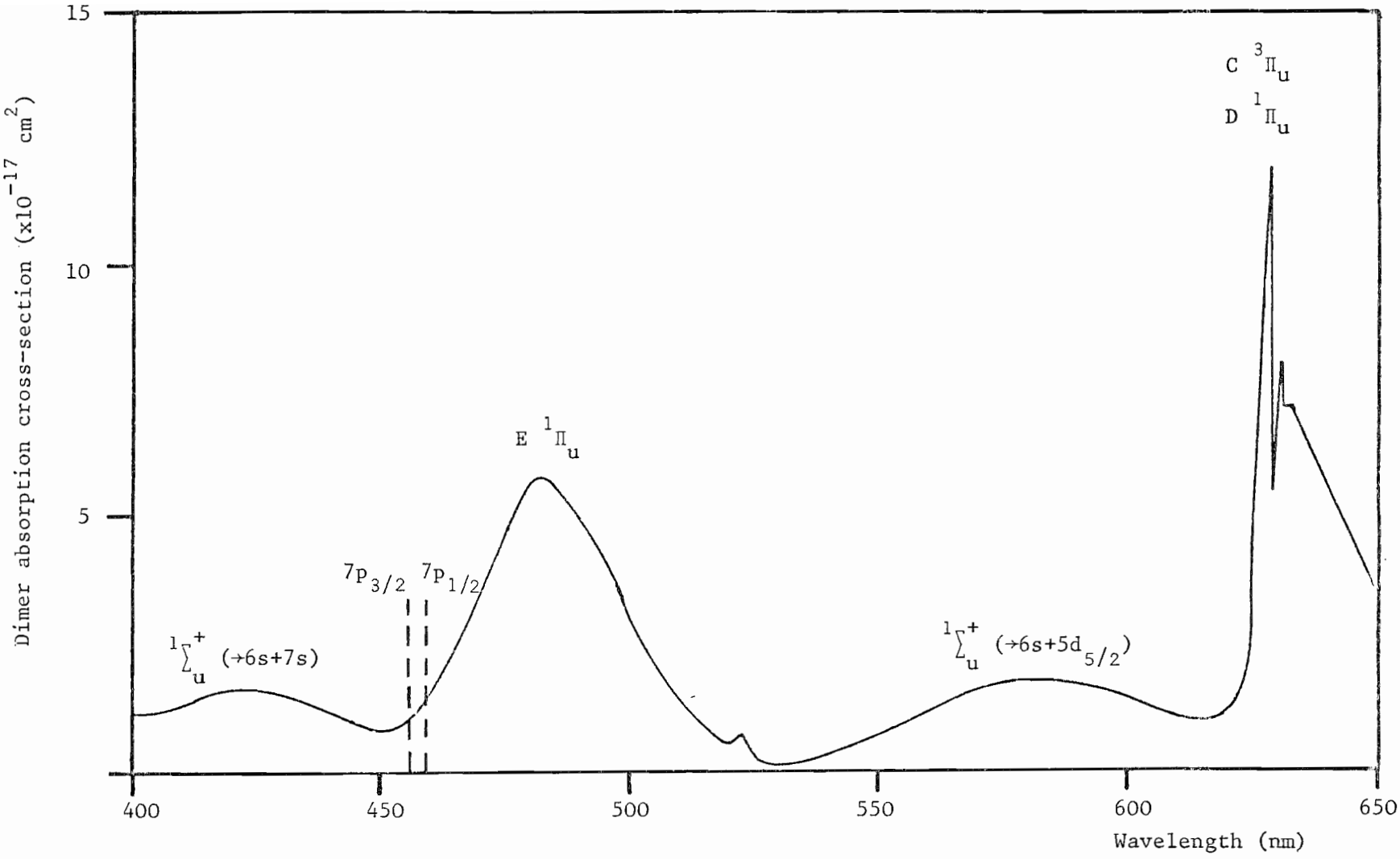

Figure 4.8a Caesium dimer absorption cross-section
(Dissociative states marked with dissociation products)

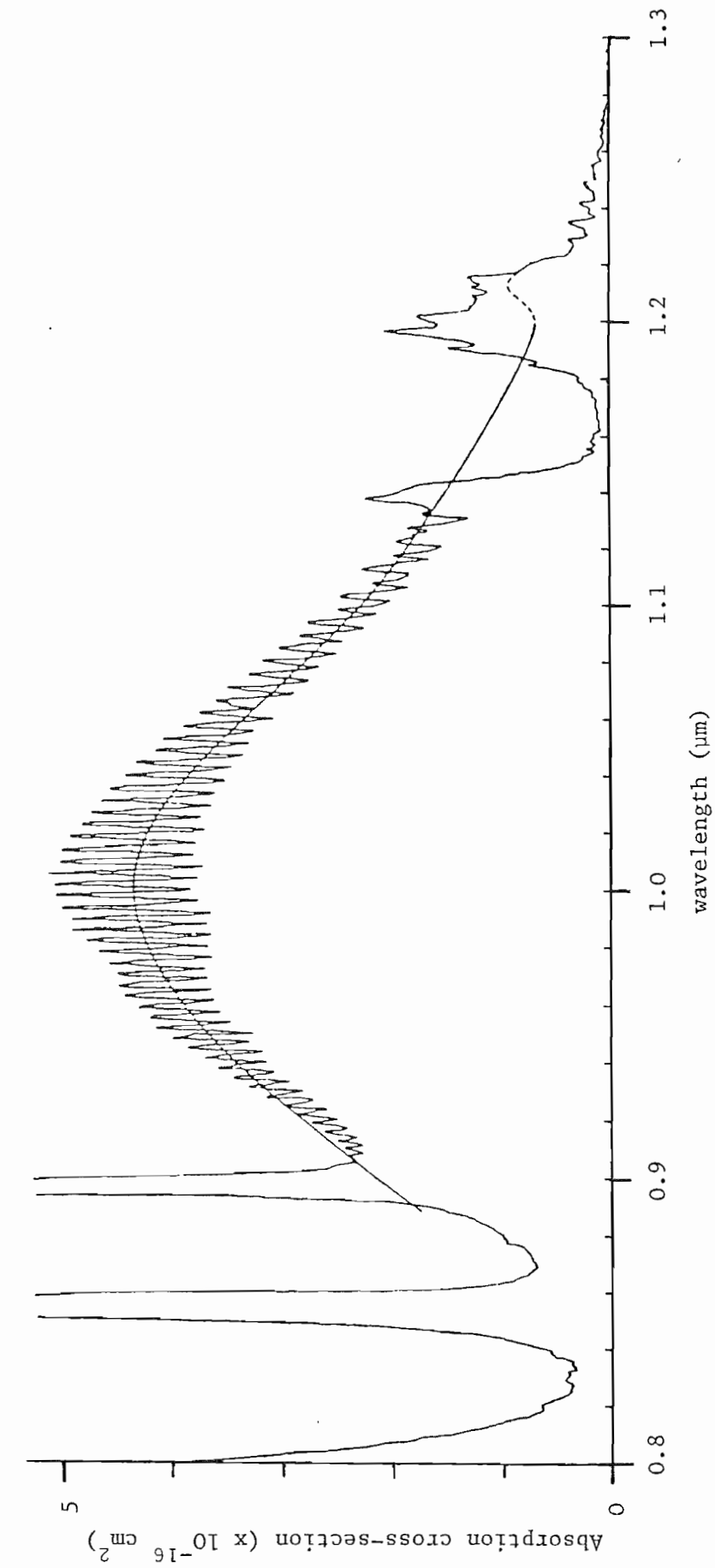

Figure 4.8b Caesium dimer absorption cross-section. (Data deduced from Benedict et al (1977).)

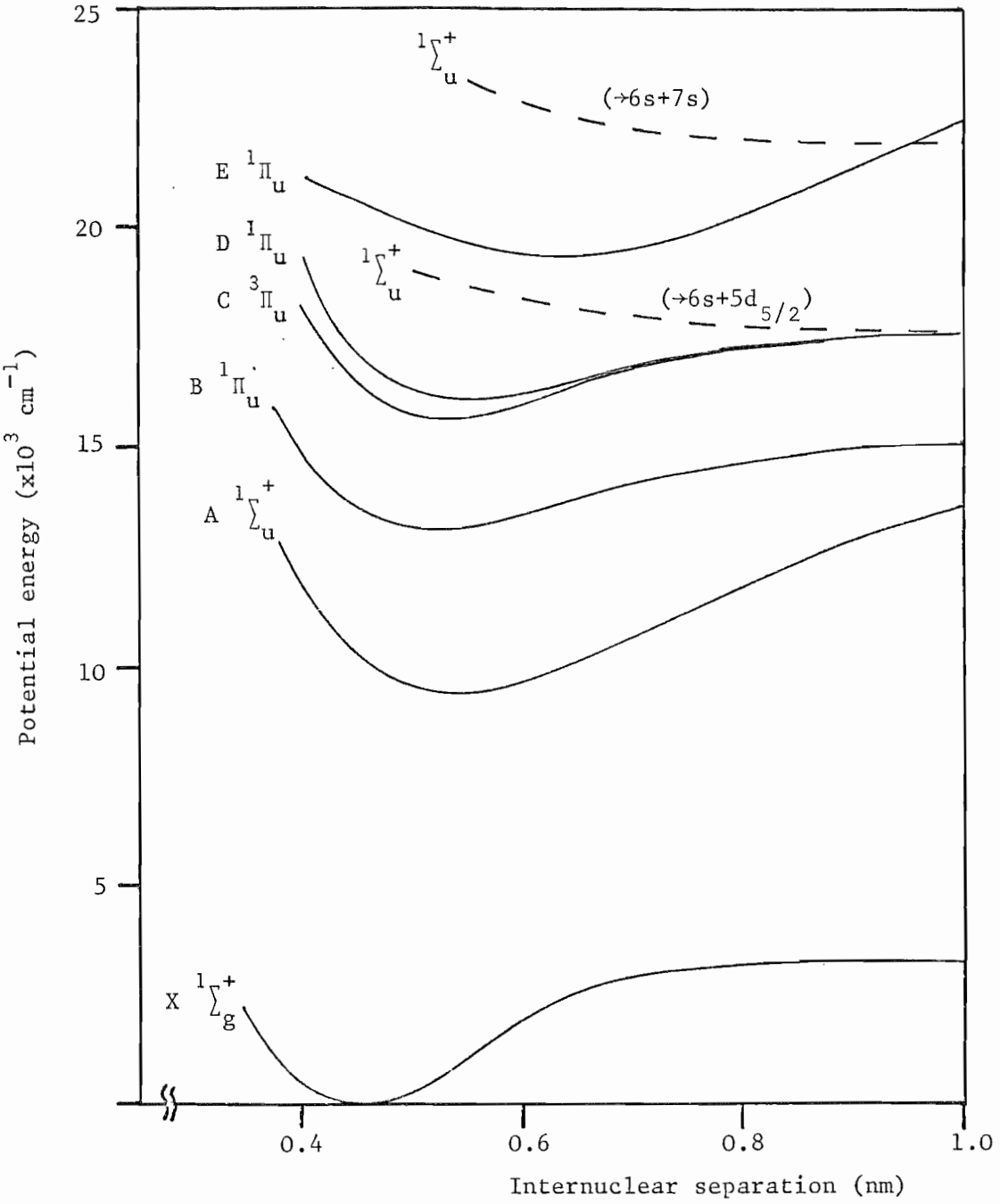

Figure 4.8c Partial potential curves for the Caesium dimer molecule showing states connected to the ground state by single photon transitions.

details of the absorption of Caesium vapour around 1 μm are included in Figure 4.8. Beyond 1.3 μm there is no molecular absorption, although high pressure (> 100 torr) studies have shown small polymeric absorption out to at least 2 μm (Zouboulis et al (1980)). For the pressures used in the work described here, this will give rise to negligible Stokes absorption.

4.5 The Properties of Barium and the Barium Vapour Cell

Barium, like Caesium, has relatively low lying excited electronic states. As this element has two valence electrons, the structure of these levels is rich and offers many possible resonant routes for the investigation of nonlinear optical effects. A partial term diagram for Barium is shown in Figure 4.9. In this work only transitions between singlet states are considered, although other works mentioned in Chapter 5 are concerned with singlet-triplet transitions.

Barium is a slightly reactive alkaline earth metal with a moderately high melting point. Unlike Caesium, the temperatures required for a few torr of vapour are in excess of 1000^{o} C and so Barium requires special materials in the construction of vapour cells. Heat-pipes were constructed of stainless steel grade 310, lagged with a 15 cm thickness of Kaowool silica fibre wool. Power was applied to the central 30 cm of the stainless steel tube using a coil of Kanthal A resistance wire wound beneath this lagging. This heater was insulated from the metal of the heat-pipe by a single turn of woven silica cloth (Refrasil C1400).

The vapour pressure data for Barium used in this work are those given by Schins et al (1977) and are presented in Table 4.1. However, large discrepancies exist in the information available in the literature; the reader is referred to the assembled data contained in Karmyshin et al (1974). In order to calculate the required inert gas fill pressure and the minimum heat-pipe wall operating temperature Equations 4.1 and 4.2 can be used just as for Caesium. Unlike Caesium, Barium vapour does not contain dimer molecules at these low pressures. In fact the observations of Djeu and Burnham (1977)

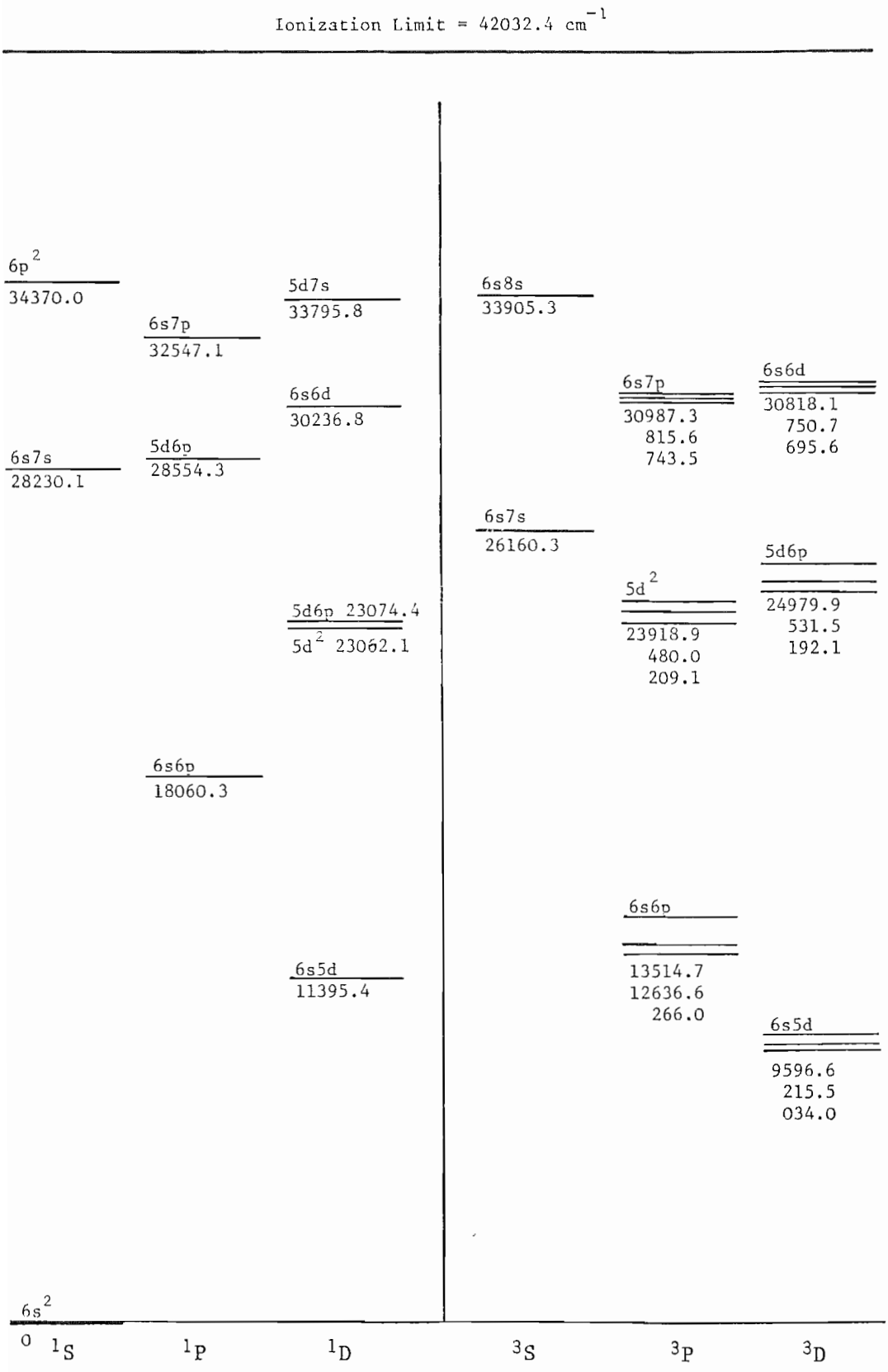

Figure 4.9 Partial term diagram of the Barium atom (energy in cm^{-1}).

suggest that for Barium pressures of over 10 torr significant formation of particles takes place. This leads to a neutral density scattering of light passing through the vapour. However, this may be due to unstable operation of their vapour cell. In view of the poor reliability of the Barium vapour pressure data, a calculation of the required temperature should only be used as a rough estimate and the minimum operating temperature should be determined by monitoring the total heat-pipe pressure.

Barium was obtained in the form of rods which were stored under oil. To avoid contamination of the heat-pipe the material was cleaned. After using a hacksaw to slice off the required fill of the metal (10 to 20 grams), the Barium was degreased with either Trichloroethylene or Acetone and then left in water to effervesce for a few minutes. The Barium was once more immersed in Acetone then dried and inserted into the cell. In operation a slow loss of metal to the cold regions of the wick was inevitable. The procedure above was repeated with smaller quantities of Barium at intervals of around 14 days to ensure a sufficient supply of the metal in the central portion of the wick. In addition, solid Barium built up at the edge of the cold regions reducing the available aperture of the vapour cell. It was found to be convenient to replenish the metal at the same time as the cell was opened to push this build-up back into the heated region.

As for the superheated Caesium oven, the high temperatures required for a Barium cell inevitably cause distortion of the cell shape. Improvements in cell design using higher temperature materials such as Titanium are called for. This material, which spontaneously ignites when heated above red heat in air, requires a vacuum or inert gas jacket around it; this can also double up as a primary insulating layer. Alternatively, the same arrangement could be used with a baked, resin impregnated graphite tube. In both cases direct ohmic heating of the cell as employed with the superheated Caesium cell could be used.

CHAPTER 5

SERS and Biharmonic Pumping in Barium Vapour

The use of alkaline earth metal vapours as nonlinear media has several advantages over the use of the alkali metals. Dimer molecules, not evident in the alkaline earth vapours, have absorption bands in the visible and near visible spectral regions and give rise to linear and nonlinear pump laser absorption. Multiphoton ionization of the dimer molecules can lead to significant ion densities during the laser pulse and result in Stark broadening and shifting of the final Raman level. Typically, the Stark shift and linewidth in Caesium vapour can be more than an order of magnitude larger than the Doppler width (Tuttlebee (1977)).

The atomic ionization limits of the alkaline earths are generally higher than those of the alkalis. For example, the ionization limit of Barium is 42032 cm^{-1} whereas for Caesium it is 31406 cm^{-1}. Atomic multiphoton ionization is likely, therefore, to be much less important for the alkaline earths when used in conjunction with visible lasers. Two photons of second harmonic light at 532 nm from a Nd:YAG laser can ionize Caesium, but a three photon process will be involved with Barium. Again, excessive Stark broadening is less likely to take place in the alkaline earths.

Wyatt (1976) considered line broadening of the 4s-5s transition in Potassium caused by amplified spontaneous emission from the final Raman level to the lower 4p state. The reduction in the lifetime of the population in the 5s state, it was concluded, can lead to a linewidth much larger than the Doppler width. The same argument can be applied to all Raman transitions in the alkalis - there is always a strong dipole allowed transition between the final Raman level and a lower level.

This is not true, however, of the alkaline earths (see, for example, Figure 4.9). The lowest lying excited singlet state in

the alkaline earths is a ^1D state, which is therefore metastable as well as being a candidate for the final Raman level. The corresponding lowest triplet state is a ^3D, again metastable and again a possible upper Raman level. For SERS in Barium using either of these states as an upper state, lifetime broadening can be neglected.

In Section 2.3 contributions to the linewidth arising from collision broadening were considered for Caesium. A broadening coefficient γ_c of 10^{-18} cm^{-1} $(cm^{-3})^{-1}$ was found to be appropriate for the $6s-5d_{5/2}$ Raman transition. Such a large value leads to a linewidth of 0.15 cm^{-1} at 10 torr. For Barium a smaller value of the broadening coefficient should be used, as the lack of dimer molecules would suggest a relatively shallow ground state potential curve. Even so, the Doppler width of the transition is only just matched by the collision width if the relevant values of γ_c for Caesium are used together with a Barium pressure of 2 torr. With a more realistic value of γ_c the Doppler width of 0.02 cm^{-1} is expected to dominate over the collision broadened width for the experiments described in this thesis. This expectation is borne out by the threshold measurements described here as well as those of Tuttlebee (1977) on a different transition, the $6s^2\ ^1S-6s5d\ ^3D$.

5.1 SERS in Barium

Barium offers many low lying singlet and triplet levels which can be used to enhance the SERS gain (see Figure 4.9). These are summarized in the following table:

Intermediate level		Transition wavelength	
Singlets:	$6s6p\ ^1P$	553 nm	(This work)
	$5d6p\ ^1P$	350 nm	(Djeu and Burnham, This work)
	$6s7p\ ^1P$	307 nm	(Burnham and Djeu, Cotter and Zapka)
Triplets:	$6s6p\ ^3P$	790 nm	(Carlston and Dunn, Tuttlebee)
	$5d^2\ ^3P$	426 nm	
	$6s7p\ ^3P$	325 nm	

The lowest lying triplet resonance was exploited by Carlston and Dunn (1975) and Tuttlebee (1977) to generate tunable infrared radiation on the $6s^2\ ^1S_o$-$6s5d\ ^3D_1$ and $^3D_2$. The Raman gain is larger for the $^3D_2$ final level and this transition allowed 130 cm^{-1} continuous tuning around 2.9 μm.

Singlet-singlet $6s^2$-6s5d Raman transitions have been studied using excimer lasers. Cotter and Zapka (1978) and Burnham and Djeu (1978) independently observed low thresholds for Raman scattering of XeCl radiation at 308 nm to its Stokes wavelength (475 nm) with photon conversion efficiencies of up to 31%. Djeu and Burnham (1977) also achieved 80% conversion of 351 nm XeF radiation to its Stokes wavelength using the $5d6p\ ^1P_1$ enhancing level.

The results obtained for the schemes above show good agreement with theoretical predictions of the Raman gain using the Doppler width for the Raman transition linewidth. This is in contrast to results in the alkalis. Here Wyatt (1976) and Cotter (1976) found that the measured threshold powers for their experiments in Caesium corresponded to an assumed Raman linewidth of around 1 cm^{-1}. This is nearly two orders of magnitude larger than the Doppler width, in agreement with the ideas of Section 2.3 where the effect of collision broadening is considered.

No use of the $6s6p\ ^1P_1$ level for intermediate resonance has been reported, although the equivalent route in Strontium has been studied by Wynne and Sorokin (1977) and Tuttlebee (1977). Their failure to reach Raman threshold on this transition, the $5s^2$-$5s4d\ ^1D_2$, was attributed to single photon absorption of the 460 nm pump laser. Tuttlebee used Equation 2.8 to calculate that, for the 500 kW dye laser used, an absorption limited maximum Stokes gain of exp(15) could be expected from 10 torr of Strontium vapour. The use of the transition in Barium, however, is not precluded by this. Using the oscillator strengths for Barium given by Miles and Wiese (1968) and taking a Barium pressure of 2 torr, a gain of exp(8000) at 1.35 μm is predicted for a 500 kW laser at 532 nm focused confocally into the vapour. Of course, the second harmonic light from a Nd:YAG is of fixed frequency. By using a dye laser pumped by this light, the Stokes wavelength will be further into the infrared.

At first sight, SERS in Barium on the $6s^2\ ^1S_o$ to $6s5d\ ^3D_2$ transition offers the possibility of highly efficient generation of tunable infrared radiation.

5.1.1 Calculation of the Expected Threshold Powers

In this section, the Raman gain coefficients relevant to SERS from 355 nm and from 532 nm are calculated. From these results, predictions of the required pump laser power to exceed Raman threshold at these wavelengths are made.

For a Raman scheme with one dominant intermediate level, and with a D level as the final level, the Raman gain is given by Equation 2.5 as

$$g_R = \frac{4\pi^2 r_e^2 c^2 N \omega_s}{\hbar \Gamma_R} \cdot \frac{f_{fi} f_{ig}}{\Omega_{if} \Omega_{ig}} \cdot \frac{1}{(\Omega_{ig} - \omega_p)^2} \qquad (5.1)$$

Substituting suitable values for the transition frequencies and oscillator strengths (Miles and Weise (1969))†, taking Γ_R as the Doppler width of the transition $\Gamma_R = \Gamma_D = 0.012\ cm^{-1}$, and $N = 1.5 \times 10^{16}\ cm^{-3}$ (which corresponds to approximately 2 torr) we obtain for the two cases

$$g_R(355\ nm) = 3.5 \times 10^{-9}\ m/W$$

$$g_R(532\ nm) = 4.6 \times 10^{-9}\ m/W$$

These values in conjunction with Equation 2.12 give threshold powers of

$$P_{th}(355\ nm) = 1.8\ kW$$

$$P_{th}(532\ nm) = 2.25\ kW$$

---

† In the data for Miles and Weise (1969) there is a typographical error. The wavenumber of the $6s^2\ ^1S_o$ - $6s6p\ ^1P_1$ transition is 18060.3 cm^{-1} and not 18080.3 cm^{-1} as stated therein.

where confocal focusing has been assumed. For 15 ns long, fast Q-switched pulses where the bandwidth ($\sim$0.3 cm^{-1}) is much larger than the Raman transition linewidth Γ_R, these powers correspond to pulse energies of

$$E_p(355\ nm) = 27\ \mu J$$

$$E_p(532\ nm) = 34\ \mu J$$

Raman threshold should, therefore, be readily exceeded by the 3 mJ of 355 nm and 20 mJ of 532 nm light available from a 160 mJ Nd:YAG laser system.

5.1.2 Single Photon Absorption at 532 nm

Failure to reach Raman threshold on the $5s^2\ ^1S_o - 5s4d\ ^1D_2$ Raman transitions in Strontium was considered (Tuttlebee (1977)) to be caused by absorption of the pump laser radiation on the $5s^2\ ^1S_o - 5s5p\ ^1P_1$ principal line. In order to see whether this would also be the case in Barium, the absorption coefficient $\beta(m^{-1})$ at 532 nm can be calculated using Equation 2.6b. The linewidth Γ_i of the upper state can be taken as resonance broadened as this is the largest of the natural, Doppler and resonance broadened linewidths. Γ_i is dependent on the atomic number density N, and in the case of $^1S_o - ^1P_1$ transitions, is given by Equation 2.7 as

$$\Gamma_i = \frac{2\pi r_e c^2 N f_{gi}}{\sqrt{3}\ \Omega_{ig}} \qquad (5.2)$$

Substituting suitable values for f_{gi} and Ω_{ig} from Miles and Weise (1969) and putting $N = 1.5 \times 10^{16}\ cm^{-3}$, we obtain a broadened linewidth of around 0.04 cm^{-1}. This would suggest a value for the absorption coefficient $\beta \simeq 0.04\ m^{-1}$. The absorption length, i.e. the length over which the pump power drops to 1/e of its original value, is therefore, around 25 metres. The same calculation for Strontium at 2 torr and for a detuning of 100 cm^{-1} gives $\beta \simeq 2.7\ m^{-1}$ and so

the absorption length is 36 cm. This is in keeping with the observation of Tuttlebee (1977) that severe pump depletion occurs in passing through a 30 cm column. On the other hand, although no accurate measurements of Barium vapour column transmission were made, it was noted that the 532 nm light passed through the heat-pipe with virtually no attenuation. (From the calculated value of β, the transmission is expected to be roughly $\exp(-\beta\ell) > 98\%$). It is therefore unlikely that SERS of 532 nm light in Barium will be inhibited by single photon absorption as was the case for the use of the principal line of Strontium.

5.2 Experimental Studies of SERS in Barium

5.2.1 SERS of Second Harmonic Radiation

An extensive search was made for the Stokes radiation at 1.35 μm from a frequency doubled Nd:YAG laser (JK lasers system 2000). The laser was operated with either a stable TEM_{oo} resonator, giving up to 1.5mJ of doubled radiation, or with an unstable resonator. The latter has been described by Laycock (1979). Using a 2.5 cm long crystal of type II phasematched KD*P, a reliable 20 mJ of 532 nm radiation could be obtained from the unstable resonator. No attempt was made to select single longitudinal mode operation of either laser resonator at this stage. The peak power available was therefore a few times that calculated from $P_p = E_p/\tau_p$ and would have been of the order of 10 MW†.

The light was focused to the centre of a 30 cm long Barium column contained in the heatpipe described in Chapter 4. The focal spotsize was determined by attenuating the 532 nm light and scanning a specially mounted monochromator slit assembly across the waist of the beam. The measured spotsize was ∿125 μm and so

---

† For N randomly phased independent laser modes of equal field amplitude, the maximum peak power can be N times that expected from a single mode. For random field amplitudes the 'average' peaks are $\sqrt{N}$ times the single mode value. The linewidth of the Nd:YAG laser was ∿0.3 cm^{-1} corresponding to ∿50 modes, and so a peak power of up to 7 times the single mode $P_p = E_p/\tau_p$ is expected.

the light was confocal over 20 cm. The heatpipe was positioned to lie symmetrically about the waist position. After passing through the necessary 1.06 μm rejecting filters, lens and heatpipe input window, the transmission and Fresnel losses reduced the 532 nm power to 65% of that produced in the crystal. The peak power entering the vapour column was therefore ∿6 MW and so a peak focal intensity of around 10 $GWcm^{-2}$ ensued.

Despite varying the input power from zero up to this maximum by making use of neutral density filters in conjunction with tilting the angle of the doubling crystal, no SERS from 532 nm to 1.35 μm could be observed with a photoconductive InSb detector. The noise limited minimum detectable energy at 1.35 μm using this detector was later found to be 0.2 nJ. This negative result was obtained with the laser operating with both the stable and unstable resonators. The experiment was repeated with the light unfocused and with the focusing lens replaced by a 3x reduction telescope. Although the peak intensity of the pulse exceeded that predicted for SERS threshold, threshold could not be reached.

For high focused input energies, the green light was observed to undergo strong defocusing. For a 2 torr vapour pressure, the threshold energy for this process was 5-6 mJ. The onset of this defocusing was accompanied by amplified spontaneous emission at 1.5 μm on the 6s6p $^1P_1$ - 6s5d $^1D_2$ transition. This transition can be pumped either by direct absorption of 532 nm light or by relaxation of highly excited Barium atoms or of Barium ions.

5.2.2 Raman Threshold for 355 nm Light

The $6s^2\ ^1S_o$ - 6s5d $^1D_2$ transition has been studied by Djeu and Burnham (1977) using a XeF excimer laser, achieving a low threshold power and a good ultraviolet to orange conversion efficiency. The wavelength of this laser is 351 nm and is therefore close to that of the third harmonic of the Nd:YAG laser at 355 nm. In the SERS schemes in Figure 5.1, they share the same intermediate enhancing level, the 5d6p $^1P_1$, with the detuning of the XeF laser being ∿10 times less than that of the tripled Nd:YAG. The detuning of the latter is 360 cm^{-1}.

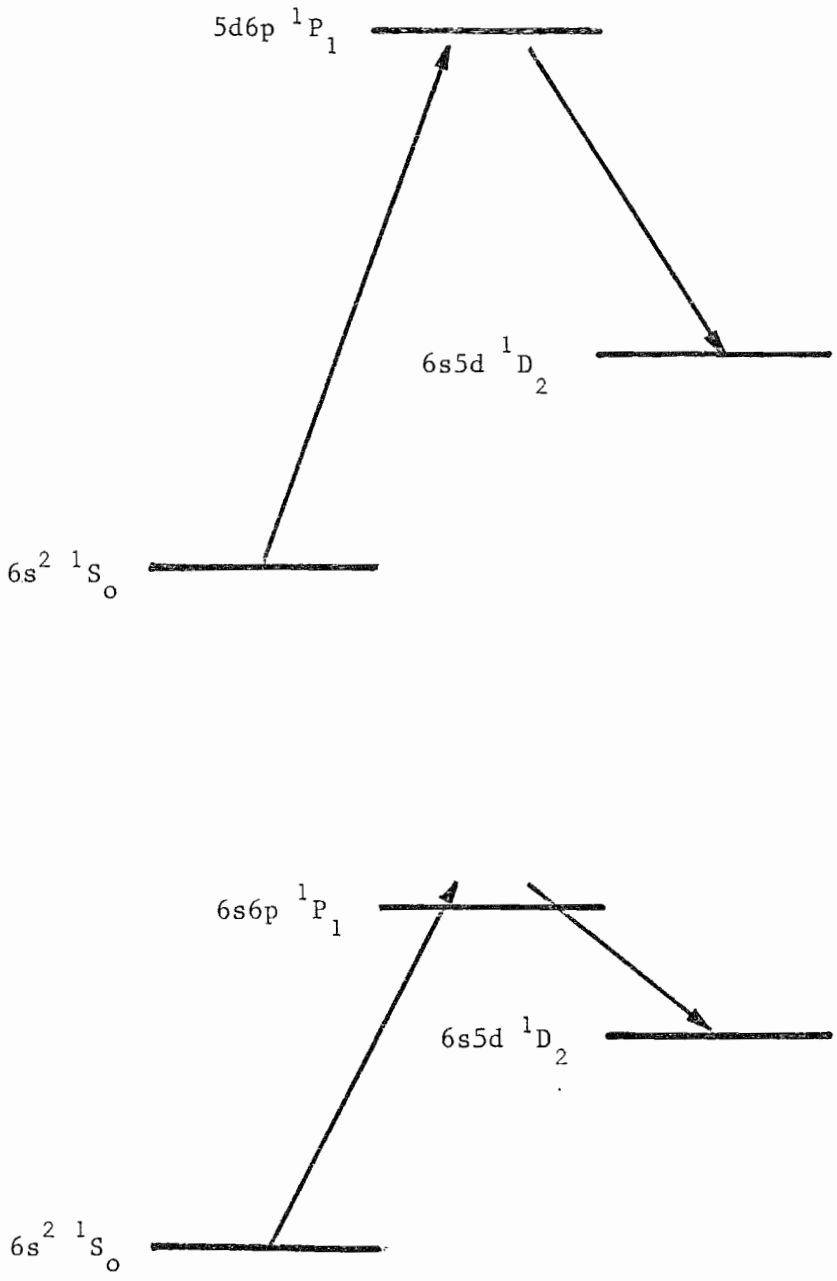

Figure 5.1 The SERS schemes investigated in this work

(a) Pump wavelength near 355 nm

(b) Pump wavelength near 532 nm

A comparison of experimental and theoretical Raman thresholds was made with essentially the same experimental arrangement as used for 532 nm. Ultraviolet 355 nm pulse energies of up to several hundred microjoules were obtained from the TEM_{oo} Nd:YAG laser, by mixing the fundamental and second harmonics in a 2 cm long KD*P crystal. This third harmonic light was then separated from the other frequencies by a combination of dichroic beamsplitters and ultraviolet pass filters. Further filters and a monochromator were used to separate the 596 nm Stokes radiation from any other emissions from the vapour and a photomultiplier tube was used to detect the 596 nm radiation; Raman threshold was measured to correspond to 7.6 μJ of ultraviolet light in a 10 ns long pulse. The light was focused confocally into the heatpipe which was run at a 2 torr Barium pressure. The linewidth of the third harmonic radiation was not measured. No attempt was made to line narrow the fundamental light to below its gain narrowed value of 0.15 cm^{-1}. The linewidth of the 355 nm light was much larger than the Doppler width of the Raman transition (0.015 cm^{-1}). The absence of Barium dimers led to the conclusion in Section 2.3 that this Doppler width is dominant in the Raman transition linewidth. The relative magnitudes of the two widths are such that, to a large extent, the medium sees the power fluctuations of the third harmonic pulse smoothed out, and responds to the average power E_p/τ_p.

The measured threshold power of 760 W compares quite well with the predicted 1.8 kW and therefore justifies the use of the Doppler broadened transition linewidth as the value of Γ_R in the Raman gain calculation. This is unlike earlier calculations of Raman gains for Caesium, where measured thresholds were nearly two orders of magnitude above the thresholds predicted using the Doppler width for Γ_R.

In addition the use of a Doppler limited linewidth is supported by a preliminary direct measurement of the linewidth of the Stokes radiation at 596 nm. A large volume TEM_{oo} mode telescopic resonator of the type described by Sarkies (1979), was used around the 3" by $\frac{1}{4}$" Nd:YAG rod, and contained a telescope of magnification 2.5x. The output radiation was line narrowed to a single longitudinal mode by

slow Q-switching the resonator (Hanna et al (1972), two papers)), and using an internal etalon of thickness 6 mm and reflectivity 65% per surface. Improvements in the design of this type of resonator, together with criteria for selection of single transverse and longitudinal mode operation are given by Hanna et al (1981) and by Sawyers (1981). This laser was frequency doubled in KD^*P and the third harmonic was produced by mixing as for the small mode volume case.

Using an airspaced Fabry-Perot interferometer, a linewidth measurement of the second harmonic 532 nm light was found, as expected, to be instrument limited at 0.013 cm^{-1} (HWHM). The second rather than the third harmonic was measured as the etalon plates had a poor reflectivity in the ultraviolet. The third harmonic 355 nm light can be deduced as having a similar narrow linewidth. The linewidth of the Stokes radiation was also close to the instrument limit, and gave fringes of width 0.015 cm^{-1}. It can be inferred from this that the Stokes radiation is no broader than the Doppler width of the Raman transition. This is in agreement with the conclusion from the threshold measurement that the Raman transition linewidth is dominated by Doppler broadening rather than collision broadening.

5.2.3 Stokes Generation

The observed conversion efficiency to 596 nm is shown in Figure 5.2 as a function of ultraviolet energy into the vapour. Results are presented for a Barium pressure of 2 torr and show pronounced atomic saturation. At high input energies the output energy is limited by the number of atoms in the illuminated volume, as can be seen from the following considerations. The final Raman level is metastable, so any atom that is excited to that level cannot take part in any further Stokes generation (within the time scale of the pulses used in these experiments). For confocal focusing over a 30 cm column, the volume illuminated is 0.02 cm^3 implying that the number of atoms in the beam path is typically a few x 10^{14}. This limits the maximum Stokes energy that can be produced to less than 200 μJ. This is in good agreement with the energy obtained at saturation.

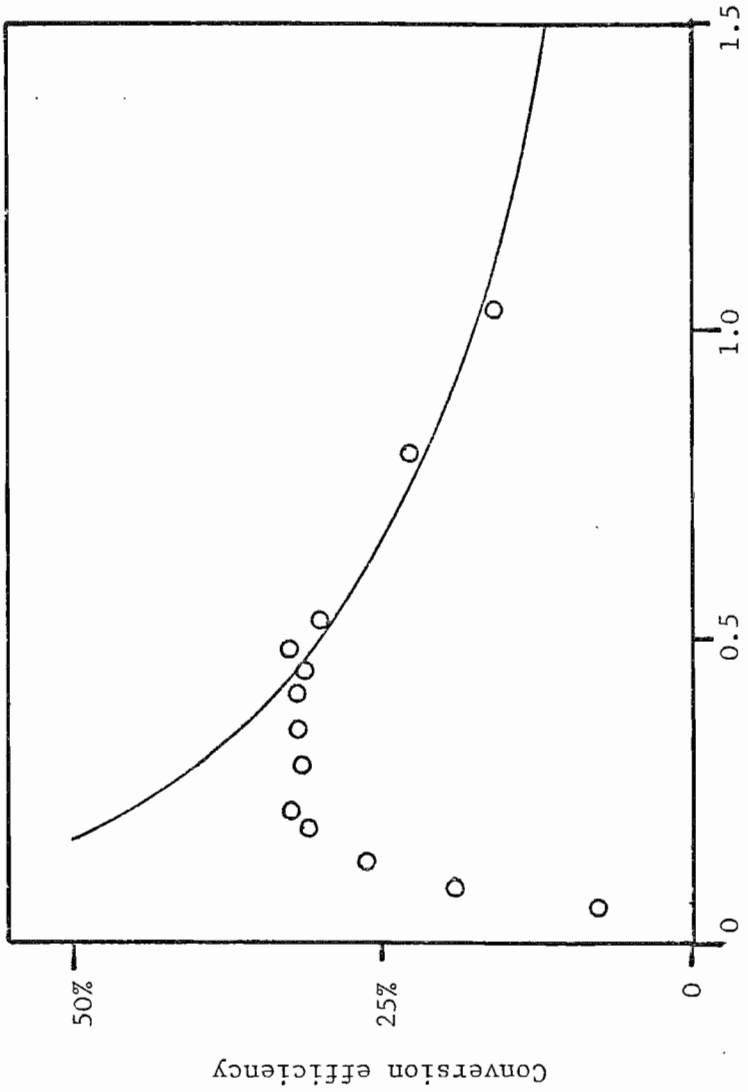

Figure 5.2 SERS in Barium; conversion efficiency from 355 nm to 596 nm showing pump and atomic saturation. (Full curve obtained by considering atomic saturation only.)

Pump saturation occurs when the number of generated Stokes photons approaches the number of pump photons and hence severely depletes the pump laser. In this regime the output energy rises linearly with increasing pump energy, giving constant conversion efficiency for a range of input energies. Figure 5.2 shows this effect on the $6s^2\ ^1S_o - 6s5d\ ^1D_2$ transition.

5.2.4 Parametric Outputs

Apart from the Raman generated light at 596 nm, other outputs generated parametrically are present in the light leaving the Barium heat-pipe. The parametric coupling schemes for the generation of light at the anti-Stokes and second Stokes wavelengths are illustrated in Figure 5.3. In looking at these outputs, the aim was not to characterize their generation but rather to see if their production would inhibit or interfere with other processes. Excessive growth of the second Stokes light would have further reduced the available atomic ground state number density; growth of the anti-Stokes radiation would reduce the available 355 nm light. Either of these processes being efficient could curtail the growth in any intentional nonlinear parametric generation of light.

a) Anti-Stokes of 355 nm

The presence of anti-Stokes light at 252 nm was first detected using a photomultiplier tube. This was placed after ultra-violet pass filters and a monochromator. The unconverted 355 nm light was reduced in intensity by passing the light from the heat-pipe through a cell containing a solution of the dye POPOP in ethanol. To measure the generated energy the beams from the heat-pipe were recollimated using a 50 cm focal length fused silica lens and passed through a silica prism. Using an iris diaphragm to select from the beams dispersed by the prism, the relative energies of the trans-mitted pump and the generated Stokes and anti-Stokes could be observed. The output anti-Stokes energy was measured for a Barium pressure of 2 torr with the input 355 nm energy ranging between 0.5 and 2.7 mJ. The output energy was found to be in linear

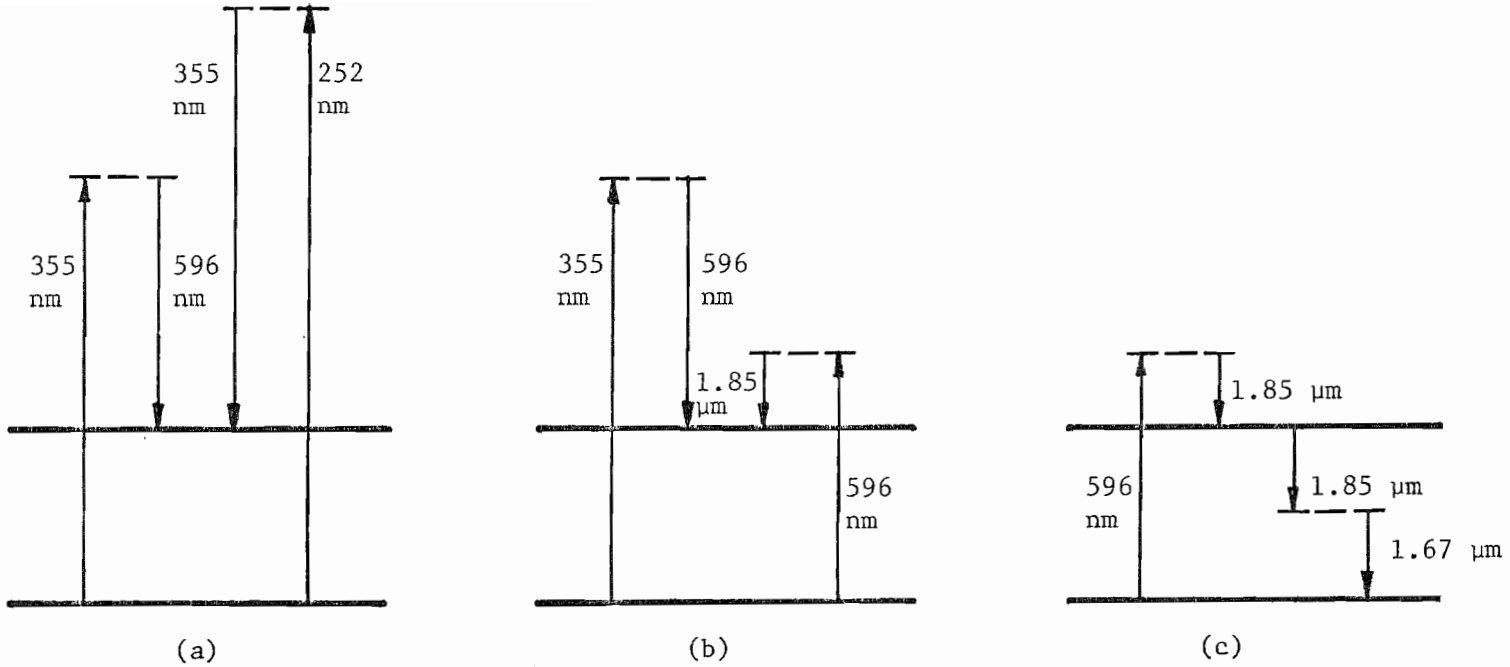

Figure 5.3 Parametric mixing in Barium pumped by 355 nm (see text).

proportion to the input energy and range from 2.6 μJ to 9.6 μJ - an overall conversion efficiency of around 0.3% from 355 nm to 252 nm.

b) Second Stokes

The detection and measurement of the second Stokes radiation at 1.85 μm was performed using a room temperature photoconductive InSb detector. This was calibrated relative to a disc calorimeter (type 14NO). The maximum energy generated at 1.85 μm was 9 nJ corresponding to an orange to infrared conversion efficiency of 4×10^{-3} %. This second Stokes generation is quite negligible on this transition and effectively plays no part in reducing the atomic ground state population. Generation of further Stokes shifted outputs is prohibited by the second Stokes frequency lying below the Raman transition frequency.

c) Difference Frequency Generation on the $6s5d - 6s^2$ transition

Raman resonant difference mixing, also shown in Figure 5.3, allows the generation of 1.67 μm radiation by the interaction of the second Stokes at 1.85 μm with the material excitation (Section 3.1.1). However, due to the low signal level of this second Stokes and the large phase mismatch of this process, $\Delta k = 7.4\ cm^{-1}$, no output at 1.67 μm corresponding to this process was observed. Had this output been efficiently generated, the growth of the second Stokes would have been enhanced since an extra photon at 1.85 μm is produced for each one at 1.67 μm.

5.3 Four Wave Mixing in Barium Vapour

5.3.1 Introduction

Failure to obtain any Raman output from Barium vapour using 532 nm input radiation and the ease with which 355 nm light produced its Stokes radiation, have been the topic of previous sections. These observations led to the examination of four wave parametric interaction as a possible method for generating 1.35 μm radiation.

The steady state theory for this type of interaction, i.e. Biharmonic Pumping, is given in Hanna et al (1979) and is summarised in Chapter 3. Figure 3.1 shows the general Biharmonic interaction and Figure 5.4 details the scheme in Barium for the specific case of the harmonics of the Nd:YAG laser. In terms of the ideas of Chapter 3, the ultraviolet and orange waves set up an excitation in the vapour and the 532 nm wave coupled with this excitation produces a polarization which radiates at 1.35 μm.

The important parameters in this four wave interaction are the phase mismatch Δk and the material ratio R (see Section 3.1.1.) As usual, Δk gives an indication of the difference in phase velocities of the generated wave at 1.35 μm and the polarization wave which is generating it. In Biharmonic Pumping, the waves fall naturally into distinct two photon resonant pairs, ω_1 with ω_{1s} and ω_2 with ω_{2s}. R is a measure of the relative coupling of the excitation in the medium to the waves of the two pairs. The values of these parameters are shown for input radiation at 355 nm and near 532 nm in Figure 5.5. For 532 nm, the values of the parameters are:

$$R = 0.96$$

$$\Delta k = 3.7 \text{ cm}^{-1}$$

The effect of the phase mismatch can be made negligible by ensuring a sufficient ultraviolet input energy - making Equation 3.16 tend to unity. This is true for Δk much less than G_R, the Raman gain per unit length for the orange light, given by $G_R = g_R I_{UV}$.

In principle, the efficiency of conversion from 532 nm to 1.35 μm is just dependent on R. As $R \simeq 1$ the limiting efficiency is given by Equation 3.15 as

$$\eta = \sin^2 \frac{R\pi}{2} = 100\% \qquad (5.3)$$

implying that total conversion from green light to infrared light could be obtained.

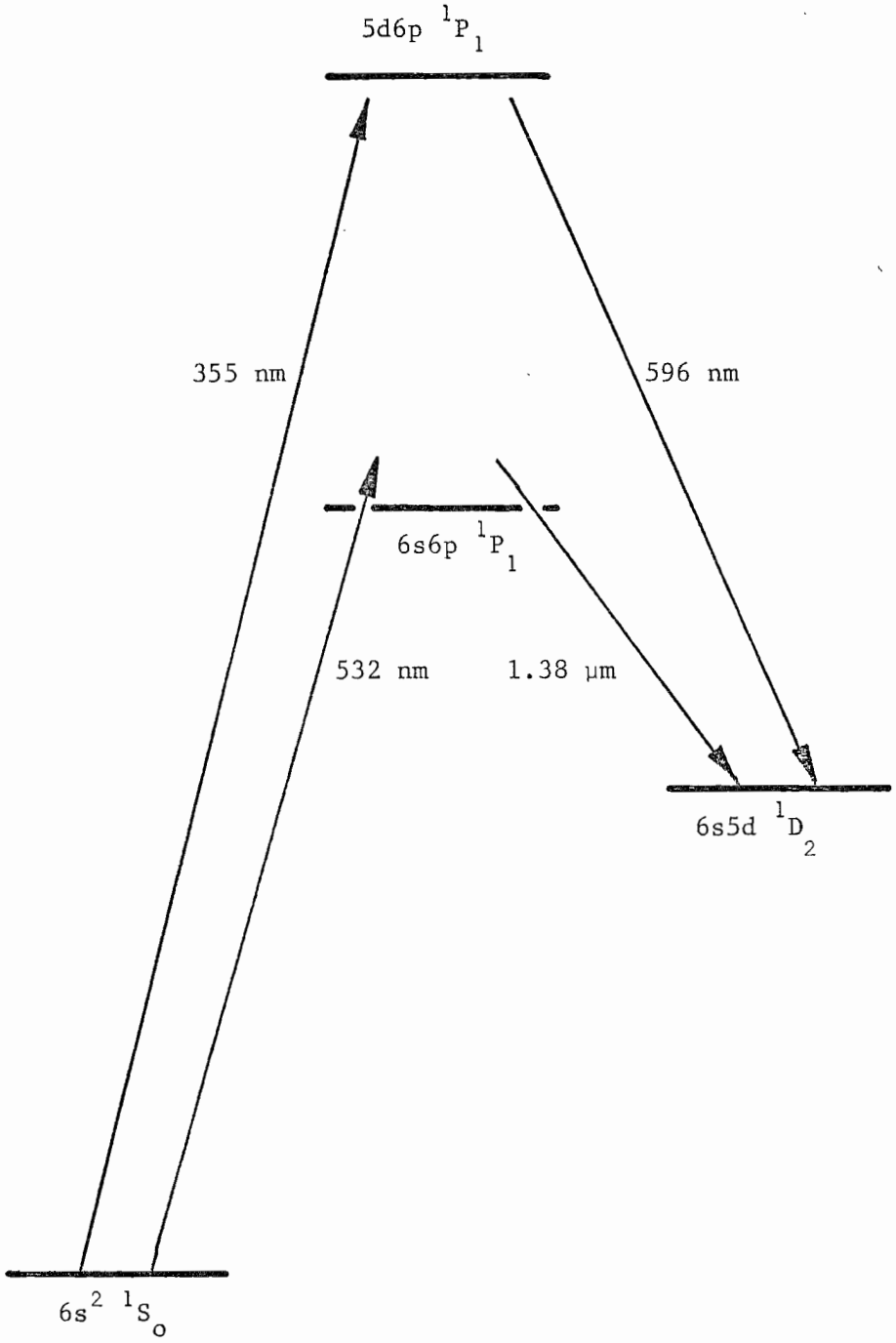

Figure 5.4 Biharmonic pumping in Barium using Nd:YAG harmonics

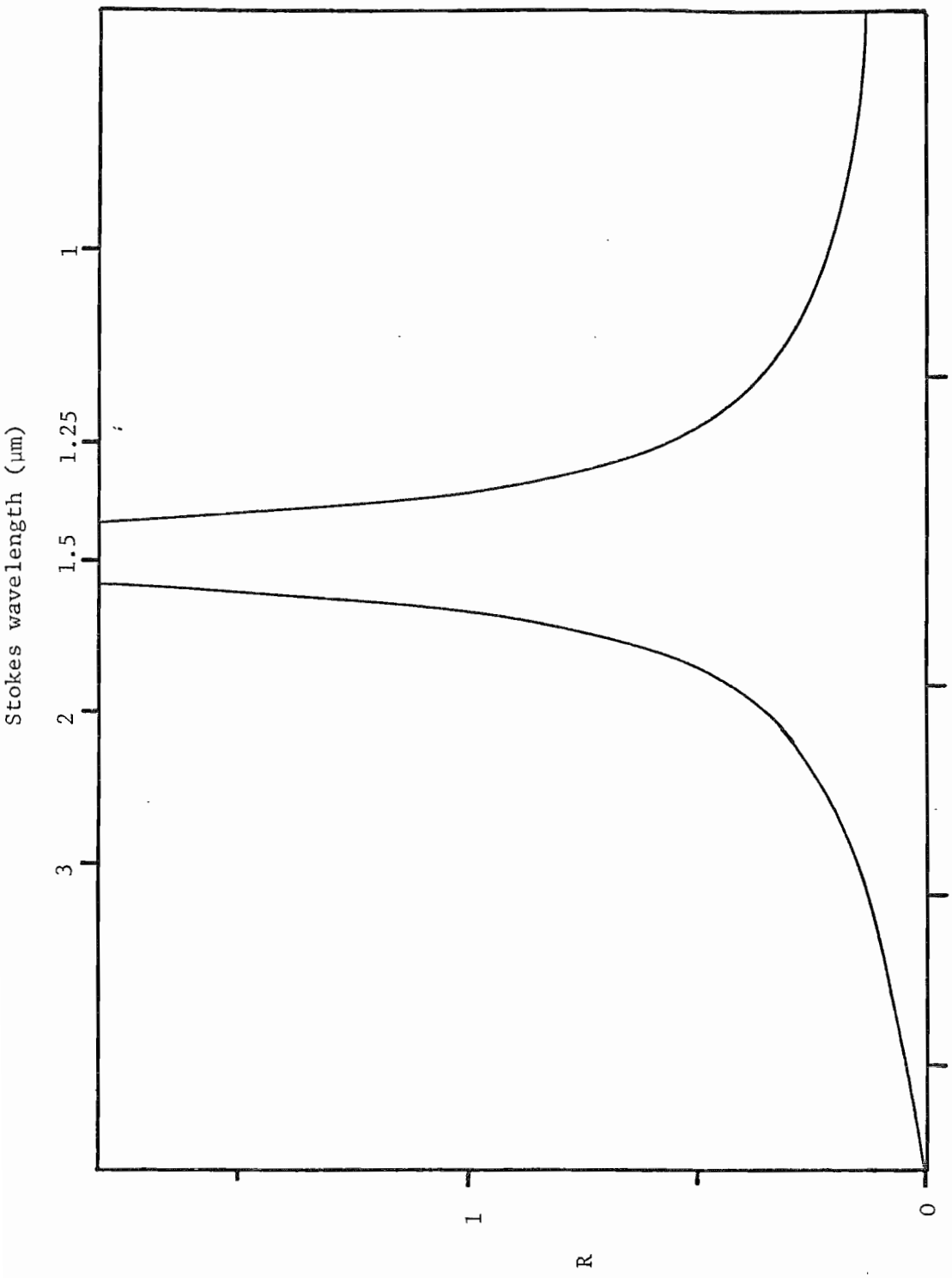

Figure 5.5a The material ratio R for biharmonic pumping in Barium. Strong pump laser at 355 nm.

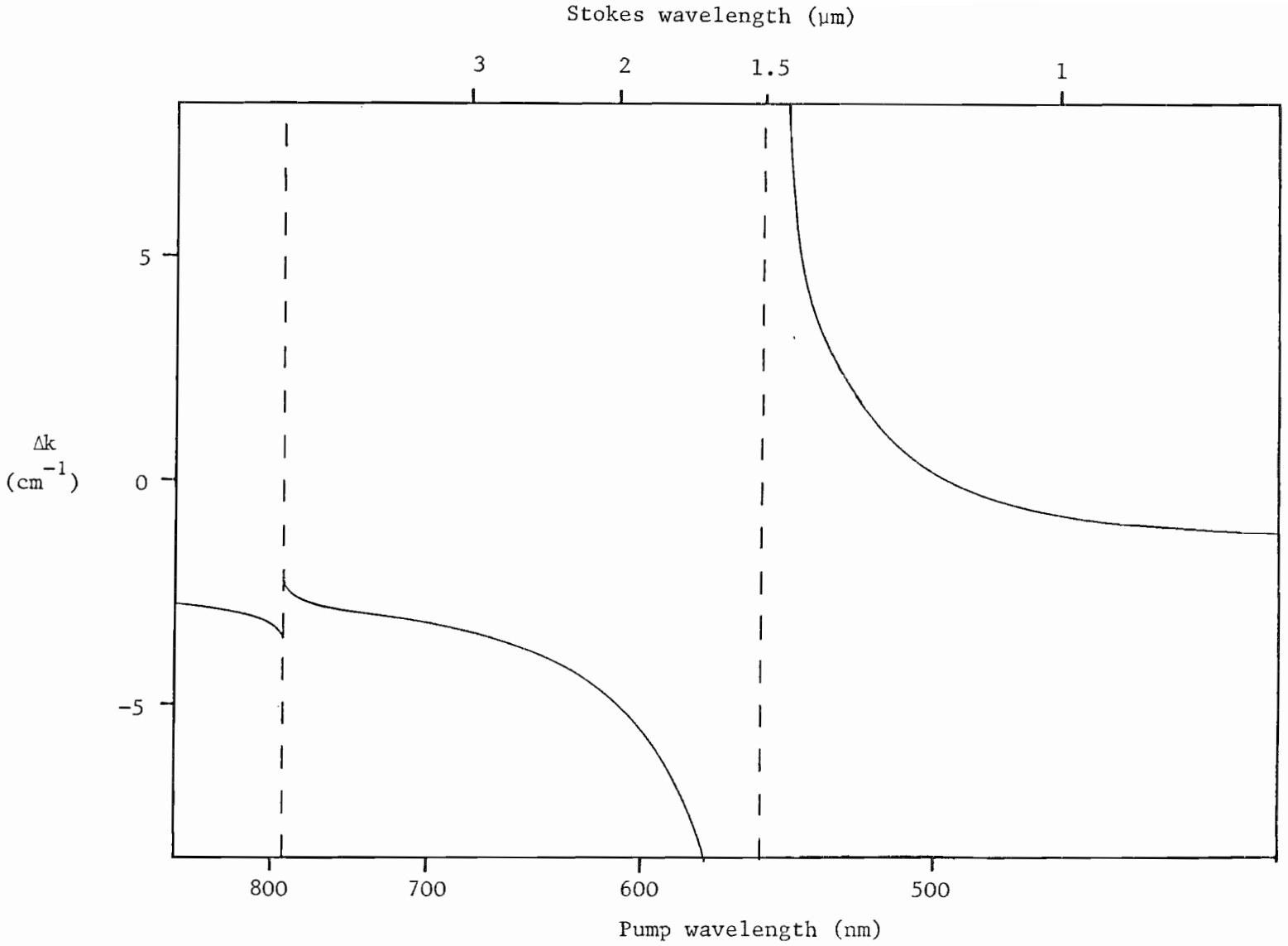

Figure 5.5b The phasemismatch Δk for biharmonic pumping in Barium. Strong pump laser at 355 nm.

In practice, however, saturation of the growth of 596 nm radiation will adversely affect the production of infrared photons. As both waves are competing for the same ground state atoms, the efficiency will be below that expected from the steady state theory. In addition to this, no account of the yet unexplained inability of 532 nm light to reach Raman threshold has been made. The processes which inhibit SERS at this wavelength are also likely to have a serious detrimental effect on four wave mixing in Barium vapour.

5.3.2 Effects which will Reduce the Biharmonic Pumping Efficiency

Most of the measurements of four wave mixing efficiency were performed using an unstable resonator Nd:YAG laser. The focused (far field) beam profile is similar to the Airy ring pattern associated with diffraction from a circular aperture. The transverse intensity distribution has a central lobe which contains a large fraction (60%) of the laser energy: this lobe has been used to approximate a Gaussian intensity distribution (Laycock (1979)). Even so, the beam profile is, in practice, far removed from either the uniform intensity or Gaussian cases considered in Chapter 3. The effects which this will have are now discussed.

a) Diffraction Loss and Gain Focusing

By keeping the transverse derivatives in the wave equation for Raman scattering, Cotter, Hanna and Wyatt (1975) were able to consider the interplay of diffraction and gain focusing in nonlinear light generation. Diffraction of the generated light was shown, in Section 2.5, to play a part in the determination of Raman threshold; the more the Stokes light tends to diffract out of the illuminated region, the higher the threshold pump power. This can be viewed, in effect, as a reduction in the effective gain seen by the Stokes wave as compared to the uniform illumination case, that is, a reduction in the growth rate of the Stokes wave.

The situation becomes more complex when the interaction of four waves is considered. The transverse dependence of gain seen

by the generated infrared wave is now dependent on the variation across the other three beams, one of which is also being generated. Attempting to solve the problem is beyond the scope of this thesis, but some idea of how the generation efficiency could be reduced can be seen as follows. In the Raman driven parametric approximation of Chapter 3, the gain seen by the infrared light being generated is proportional to the product of the field amplitudes of the other waves. This gain is therefore only present over the diameter of the smallest of the interacting beams, and so energy can only be given to the infrared wave in that region. This will severely limit the generation efficiency as only a fraction of the energy entering the heat-pipe will pass through this area. The role played by diffraction becomes more important the smaller the diameter over which generation takes place.

b) Beam Overlap Inside the Heat-pipe

The beams of 532 nm and 355 nm radiation were regularly checked for overlap outside the heat-pipe. They remained collinear over several metres and consequently they would be expected to overlap very well inside the vapour column. The waists of the harmonic beams of the Nd:YAG laser are coincident with the waist of the fundamental and, neglecting dispersion, they will be focused to a waist at the same point along the vapour column. By considering the propagation of the beams and their transformation by a lens, the confocal parameter of both beams in the heat-pipe is found to be the same. However, the light with shorter wavelength is focused to a smaller waist size. For the case of Gaussian TEM_{oo} beams, the 355 nm light would have a beam area two thirds that of the 532 nm light and so effectively one third of the green light is unable to take part in a four wave interaction. Overlap of the lower intensity outer rings of the two beams will be rather poor due to their different sizes. The usable input energy is almost entirely contained in the central lobe of each beam and so the expected efficiency will be lower than for TEM_{oo} beams.

c) Temporal overlap

There is considerable structure on the time profile of a Q-switched Nd:YAG laser when it is allowed to operate on many longitudinal modes. A characteristic time for these fluctuations can be found from the inverse of the laser bandwidth. Taking a bandwidth of 0.15 cm^{-1}, an inherent time scale of around 100 ps for the intensity variations is calculated. The scale of these changes in the light wave corresponds to a distance of 3 cm. The temporal behaviour of the harmonics of the laser are a complex function of the time structure of the fundamental radiation, but their structure will have a characteristic scale of the same order.

As has been noted before, the gain seen by the generated infrared wave is dependent upon the product of the amplitudes of the interacting waves. The production of light at the weak Stokes wavelength can only occur by the interaction of the weak pump with the excitation set up by the strong wave pair. The decay of this excitation is determined by the Raman linewidth of the transition; the medium remembers the presence of the strong wave pair for a time Γ_R^{-1}. The production of the weak wave will therefore show a marked dependence upon the temporal and spatial behaviour of the orange light at 596 nm.

The tremendous task of analysing the effects of overlap in time has not been attempted, although it can be seen as another major limitation to efficiency.

d) Atomic Saturation of the Medium

The conversion of the strong pump to its Stokes at 596 nm has been shown to suffer strong atomic saturation. This saturation is due to a rapid reduction in the population difference between the ground state and the upper Raman state over part of the vapour column. This has the effect of scaling down the Raman gain per unit length over this region as seen by the Stokes wave. At the same time, the material excitation set up by these waves will also be dramatically reduced. The growth of an infrared wave through biharmonic pumping in an atomic medium will be substantially less than the large signal growth expected from steady state four wave

mixing theory. In biharmonic pumping the waves at 596 nm and 355 nm, take away on one hand almost as much as they give on the other; they provide the excitation with which the 532 nm light interacts but the strength of the excitation is very small due to the reduced population in the ground state.

Far above Raman threshold, the saturated 596 nm Stokes generation will cause the populations of the two levels to become equal nearly instantaneously. In this case the growth of the infrared Stokes light will never leave the small signal regime. This can be seen by considering the point at which the growth of 596 nm light becomes saturated. This occurs at a threshold distance into the medium, ℓ_{th}, given approximately by $G\ell_{th} = 30$. For vapour columns shorter than ℓ_{th} the Raman scattering processes are 'below threshold'. Beyond this threshold length the small signal treatment of SERS breaks down as pump and atomic depletion become important. It is also at this distance that the four wave mixing process is effectively stopped. In this approximation then, it is only the exponential part of the 596 nm growth which is impressed upon the growth of the infrared wave.

The typical photon conversion efficiencies expected from this four wave process can be calculated from the small signal growth equation. This equation (3.12), re-expressed in terms of pulse energies by factorizing out pulse areas and durations, is

$$E_s = E_{so} \frac{\omega_{355} E_{532}}{\omega_{532} E_{355}} R^2 \exp(G\ell_{th}) \qquad (5.4)$$

When a starting noise energy E_{2so} of the order of 1 photon ($h\omega_{2s}$) is assumed and the relationship between the frequencies of the Nd:YAG harmonics is recognized, the photon conversion efficiency is

$$\eta = \frac{\omega_{532} E_s}{\omega_s E_{532}} = \frac{3h\omega_{532} R \exp(30)}{2E_{355}} \qquad (5.5)$$

Here $G\ell_{th}$ has been taken as 30. With values typical of the experimental conditions, viz. $h\omega_{532} = 3.7 \times 10^{-19}$ J, R = 1 and

$E_{355} \simeq 1$ mJ, η is of the order of 1%. This is not inconsistent with observed efficiencies of up to 0.6%, despite the assumptions made. Of course this estimate totally neglects the growth which may occur in the large signal region, and is strictly only applicable for infinite plane waves. However, the role of atomic saturation in four wave mixing is seen to be an important one; the limitation it imposes on parametric growth contributes heavily to the observed conversion efficiencies being much less than expected from present steady state theory.

A full treatment of saturation of SERS and four wave mixing requires a time-dependent approach. This is far from trivial even in the case of SERS. Cotter (1976) obtained numerically the expected Stokes energy from Caesium using the 6s-7s Raman transition. This has not yet been attempted for biharmonic pumping in Barium.

5.4 Biharmonic Pumping Experiments

5.4.1 Fixed Frequency behaviour

In the previous section calculations applicable to biharmonic pumping in Barium vapour were discussed and some limiting mechanisms put forward. The subject of this section is an experimental investigation into this four wave mixing process. The conversion efficiency from second harmonic Nd:YAG radiation at 532 nm to its Stokes shifted wavelength is seen to be limited by atomic saturation.

To investigate the parametric generation of infrared light, the arrangement of Figure 5.6 was used. After rejection of the Nd:YAG fundamental light with a dielectric coated mirror and filters, the harmonics were separated from one another by a dichroic beamsplitter. By placing neutral density filters in these two beams, the relative energy in each could be adjusted. The beams were then recombined using another dichroic beamsplitter and focused into the Barium heat-pipe oven by a 50 cm focal length silica lens. All wavelengths shorter than 715 nm were removed from the light leaving the oven by a filter type RG715. The

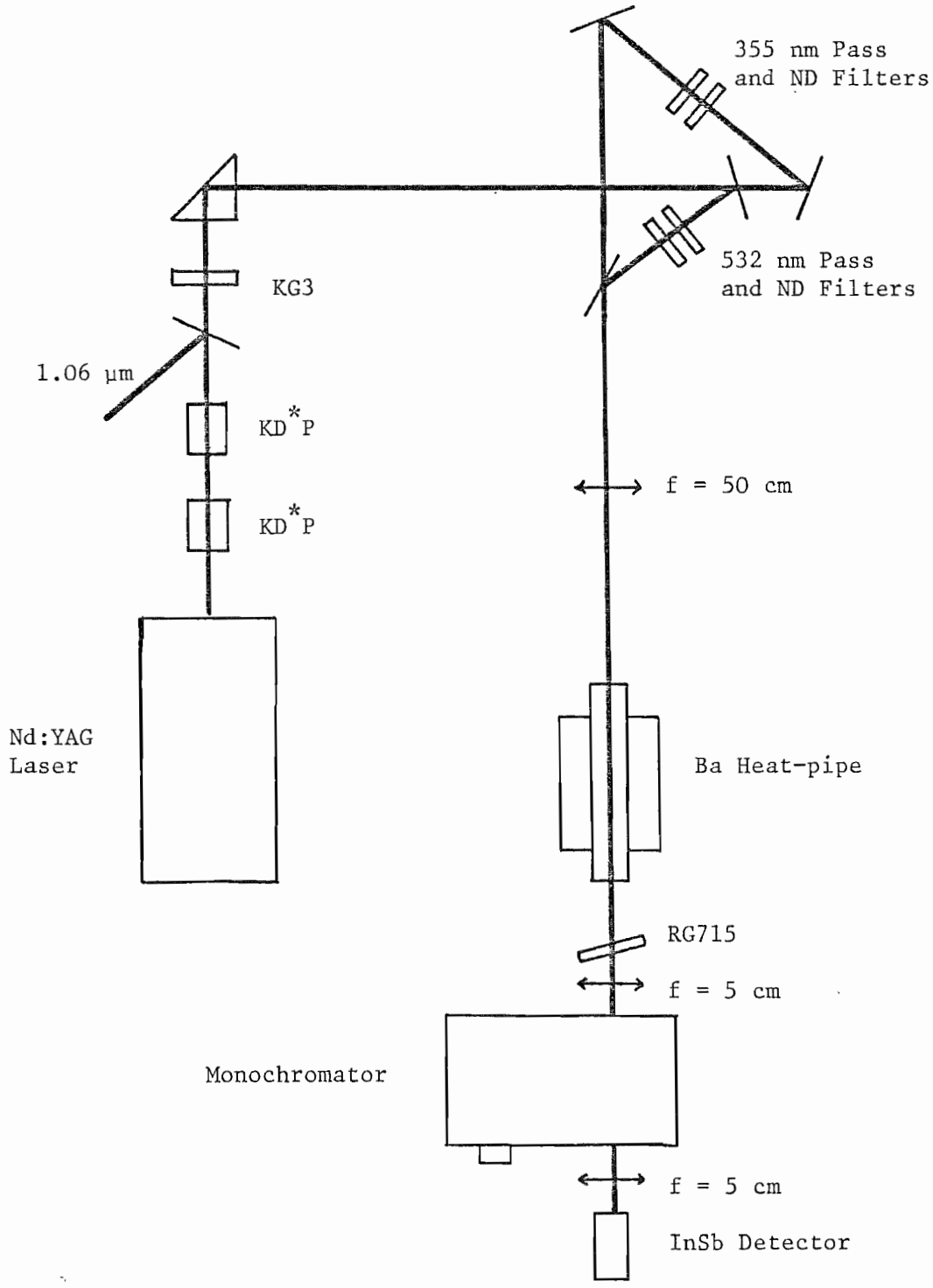

Figure 5.6 Experimental arrangement used to study biharmonic pumping with fixed frequency inputs

remaining light was focused onto the entrance slit of a Hilger Watts D330 monochromator with a KBr lens. A calibrated photoconductive InSb detector, placed after the monochromator, was used to monitor the generated 1.35 μm radiation as the pulse energies of the two beams were varied. Throughout the measurements a Barium pressure of 2.5 torr was used, corresponding to a number density of 1.5×10^{16} cm^{-3}.

Measurement of the generated infrared energy as a function of ultraviolet input, for fixed 532 nm energies, was hindered by a dearth of ultraviolet reducing filters. Only filters with ultraviolet transmissions of 44% and 19% were available. It was therefore easier to study the generated infrared as the 532 nm energy was varied. Despite this, Figure 5.7 shows the results that could be obtained. With 355 nm energies below 1 mJ the infrared energy is seen to have a strong dependence on the ultraviolet input. (This is a reflection of the unsaturated nature of the 596 nm Stokes generation - atomic saturation becomes severe for 355 nm energies > 1 mJ.)

For fixed 355 nm input energy the infrared output grows with increasing 532 nm input. Figure 5.8 shows the generated Stokes energy for ultraviolet pulse energies ranging from 300 μJ to 3 mJ. The curves in this Figure show that the generated infrared energy increases nearly linearly with increasing 532 nm input. For moderate input energy, the efficiency is roughly constant at around 0.3%, in agreement with the model of saturation developed in Section 3.1, and the estimate of efficiency given by Equation 3.12. This trend is quite noticeable for 532 nm pulse energies of less than ∿50 μJ.

At low input energy the efficiency decreases with increasing ultraviolet input. This qualitative behaviour was suggested by Equation 3.12, although the amount that the generation efficiency is reduced is not as large as would be expected from this Equation. In view of the rather simplistic way this question was dealt with, this result is not surprising.

At higher 532 nm inputs the curves deviate significantly from the constant efficiency described above. In this region the 532 nm

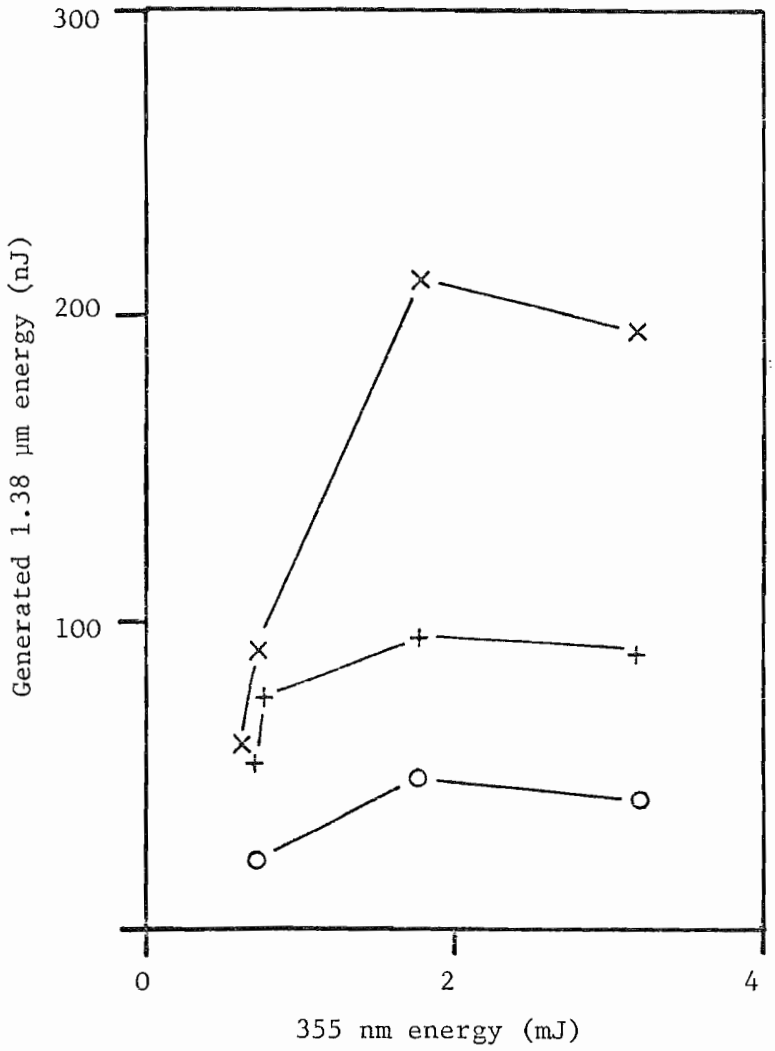

Figure 5.7 Biharmonic pumping in Barium; Stokes generation with fixed 532 nm energy:

o - 40 μJ

\+ - 110 μJ

X - 300 μJ

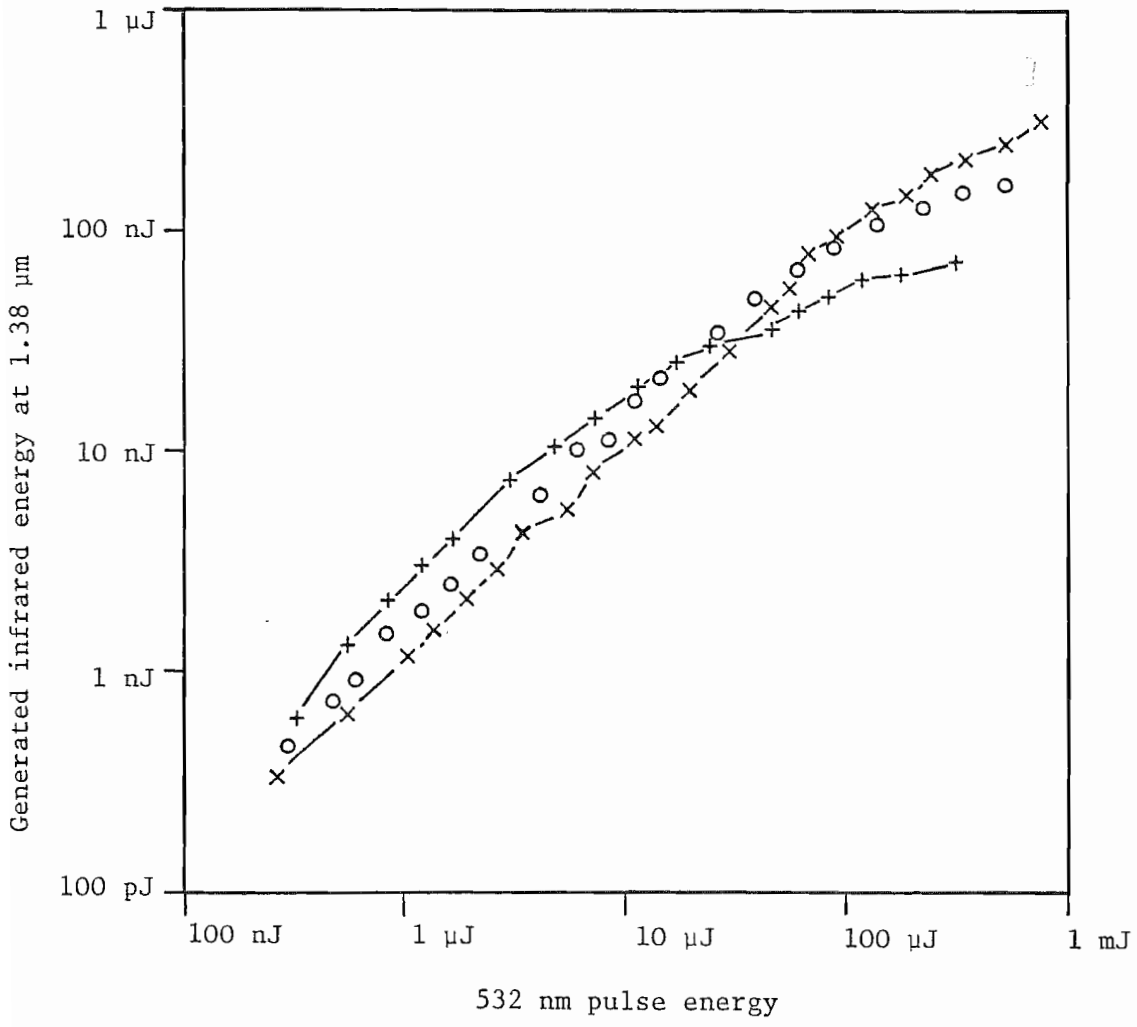

Figure 5.8 Fixed frequency biharmonic pumping in Barium; the variation of generated energy with 532 nm input.

355 nm input energies:

\+ - 320 µJ

o - 1 mJ

X - 3 mJ

input energy approaches the energy of the 355 nm pulse. The presence of the green light is seen no longer to be weak compared to the 355 nm and 596 nm of the SERS process. If the 532 nm could independently reach Raman threshold, the infrared generation efficiency would be expected to rise above that obtained from biharmonic pumping. It should be noticed that the efficiency drops off more rapidly for small ultraviolet input, again reflecting the fact that the 532 nm energy is becoming comparable to that at 355 nm. The reduction in efficiency evident in Figure 5.8 is therefore likely to be due to a competing process. It is quite possible that it is this same process which inhibits the independent generation of 1.35 μm light by SERS of 532 nm. As this mechanism is not currently understood, it is not possible to draw any further conclusions.

5.4.2 The Tuning Behaviour of Biharmonic Pumping

Having investigated biharmonic pumping with fixed frequencies, attention is now turned to the more useful application of four wave mixing, in which a tunable Stokes output is produced. In order to do this the 532 nm input was replaced by a Coumarin 522 dye laser whose wavelength could be varied from 500 to 549 nm. The infrared tuning range expected using this dye laser was 1.16 to 1.47 μm.

The experimental arrangement is shown in Figure 5.9. The grazing incidence grating dye laser described in Section 4.1 was pumped by 10% of the ultraviolet 355 nm light. This was split from the unstable resonator Nd:YAG laser beam by a dielectric mirror. The beam from this dye laser was adjusted by means of a telescope to be collimated and about the same size as the ultraviolet beam. This was then focused into the heat-pipe by the same 50 cm focal length silica lens.

In order to achieve the best temporal overlap of the two lasers, a delay of 5 ns had to be introduced into the ultraviolet path. Allowance was made in this way for the (short) build up time of the dye laser and the time taken for the dye laser light to reach the dichroic recombining mirror. This was not necessary for

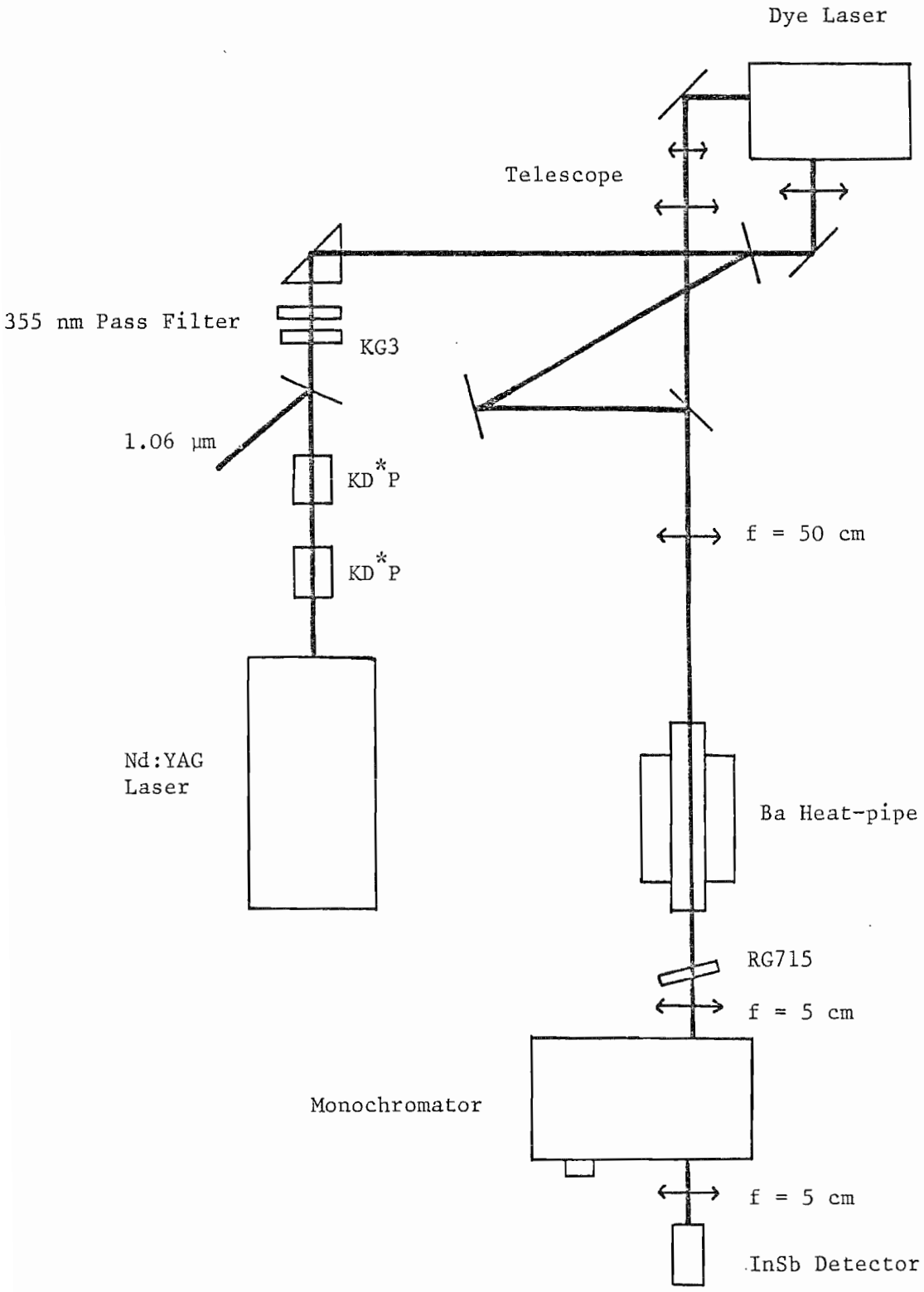

Figure 5.9 Experimental arrangement used to study biharmonic pumping with a tunable dye laser

the experiments with 532 nm second harmonic light as the harmonics are produced simultaneously.

A typical tuning curve is shown in Figure 5.10, in which up to 9 nJ of infrared light is generated from less than 40 μJ of Coumarin 522 dye laser light. Continuous tuning from 1.16 μm to 1.47 μm was obtained with this particular dye; the dye laser was shifted into the infrared over its entire tuning range by the biharmonic pumping process.

The dye laser to infrared photon conversion efficiency is shown in Figure 5.11. This curve peaks up when the dye laser wavelength is near to the $6s^2\ ^2S_o - 6s6p\ ^1P_1$ transition. This behaviour is expected from the small signal treatment of Section 3.3. As intermediate resonance is approached, the two photon polarizability α_R (defined by Equation 3.5) increases as Δ^{-1}, where Δ is the detuning from resonance. Furthermore, the material ratio R increases in proportion to α_R. Single photon absorption on the same transition also depends on Δ. Assuming a Lorentzian lineshape the absorption coefficient β is proportional to Δ^{-2}. From Section 3.3.1 the efficiency expected in the small signal regime will have the form:

$$\eta = \frac{a}{\Delta^2} \exp \frac{-b}{\Delta^2} \qquad (5.6)$$

where a and b are constants which depend on the atomic number density, the ultraviolet 355 nm intensity, the absorption linewidth of the transition and to a lesser extent on the dye laser and generated infrared wavelengths. The value of a will be critically dependent on such factors as beam overlap in the cell, beam quality and temporal overlap as discussed in Section 5.3.2.

Far from resonance ($b < \Delta^2$) the effect of the exponential is swamped by the $a\Delta^{-2}$ term. In this limit, a can be found from a graph of η against Δ^{-2}. The efficiency curve can then be fitted using $b \simeq \Delta_o^2$, where Δ_o is the detuning at which the process has its peak efficiency. Figure 5.12 shows a fit to experimental data performed along these lines, but with the dependance of a on the dye laser and Stokes wavelengths retained.

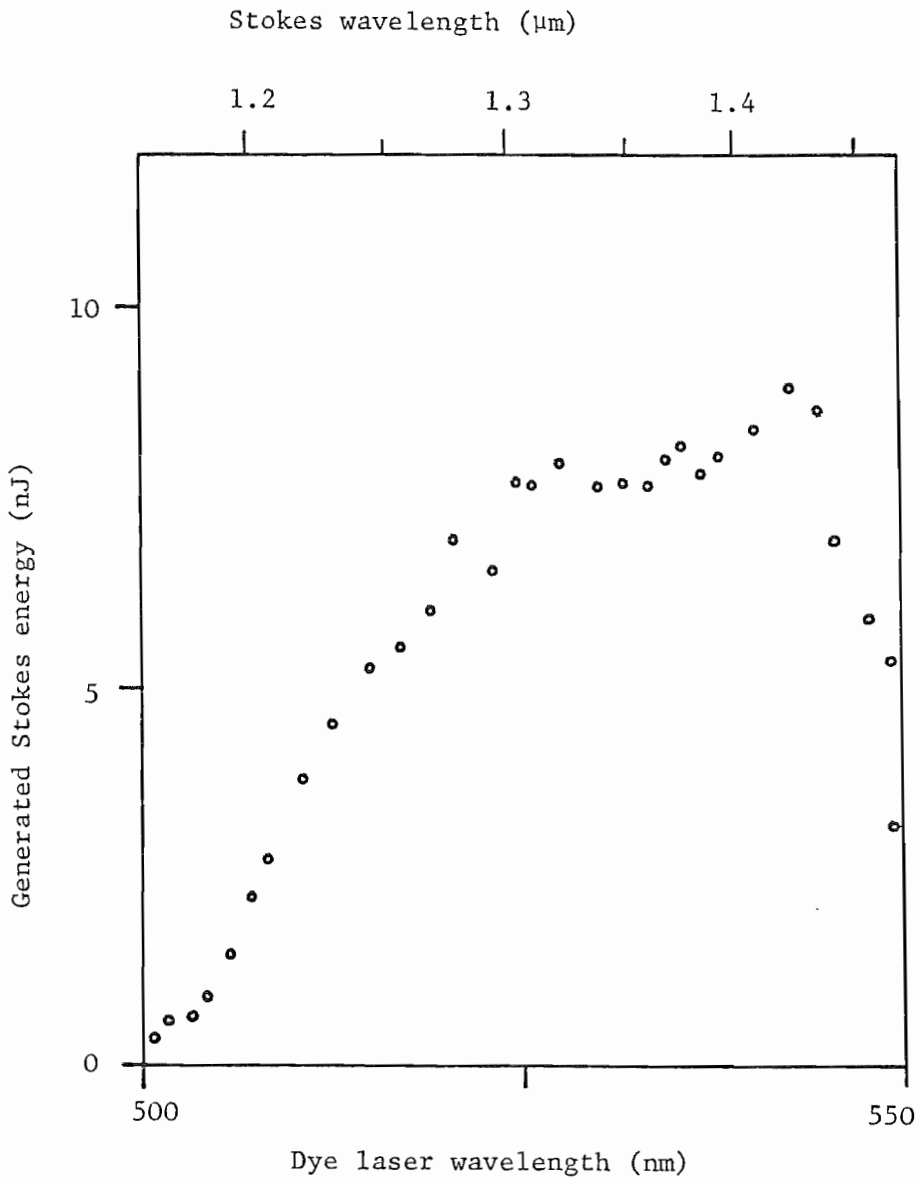

Figure 5.10 Biharmonic pumping in Barium; infrared energy generated from Coumarin 522 dye laser light

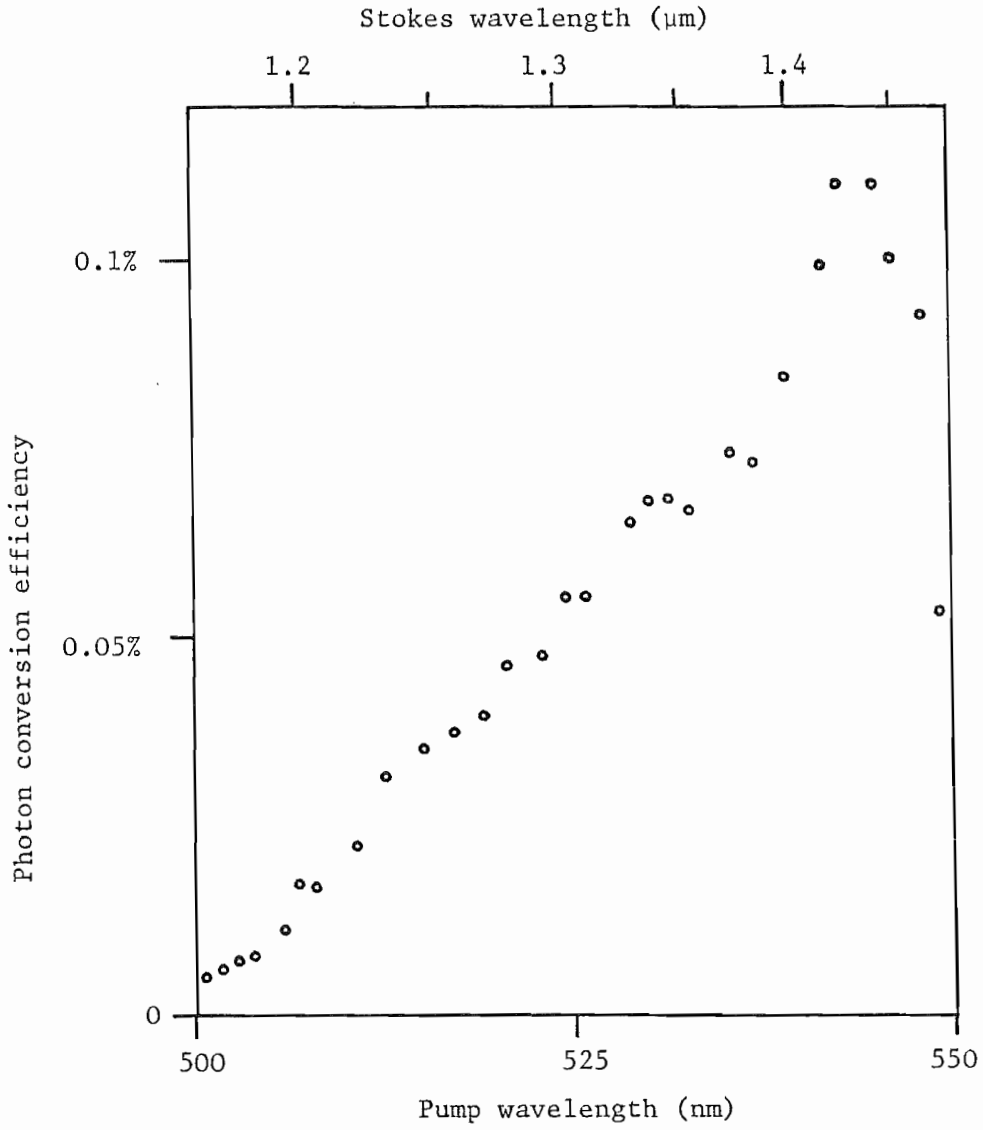

Figure 5.11 Biharmonic pumping conversion efficiency from 532 nm to 1.38 μm.

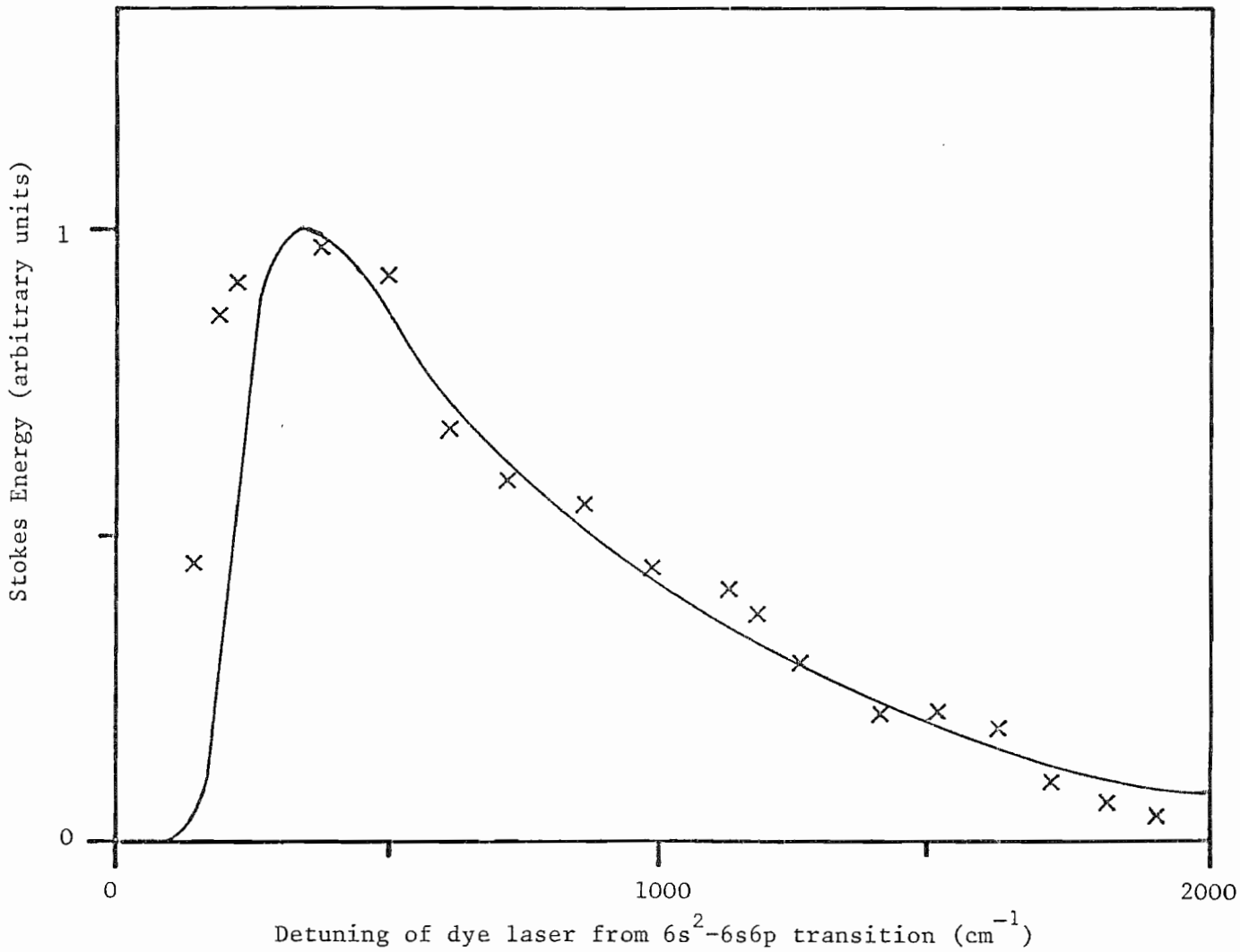

Figure 5.12 Biharmonic pumping in Barium; fit of generated Stokes output to theoretical tuning curve. (see text)

5.5 Conclusions

In this chapter, stimulated electronic Raman scattering and biharmonic pumping in Barium have been considered. Both techniques have been found to allow efficient generation of Raman shifted light.

As with Strontium, the use of close resonance with the principal line to give enhancement of the Raman gain failed to produce a Stokes output. In Barium, however, the cause is not single photon absorption as it was for Strontium. Partial blame for this failure must go to the lack of accurate Barium oscillator strength data especially for the 6s6p ^{1}P to 6s5d ^{1}D transition. Miles and Wiese (1969) give estimated uncertainties for their tabulation of the Barium oscillator strengths. In general these are quite large and are typically 50% for the transitions considered here and >50% for the 6s6p ^{1}P-6s5d ^{1}P†. However these uncertainties are not sufficient to account for the lack of Raman output for high 532 nm input energy. The inability to reach threshold is probably caused by a competing process; the possible nature of this process is currently unknown.

The use of the higher lying 5d6p ^{1}P level for intermediate resonance has been seen to allow efficient low threshold SERS. As in the related experiments of Djeu and Burnham (1978), this scheme has efficiently Raman shifted ultraviolet light into the visible part of the spectrum. As the small signal Stokes gain offered by a 355 nm pump laser is smaller than that obtained from their XeF laser, the maximum photon conversion efficiency measured here is less than the 80% that they reported. However, it has exceeded 30%.

Biharmonic pumping using fixed and tunable lasers has been demonstrated on the same Raman transition, allowing the production of Stokes outputs when one of the lasers is incapable of independently exceeding Raman threshold. Conversion efficiencies of nearly 1% have been obtained, two orders of magnitude larger than previously reported for this type of process in atomic media (Karkkainen (1977)).

---

† This spread must reflect itself in the value of R used for Biharmonic pumping. For this work the stated values of Miles and Wiese have been used throughout.

The generated output was tuned over almost 2000 cm^{-1} of the near infrared from 1.16 μm to 1.47 μm.

CHAPTER 6

Stimulated Electronic Raman Scattering in Caesium Vapour

In this chapter, investigations into SERS in Caesium vapour are described. Experiments originally aimed at improving the infrared tuning range which could be obtained using the 6s-7s Raman transition are detailed and finally the measurement of the Raman threshold for 532 nm light on the 6s-5d transition is discussed.

The original impetus for the 6s-7s work was to obtain an improved output tuning range in the infrared. Calculations of the Raman gain on this transition were performed by Cotter (1976) and Wyatt (1976), who predicted that wide Stokes tuning (2-10 μm) should be obtained. Initially they assumed a Doppler broadened linewidth which gave predictions contrary to experiments; typically a tuning range of 2.5-3.5 μm was obtained. Later the measured Stokes output linewidth was used to recalculate the gain and tuning which now agreed quite well with the measured Raman threshold and tuning. The disagreement between these linewidths was considered by Wyatt and also Tuttlebee (1977). It was felt that the presence of a significant number density of Caesium dimer molecules was responsible for increasing the required Raman threshold power. In addition, they also invoked various line-broadening mechanisms, such as upper state lifetime broadening, resonance broadening as well as dynamic line-shifting, to resolve the discrepancy. In general, however, these suggested mechanisms would give rise to a broadening of the output linewidth after Raman threshold had been reached, and in terms of threshold calculation these effects have little relevance.

The conclusion which arises from the above ideas is that some method of reducing the dimer concentration would probably the Raman threshold. The aim of the experiments described here was, therefore, to remove dimers and allow the Doppler linewidth

of the Raman transition to be utilized. With this goal in mind, two methods were used. Firstly, bleaching of the molecular absorption by excitation with a Nd:YAG laser at 1.06 μm was tried, and gave a degree of improvement to the tuning range. Secondly a technique involving superheating the vapour column was found to offer a large reduction in dimer density and a significant extension of the SERS tuning.

After this work was performed the importance of collision broadening of the Raman linewidth was realised. Careful measurement of the Raman threshold on the 6s-5d transition allows a direct comparison of experimental results with the theoretical prediction of the threshold power using a collision broadened linewidth. These measurements were performed at 532 nm using a frequency doubled single mode Nd:YAG laser and gave very good agreement with theory. However, the effect of two photon ionization was found to limit the application of the simple Raman gain calculations for tight focusing or long laser pulse durations.

6.1 The 6s-7s Transition Pumped by a High Energy Dye Laser

The work of Cotter (1976) on the 6s-7s Raman transition in Caesium showed this transition to be an efficient method of producing tunable infrared radiation between 2.5 μm and 3.5 μm. In this work a 7D4MC dye laser having a peak power of 30 kW (corresponding to a pulse energy of 120 μJ) was used to pump this transition. The observed infrared output had pulse energies of up to 10 μJ and a photon conversion efficiency of nearly 60%.

The long wavelength tuning limit of 3.5 μm was thought likely to have been set by a combination of molecular absorption and ionization. Absorption would cause attenuation of the pump laser by single photon excitation of the molecules. Multiphoton ionization of the dimer molecules at these pump laser wavelengths, by both direct and stepwise excitation, would lead to a reduction in the Raman gain by Stark broadening of the final Raman level. At wavelengths where multiphoton ionization of the molecules is the predominant factor in preventing Stokes output, the increased pump

power (and therefore, also ionization rate) will lead to a further reduction in the Raman gain. In this limit Raman threshold will never be reachd by a dye laser of such a wavelength without the dimer population being reduced beforehand by some other means. Experiments in which techniques to do this were employed will be described in later sections.

In order to assess the effect that ionization has on the 6s-7s Raman process, some of the Cotter experiments were repeated using a dye laser of substantially higher pulse energy. The use of a high pulse energy ensures that the molecular absorption has only a small effect on the pump laser intensity. For typical dimer densities of between 10^{15} and 10^{16} cm^{-3}, between 20 μJ and 200 μJ of dye laser energy will be absorbed in the process of bleaching the dimer absorption. The use of significantly higher dye laser energy will allow the maximum possible Stokes gain to be obtained from the medium.

To observe the effect of a high laser input energy, the 2 mJ per pulse dye laser/amplifier system described in Section 4.1 was used in the experimental arrangement of Figure 6.1, which is similar to that used by Cotter. The laser was focused confocally over the 30 cm vapour column of the air-cooled heat-pipe. The generated infrared light was separated from the transmitted dye laser light by a 1 cm thick polished Germanium filter. To ensure that the blue light from the dye laser was not causing free carrier absorption of the Stokes output in the filter, a measurement of the generated energy at 2.65 μm was performed with and without an additional filter of glass type RG715. This was placed between the heat-pipe output window and the Germanium filter. The RG715 totally stopped the blue light from reaching the other filter. The Stokes energy falling onto the pyroelectric energy meter was found to be reduced by an amount consistent with the transmission of the RG715 filter, indicating that free carrier absorption could be neglected. The RG715 filter could not be used independently as it becomes opaque beyond 2.7 μm and is transparent to the main amplified spontaneous emissions (ASE) from Caesium vapour in the range 1.3 μm to 1.5 μm. The emissions are produced on the 7s-6p and 7p-5d atomic transitions.

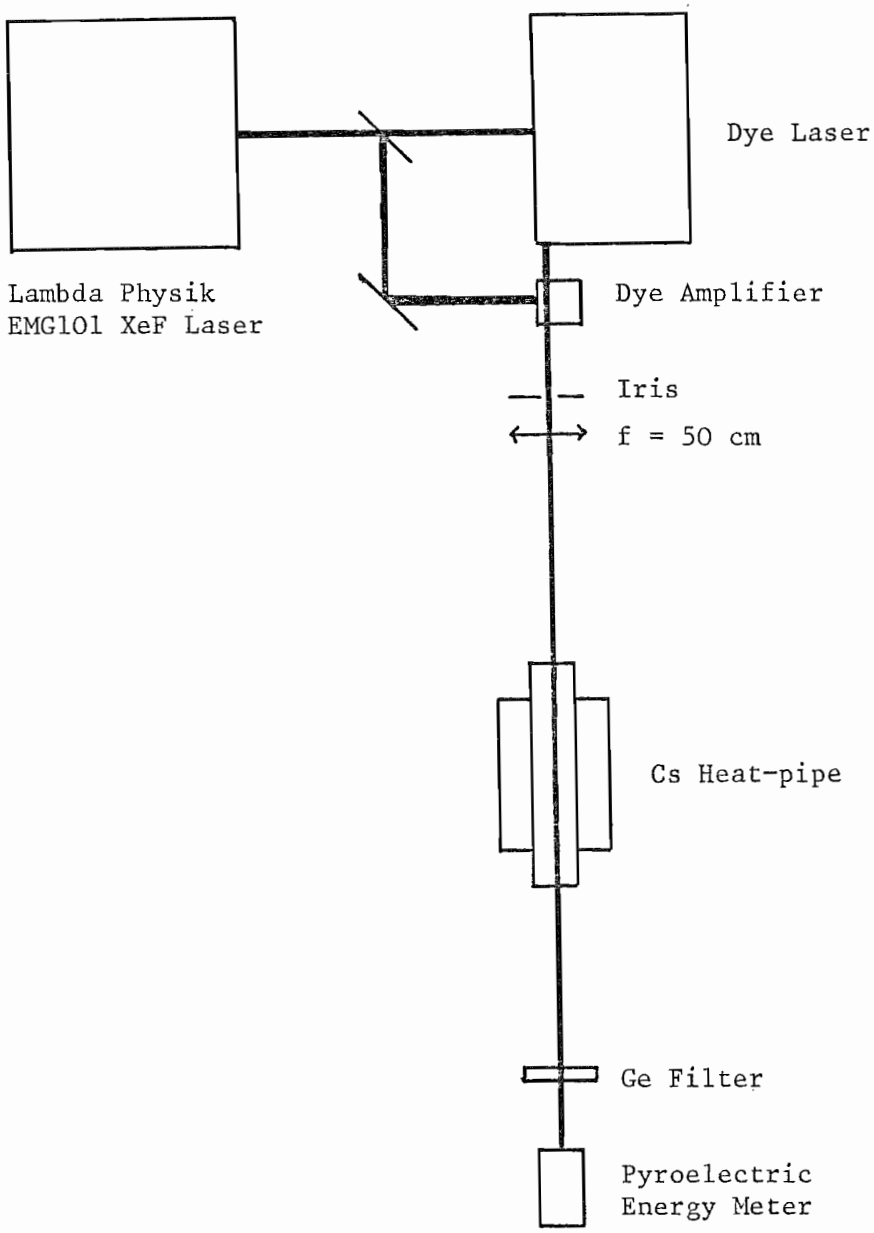

Figure 6.1 Experimental arrangement used to examine long wavelength 6s-7s SERS tuning in Caesium

A typical SERS tuning profile is shown in Figure 6.2. The short wavelength tuning limit is set by the end of the dye laser tuning range. (The use of a shorter wavelength dye laser will be considered later.) The long wavelength limit occurs before the dye laser energy has fallen far from its peak value. This limit is therefore set during the SERS process rather than by the dye laser. It should be noted that the tuning limit of 3.7 μm is not much further into the infrared than that which is obtained using a 120 μJ dye laser. Despite having increased the laser intensity by a factor of 10 the Raman gain would appear, from the dependence of gain and threshold on Stokes wavelength, only to have doubled. It is felt that this is a direct consequence of molecular ionization.

A calculation of the effect of Stark broadening on the 6s-7s Raman transition was performed using the formulae which will be given in Section 6.6. It was found that ionization greater than ~1%. would lead to a significant reduction of the Raman gain from its collisionally broadened value. Using the molecular two photon ionization cross-section determined by Granneman et al (1976), the laser energy at which the Stark broadened linewidth equals the collisional linewidth is found to be 0.2 mJ over the pulse duration of 15 ns. This calculation was performed at a pump wavelength of 472 nm where $\sigma_D = 6 \times 10^{-41}$ cm s^{-1}. The Stokes wavelength of 3.75 μm would lie just inside those obtainable under these conditions. Atomic ionization was neglected.

6.2 Bleaching of Caesium Dimers by 1.06 μm radiation

Having seen that only a small increase in SERS tuning could be obtained using a high power dye laser, due to the presence of dimer molecules, attention is now turned to methods of reducing their effect. Two techniques were tried; excitation of the molecules by a Nd:YAG laser to reduce their absorption and in addition, superheating the Caesium vapour to thermally dissociate them. The first method was tried by Hodgson (1979) in an unsuccessful attempt to lower the Raman threshold on the 6s-$5d_{5/2}$ transition in Caesium. The second method was successfully demonstrated by Wyatt and Cotter (1979) on the same transition.

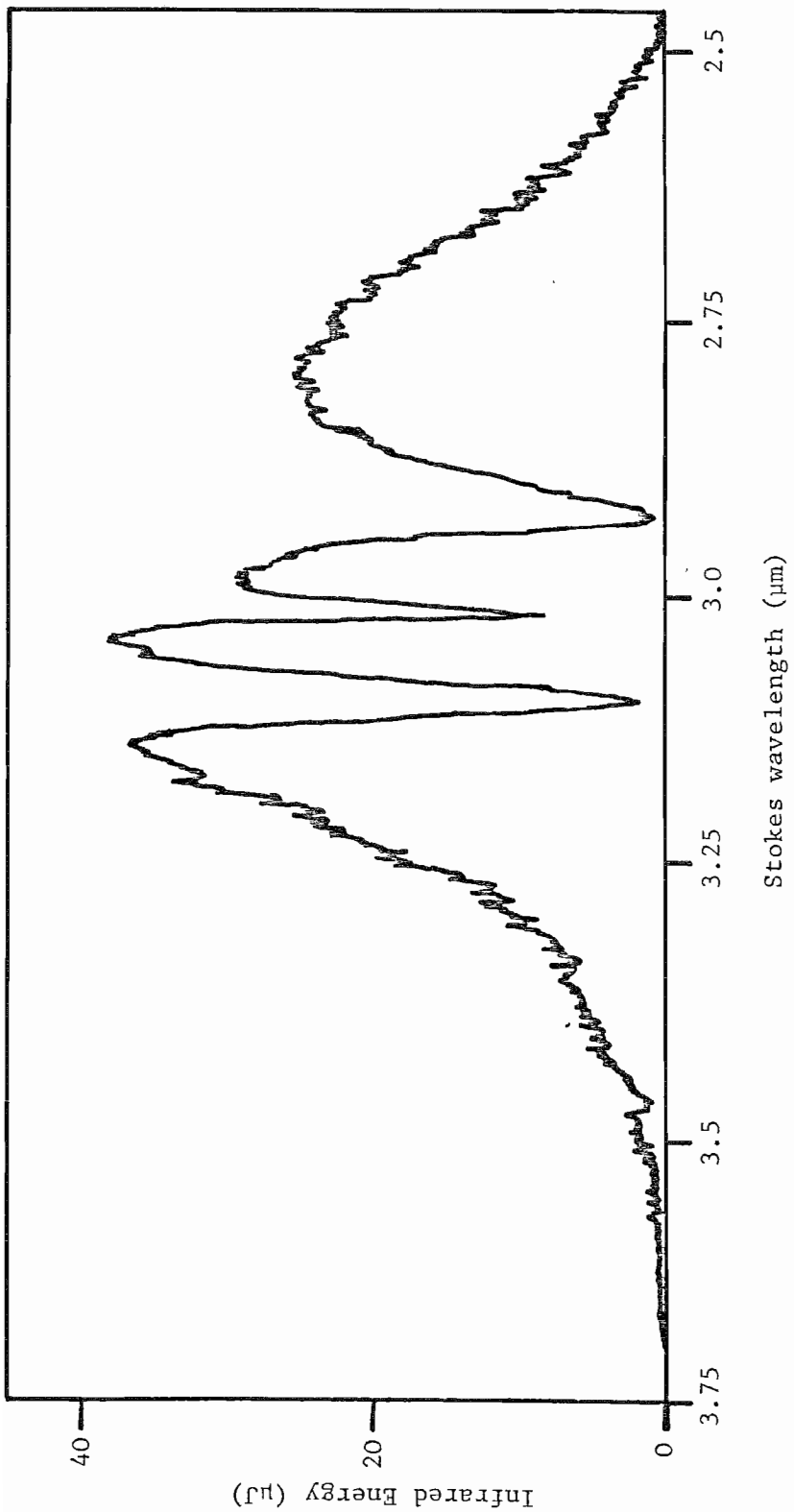

Figure 6.2 Output tuning on the 6s-7s transition for high energy blue dye laser.

The light from a Nd:YAG laser operating at 1.06 μm also falls within a strong absorption band of Caesium dimers (see Figure 4.8). A partial potential energy curve for these molecules is shown in Figure 6.3. Superimposed upon it are the energies of one and two Nd:YAG photons. As can be seen, direct single photon and stepwise two-photon excitation of the molecule are possible. Population in the $A\ ^1\Sigma_u^+$ state can either decay back to the ground state or be further excited to one of the higher lying states. (Sorokin et al (1971) made use of two step excitation of Caesium molecules to this dissociative state, to pump laser transitions in atomic Caesium.)

Measurements of the decay times of the various bound upper molecular states have been performed by Baumgartner et al (1970). These ranged from 6 ns to 30 ns and are, therefore, short. Molecules excited to these states are expected to decay quite rapidly back to the ground state. However, molecules excited to the dissociative state are lost from the ground state pool of dimers. Recombination of Caesium dimers will involve a three body interaction, as the excess energy released in forming the strongly bound ground state must be removed as kinetic energy of a third Caesium atom. These three body collisions will occur quite infrequently, giving rise to a long (100 μs < t < 10 ms) recombination time. Once molecules have been dissociated, the dimer ground state number density will remain reduced for a time which is long compared to typical laser pulse lengths.

In his work on the $6s\text{-}5d_{5/2}$ Raman transition, Hodgson (1979) attributed his inability to exceed threshold at 601 nm to the presence of Caesium dimer molecules. Caesium molecules absorb quite strongly at this wavelength. In an attempt to reduce the dimer absorption, he allowed 1.06 μm radiation - the fundamental of his Nd:YAG laser - to enter the heat-pipe. At the same time he monitored the Raman scattered output at 2.38 μm generated from the second harmonic light of the same laser. With 1.06 μm radiation present there was an overall worsening of the situation. At best Hodgson saw no change in the amount of Stokes light generated. At worst the 532 nm and its Raman shifted output were extinguished by plasma sparks at the focus of the laser in the heat-pipe.

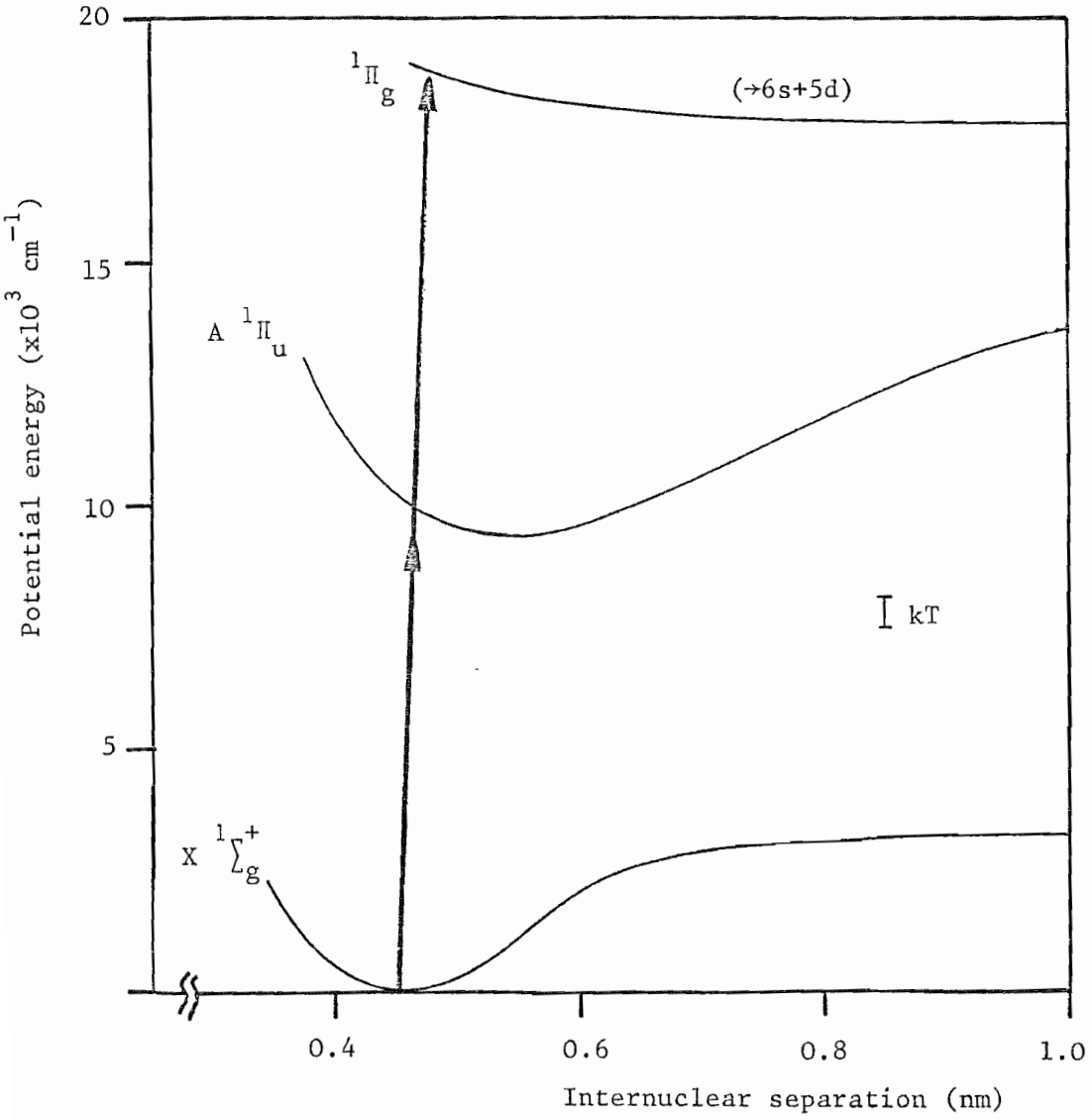

Figure 6.3 Partial potential diagram of the Caesium dimer molecule showing likely excitation route during bleaching by a Nd:YAG laser.

The transmission of a He-Ne laser at 632.8 nm through a 30 cm column of Caesium vapour was studied by Tuttlebee (private communication). He monitored the transmitted power while allowing 1.06 μm pulses to enter the column. It was noted that the transmission of the vapour increased, but even in this preliminary experiment it was obvious that the transmission maximum occurred some time after the Nd:YAG pulse had entered the vapour†.

6.2.1 Bleaching Measurements at 632.8 nm and in the Blue

Before turning to the improvement in the SERS process produced by prior bleaching of the molecular absorption, it is apt to consider the enhancement this has to offer to the transmission of light through the vapour. Two sets of measurements were made in this context. Initially, the transmission of a He-Ne laser at 632.8 nm, which lies in a strong absorption band of the molecules, will be dealt with. Finally, the improvement in the transmission of the blue dye laser used for SERS will be discussed.

The He-Ne laser wavelength lies in the midst of the strong $X\ ^1\Sigma_g^+ - B\ ^1\Pi_u$ molecular absorption band (see Figure 4.8). The absorption cross-section of a Caesium dimer molecule at this wavelength is 7×10^{-17} cm^2. At a typical dimer density of 2×10^{15} cm^{-3}, the transmission of a 30 cm vapour column is only 1.5%. A reduction in the dimer density would lead to a large increase in vapour transmission. Hence, the use of a Ne-Ne laser is well suited to the study of bleaching in Caesium vapour.

In order to investigate the effect of Nd:YAG laser light, and to determine how useful it is in reducing dimer absorption, the experimental arrangement of Figure 6.4 was used. The light from the Nd:YAG laser was made coaxial with that of the He-Ne laser by an iterative adjustment of the two 45° beam steering mirrors. The remaining 1.06 μm radiation, together with any generated infrared light, was removed using a filter of glass type KG3.

---

† The same effect has been noted by Cotter (private communication), who in a similar experiment found that the transmission of a He-Ne laser increased after a blue dye laser pulse.

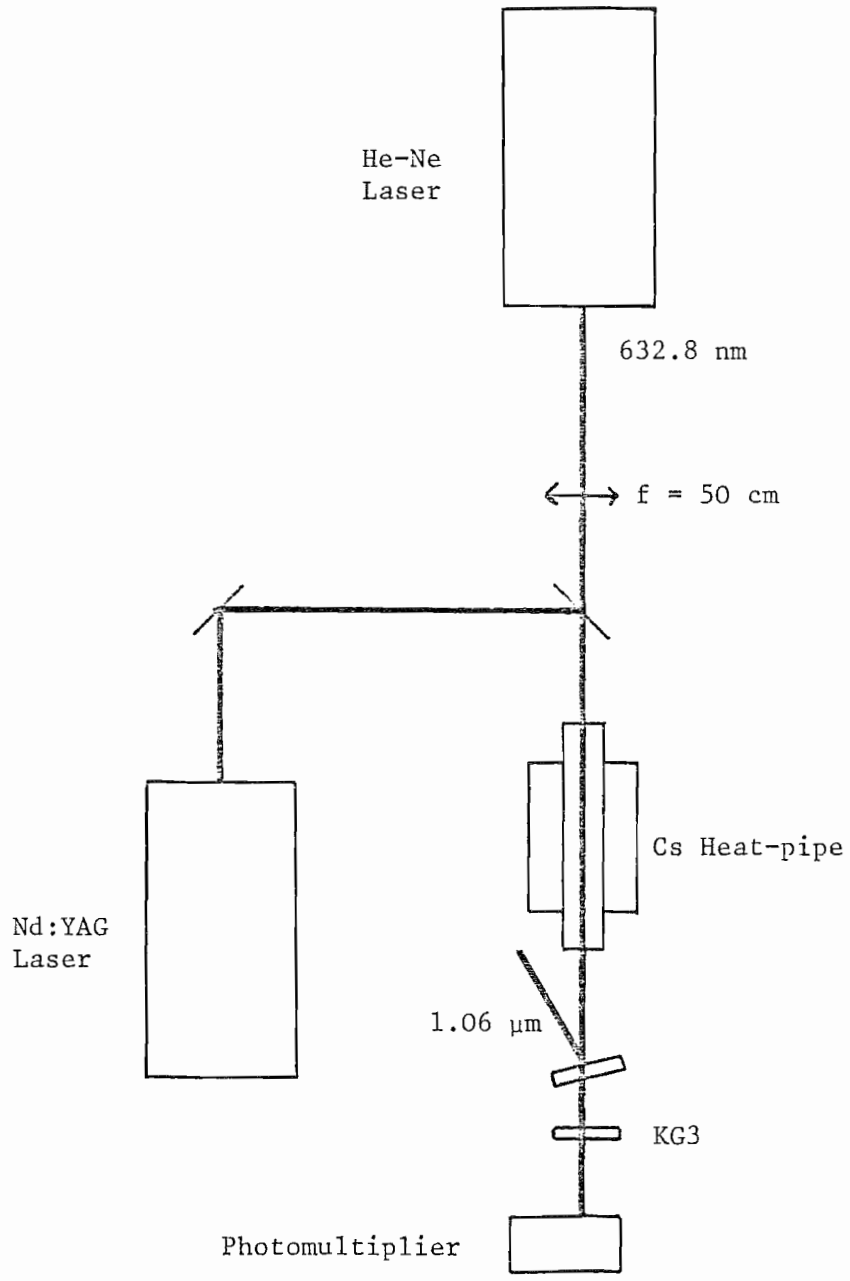

Figure 6.4 Experimental arrangement used to observe Nd:YAG bleaching of Caesium vapour at 632.8 nm.

In a separate experiment various amplified spontaneous emissions in the infrared were observed from the Caesium vapour; these are the Caesium laser outputs which were produced in the experiments of Sorokin et al (1971).

The transmitted 632.8 nm light was monitored using a photomultiplier. A typical oscilloscope trace showing the temporal behaviour of the vapour transmission is shown in Figure 6.5. As can be seen, the transmission of the cell is quite dramatically improved after the passage of a pulse from the Nd:YAG laser. This increase in transmission dies away after approximately 1 ms, as is expected from the discussion of dimer recombination times in the last section.

Attention is now turned to the effect that Nd:YAG bleaching has on dimer absorption of blue light around the atomic 6s-7p absorptions. The dimer absorption cross-section changes significantly over the range 450 nm - 480 nm as was seen in Chapter 4. Temporal measurements of the vapour transmission were made for three blue laser wavelengths.

To observe the temporal behaviour, the arrangement of Figure 6.6 was used. A delay generator was used to vary the separation in time of the pulses from the two lasers. This could be varied continuously over the range 0-80 ms; the upper limit was the interval between Nd:YAG pulses. The transmitted blue light was monitored using a pyroelectric energy meter. The light leaving the vapour was filtered using a piece of KG3 glass which removed any generated infrared light. The blue dye laser energy was attenuated before entering the heat-pipe to a level of around 2 μJ per pulse to inhibit Stokes generation, which would have reduced the transmitted blue energy.

A plot of the transmission of the vapour at times after the Nd:YAG pulse is shown in Figure 6.7 for both Q-switched and fixed-Q operation of the Nd:YAG laser. As for the He-Ne experiments described earlier, the transmission increases and then decays back to its steady state value as dimers reform in the vapour. Due to the long recombination time, it was found that the medium integrated the effect of all the relaxation oscillations in the

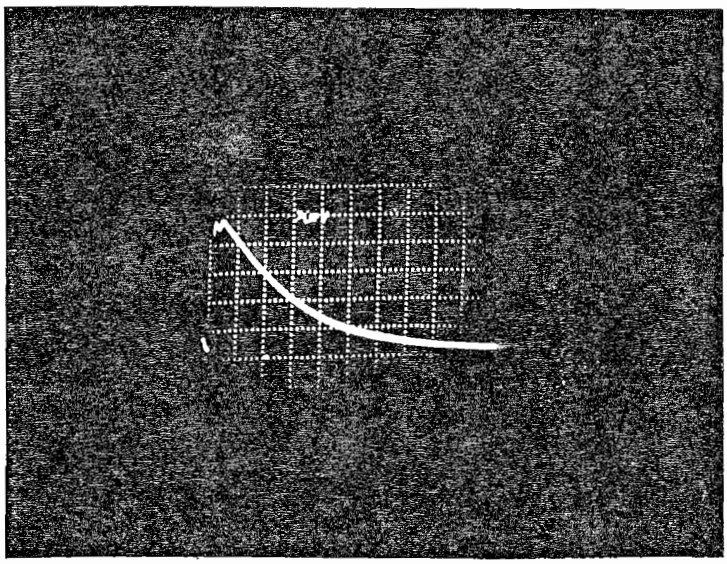

Figure 6.5 - Relative transmission of He-Ne laser through a 1 metre Caesium vapour column at times after a Q-switched Nd:YAG pulse

(Horizontal scale 200 μs/div)

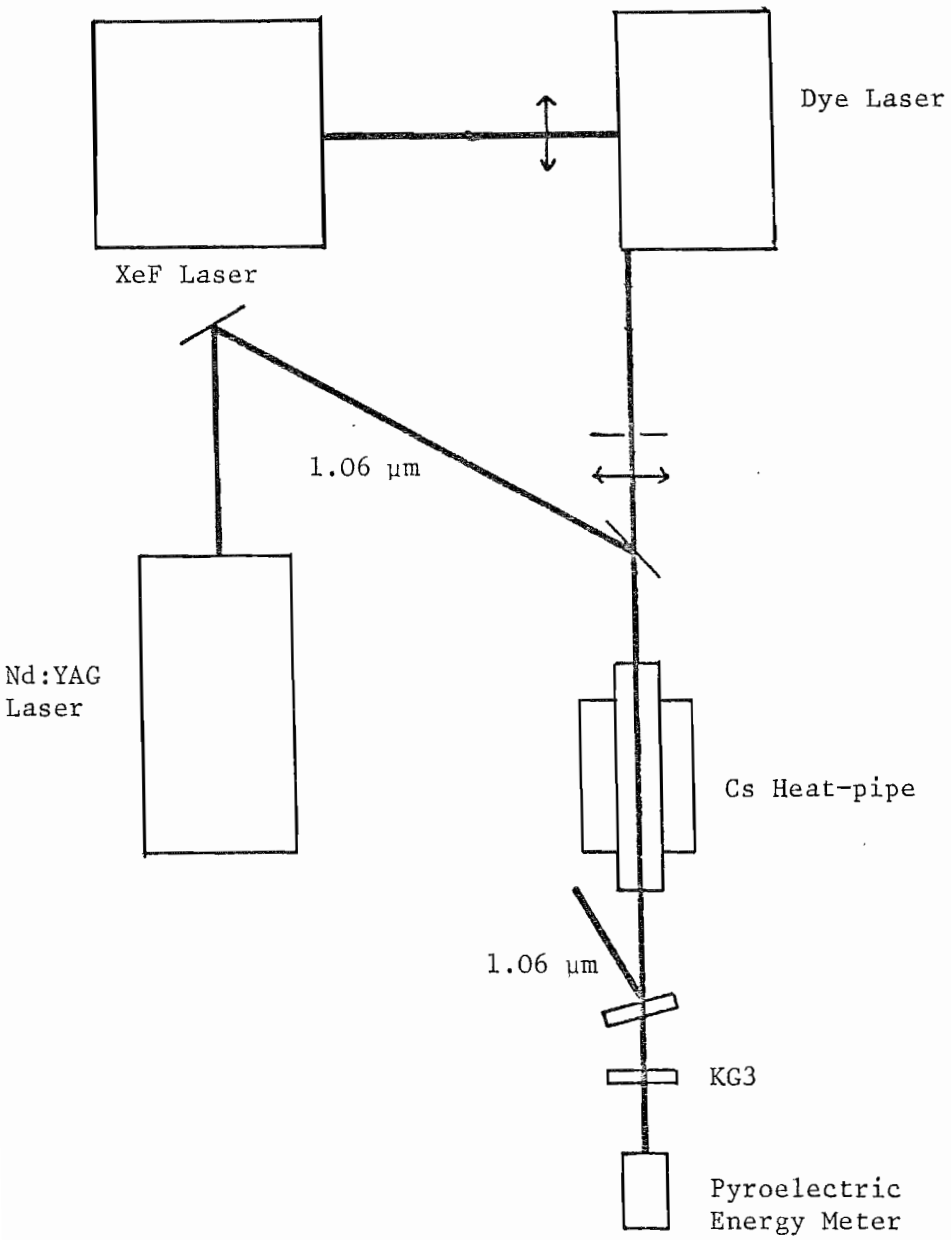

Figure 6.6 Experimental arrangement used to study the temporal behaviour and wavelength dependence of bleaching of Caesium dimers.

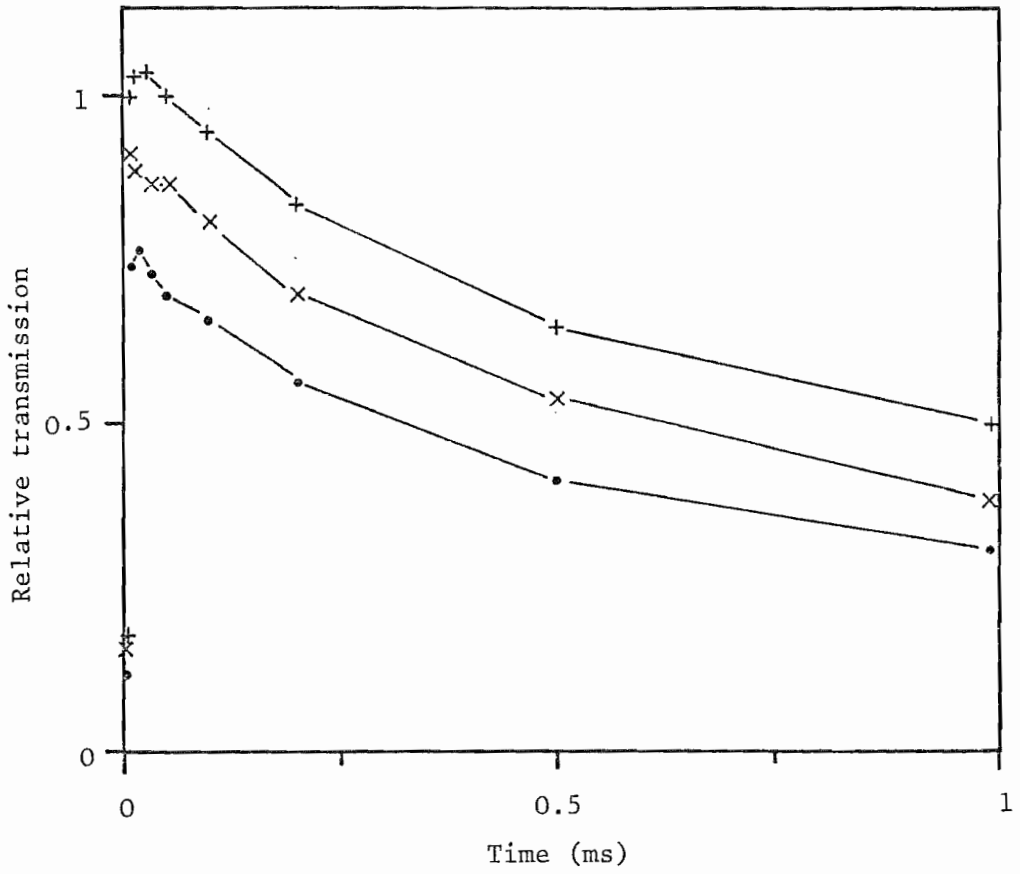

Figure 6.7a Blue transmission of Caesium vapour at times after a Q-switched Nd:YAG pulse.

. - 467 nm

x - 465.5 nm

\+ - 464.5 nm

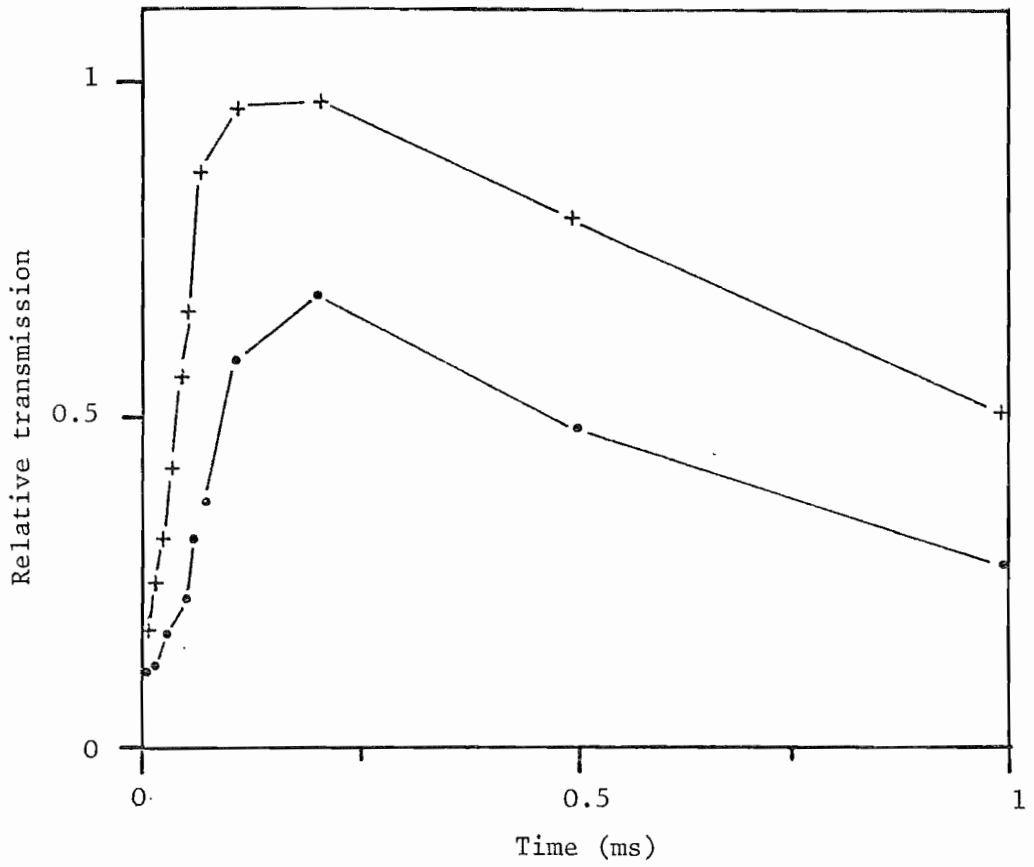

Figure 6.7b Blue transmission of Caesium vapour at times after a fixed-Q Nd:YAG pulse

. - 467 nm

+ - 464.5 nm

(Time measured from start of fixed-Q pulse train.)

fixed-Q pulse train. This gave little difference between fixed-Q and Q-switched operation, other than the time taken to reach maximum transmission. The medium responds to a large extent, therefore, to the total energy placed into it rather than to the maximum intensity.

As the dimer absorption cross-section is wavelength dependent, the effect of bleaching is dependent on the blue laser wavelength used. By performing the above experiment at several wavelengths, it was verified that the same behaviour occurred over the range which could be covered by the dye laser. The peak transmission was always reached a set time after the beginning of the Nd:YAG pulse. For fixed-Q operation this peak occurred at the end of the fixed-Q pulse train as may be expected. However, with the laser operating Q-switched, the maximum was reached approximately 25 μs after the pulse. Initially this was thought due to non-coaxial misalignment of the two laser beams within the vapour. However, this was found not to be the case. Misalignment varied this delay only slightly; a minimum delay of 25 μs was found to correspond to perfect alignment. This effect could be due to absorption by excited Caesium atoms formed by the bleaching process. The full transmission is only achieved when these have decayed back to the ground state.

Comparative wavelength measurements of the transmission were made by setting the delay between the lasers to correspond to the time of maximum vapour transmission. By tuning the dye laser wavelength while monitoring the transmitted blue energy, an absorption spectrum could be produced. The output from the pyroelectric energy meter was fed into a Brookdeal sampling gate and the output of this was displayed on a chart recorder. Typical bleached and unbleached transmission curves are shown in Figure 6.8. The short wavelength end of these curves drops off, reflecting the falling output energy of the dye laser near the limit of its tuning range. The long wavelength transmission is somewhat lower than that at short wavelengths as the dimer absorption cross-section is higher for longer wavelengths. The absorption of the dye laser by the atomic 7p doublet is clearly seen. The improvement in transmission obtained by this technique is marked.

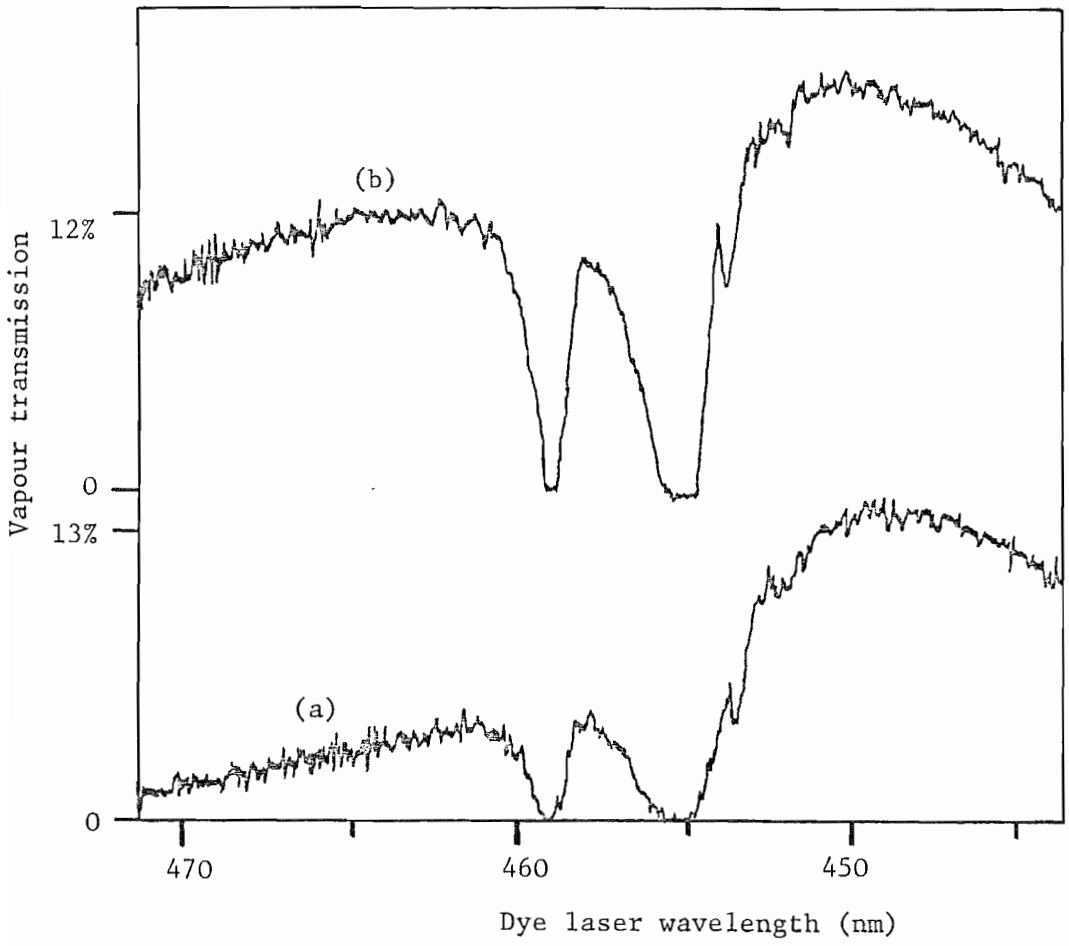

Figure 6.8 Bleached and unbleached transmission of Caesium vapour.

(a) unbleached

(b) bleached by fixed-Q Nd:YAG laser

As a check on the self-consistency of the measurement as a function of wavelength, the fraction of dimers removed was calculated. If the bleaching is assumed to be uniform along the length of the vapour then the transmission at wavelength λ will be given by Beer's Law:

$$T_\lambda = \exp(-N_D \sigma_\lambda \ell) \tag{6.1}$$

where N_D is the number density of dimers, σ_λ is the dimer absorption cross-section at wavelength λ, and ℓ is the cell length. By taking the ratio of the bleached and unbleached transmissions, T'_λ and T_λ, the reduction in dimer density ΔN_D is given by†:

$$\sigma_\lambda \Delta N_D = \frac{1}{\ell} \ln\left(\frac{T'_\lambda}{T_\lambda}\right) \tag{6.2}$$

Using the data from the transmission measurements in Figure 6.8, $\sigma_\lambda \Delta N_D$ was calculated and is plotted against λ in Figure 6.9. For comparison, a curve of $\sigma_\lambda \Delta N_D$, calculated from the absorption cross-section data of Gupta et al (1978), together with a 'best fit' value of $\Delta N_D = 5.2 \times 10^{14}$ cm^{-3}, has been also added to the graph. The figure shows the increase in transmission to be a genuine manifestation of dimer reduction.

6.2.2 SERS Output with Prior Nd:YAG Bleaching

The reduction in dimer absorption observed in the experiments of the last section should lead to improved SERS performance. As the SERS pump laser is no longer strongly attenuated, the effective length defined by Equation 2.8 is increased; the total Raman gain increasing in proportion. As the molecular absorption is reduced the contribution stepwise excitation makes to ionization is also reduced.

---

† Taking this ratio allows uncertainties in the absolute transmission to be factored out. In fact the relative output energies in the two cases can in this way be used.

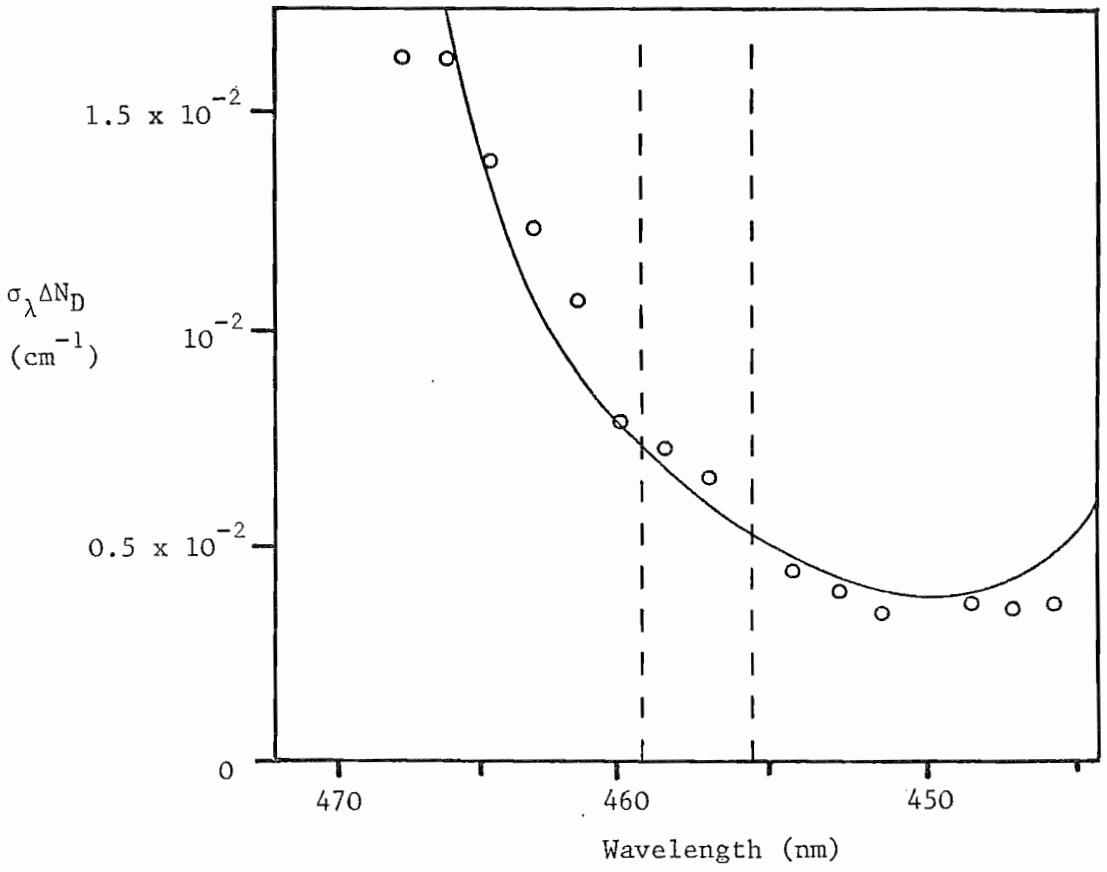

Figure 6.9 Dimer reduction by bleaching in Caesium (see text).

The arrangement used in the bleaching experiments was modified to allow a measurement of Stokes energy as a function of wavelength to be made. A 1.06 μm mirror on a CaF_2 substrate was placed after the heat-pipe to block the transmitted Nd:YAG laser light. The transmission of this mirror between 2.5 and 5 μm was roughly constant, but with some small ripples (∿10%) due to interference in the multi-layer dielectric coating. As usual, a Germanium filter was used to separate the generated infrared Stokes light from the remaining blue dye laser light. A silica plate was used at Brewster's angle to the blue dye laser beam to couple the Nd:YAG light into the heat-pipe as no suitable dielectric mirrors were available. Unfortunately this plate only reflected 30% of the incident 1.06 μm radiation along the heat-pipe axis. The reduction in dimer density was therefore somewhat less than in the previous section, and was estimated to be around 15%.

Best Stokes generation occurred at the same time delay as measured for the maximum transmission of the vapour. Figure 6.10 shows the generated infrared at several wavelengths as a function of delay after a fixed-Q Nd:YAG bleaching pulse. Measurements with a Q-switched bleaching pulse were hampered by strong ASE output at 3.49 μm. (When measurements were made in this mode of operation the 'background' signal from this $5d_{5/2} - 6p_{3/2}$ ASE could be balanced out by adding a d.c. offset to the signal derived from the pyroelectric energy meter, although this was found not to be very satisfactory.)

As with the transmission measurements, the delay was set to give optimum SERS output. The output tuning profile was observed using box car averaging and then displayed on a chart recorder. Results obtained using this laser bleaching technique in the 1 metre standard heat-pipe are shown in Figure 6.11 for a Caesium pressure of 15 torr, together with an unbleached curve. The tuning range is increased over that obtained without prior bleaching and extends a further 135 cm^{-1} into the infrared. In addition the output energy at longer wavelengths, usually hampered in this length heat-pipe by pump absorption, is improved significantly. However, the improvement is only back to that tuning range expected from a short 30 cm heat-pipe, but in view of the small reduction in dimer density

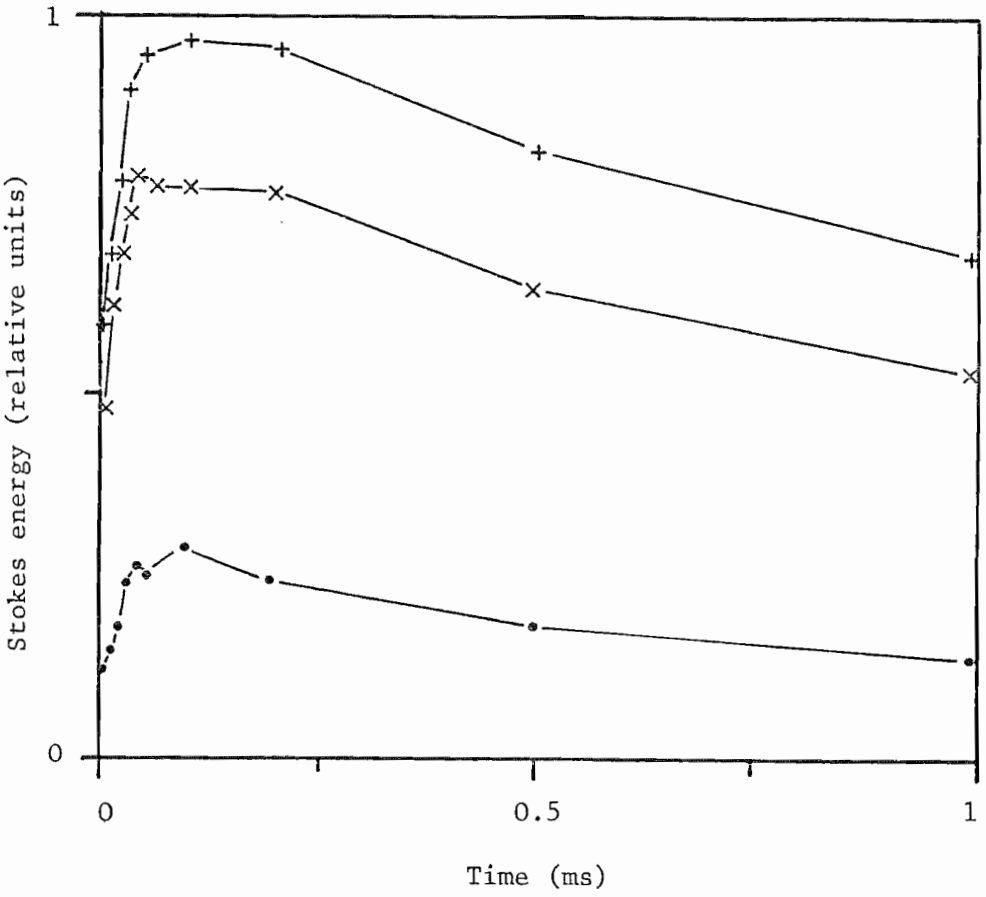

Figure 6.10 Generated Stokes signal from bleached Caesium vapour. (Time measured from start of the fixed-Q Nd:YAG pulse train.)

Stokes wavelengths . - 3.3 μm
x - 2.78 μm
\+ - 3.2 μm

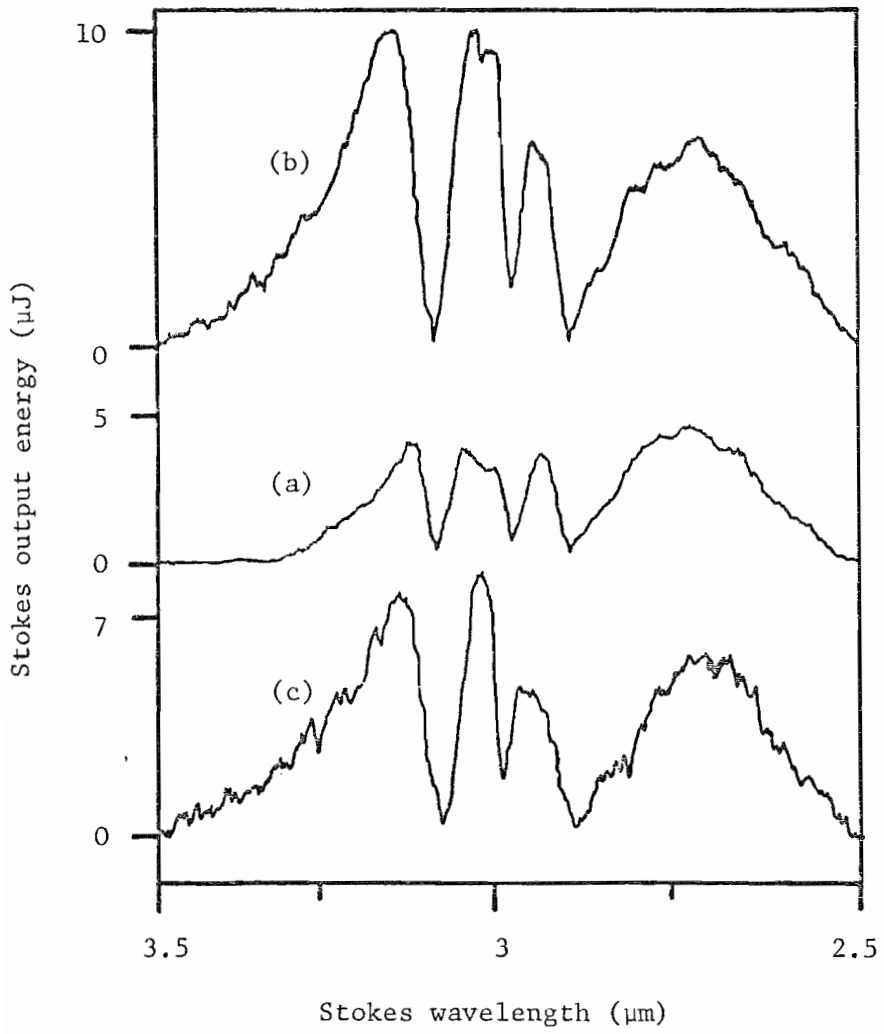

Figure 6.11 Bleached and unbleached SERS outputs from a 1 m Caesium heat-pipe

(a) unbleached

(b) bleached by fixed-Q Nd:YAG

(c) bleached by Q-switched Nd:YAG

which could be obtained in this arrangement, this is very promising. As with the measurements described in Section 6.1, the goal of wider Stokes tuning was not achieved†. Despite this, the bleaching technique has been demonstrated as a method of overcoming strong molecular absorption.

If a large amount of 1.06 μm laser energy could be deposited into the medium it is likely that the maximum available tuning of the 6s-7s transition could be realized. Coupled with a high power dye laser, a long bleached Caesium heat-pipe offers the possibility of widely tunable infrared light being produced. In such a system, the weakly focused pump laser would not give rise to a large number of intensity dependent competing effects and the output energy over most of the tuning range is likely to be limited by pump rather than atomic saturation. Unfortunately, such a system could not be assessed. As dielectric mirrors with both a high reflectivity at 1.06 μm and a high transmission in the blue were not available, the amount of 1.06 μm energy which could be placed into the medium was limited. In addition, the high power dye laser and the Nd:YAG laser were not free to be used concurrently.

6.3 The Use of a Super-heated Caesium Vapour Column

Use of a separate laser to bleach the molecular absorption, although being a viable way to increase the available 6s-7s tuning range, is far from being a simple solution. Reduction of the dimer absorption by superheating the vapour is a method that is much more reliable. This technique has been used by Wyatt and Cotter (1980) to reduce the Raman threshold on the 6s-5d transition in Caesium. They suspended a coil of heating wire along the axis of their vapour cell. Despite only having a short working life (this arrangement tends to sag into the beam path after only a few hours of use) a useful reduction of Raman threshold by a factor of 7 was observed for SERS of 565 nm, where the dimer absorption is strong.

---

† As will be discussed in Section 6.3.1, this is believed to be due to collision broadening of the Raman linewidth.

An alternative solution with a more extended lifetime is to superheat the walls of the vapour cell. This can be achieved using the split wick cell described in Section 4.3. In this cell, heat-pipe operation takes place in two 15 cm long wicks near the cool ends of the vapour column. The central 90 cm contains no wick and is heated to around 900^{o}C. This part of the cell is in thermal contact with the vapour which therefore attains this elevated temperature. In this region, the equilibrium partial pressure of Caesium dimers is reduced compared to that of a saturated vapour. Two short regions of saturated vapour remain at the ends of the vapour column, but the total integrated dimer absorption over the vapour is much less than that which is present in a normal heat-pipe cell of the same length.

Smith (1982) has performed a computer analysis of this type of superheated split wick pipe. The predicted transmission at the He-Ne wavelength of 632.8 nm, for typical operating conditions, is 14%, which can be compared to the negligible transmission (10^{-12}%) through 1 m of normal saturated vapour. The transmission measured using an unfocused He-Ne laser was 6%. This figure is slightly lower than expected. However, the low level transmission at 532 nm, where the absorption cross-section is a minimum, was 54%. Here the major attenuation was found to be scattering from Caesium dust, transported by the vapour in the transition regions at the ends of the vapour. Correcting for this neutral density 'fog', the He-Ne laser transmission is closer to 11% in good agreement with the theoretical prediction. This measurement, however, does not convincingly show that the vapour cell is operating as intended. If the high Caesium dimer density regions at the ends of the cell are longer than expected from theory, and if the central region contains no Caesium vapour, the same result could ensue. Only an additional direct measurement of the integrated atomic Caesium density-length product will verify correct operation. A method by which this measurement was performed using electric quadrupole transitions will be discussed in Section 6.4.

6.3.1 SERS Output from the Superheated Cell

Using the technique of Section 6.4, it was confirmed that the transmission of the long superheated pipe was consistent with that expected for the vapour. Following this, SERS behaviour on the 6s-7s transition was studied in this vapour cell. With the high energy dye laser focused confocally over the vapour, the long wavelength tuning profile shown in Figure 6.12 was obtained for an input of ∿1 mJ. The SERS output fell below 0.01 μJ per pulse at a Stokes wavelength of 4.2 μm, defining an end to the useful available tuning. A peak output energy of nearly 70 μJ occured at 3.25 μm and corresponds to a good photon conversion efficiency of over 30%. The output tuning is seen as a welcome extension to that obtainable from a normal heat-pipe using the same dye laser input energy.

In addition to the SERS output, an ASE output was observed. Using a monochromator this was found to be due to 5d-6p relaxation at 3.47 μm. The maximum ASE output occured when the dye laser was tuned to 467 nm, where the Stokes output has the same wavelength as the ASE. Initially, it was thought that the ASE was 'seeding' the SERS. However, the large ASE output remained even when the Stokes wavelength was tuned away from this ASE wavelength. Referring to the partial poential curve of the Caesium dimer (shown in Figure 4.8), it can be seen that the absorption around 460-490 nm arises from exciting ground state molecules to a dissociating state. Molecular fragments comprise one ground state atom and one atom excited to the 5d levels; from this state the atom decays emitting at 3.47 μm. Away from this wavelength, the SERS process is generally improved with the superheated vapour column. If a comparison is made with the 30 cm heat-pipe, several distinct advantages of this superheated cell are apparent.

(i) The molecular absorption in the superheated pipe is reduced while maintaining a useful atomic number density.

(ii) The loose focusing which can be used with a long pipe, allows a reduction in the overall pump intensity. Competing processes such as two photon ionization will not occur so readily.

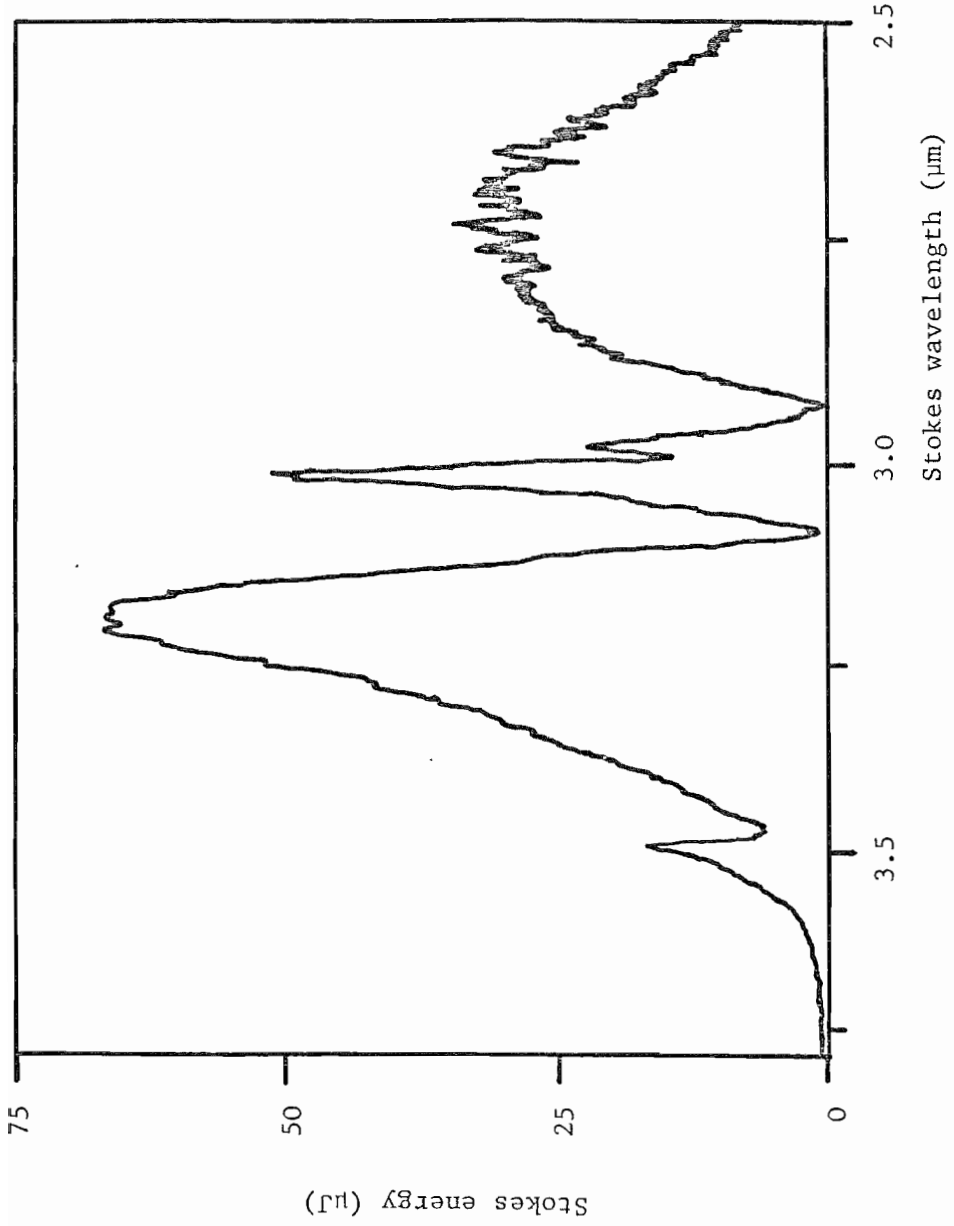

Figure 6.12 6s–7s SERS output from the superheated split-wick vapour cell

(iii) The greater length of vapour allows highly efficient generation of Stokes radiation; when operated at reduced pressure (~5 torr) the cell has produced Stokes outputs in excess of 100 μJ from 1.5 mJ of dye laser input. This is in contrast to a 1 m long standard heat-pipe, in which the molecular absorption leads to substantially lower output energy and a diminished tuning range.

The previous work of Cotter (1976) and Wyatt (1976) left the suggestion that if the dimer population could be reduced to a sufficient degree, the SERS process would ultimately be limited by the Doppler broadened Raman linewidth. The predictions which they made upon this assumption, suggested that SERS on the 6s-7s transition in Caesium would be capable of vastly improved performance. The transition linewidth and thus the Raman gain is likely, however, to be ultimately limited by collision broadening as discussed in Section 2.3. The tuning range which can be obtained using dye lasers having peak powers of around 200 kW, has been calculated using linewidth broadening coefficients similar to those suggested by Sayer et al (1971) for the 6s-5d transition. If such values are applicable, the tuning range will not be significantly larger than that obtained in this work. Using $\gamma_c = 6 \times 10^{-19}$ cm^3 cm^{-1} Stokes light on the 6s-7s Raman transition will tune over the approximate range 2-4.2 μm. The long wavelength limit has been reached. In the next section an investigation of the short wavelength limit will be discussed.

6.3.2 Short Wavelength Production on the 6s-7s Transition

During the work with high pump laser energies, it was found that the short wavelength tuning limit (2.33 μm) was set not by the process but rather by the output tuning range of the 7D4MC dye laser. It was therefore decided to use a shorter wavelength dye; namely Coumarin 120, which emits light over the range 424 nm to 460 nm.

The dye laser was pumped by the XeF laser with the same focusing conditions as for 7D4MC. The dye concentration which gave optimum beam quality was found to be 2.5×10^{-3} Molar for both the dye oscillator and amplifier. This gave output pulse energies

of around 180 μJ from the oscillator and between 0.7 and 1.0 mJ from the oscillator/amplifier combination. This laser was focused into the long superheated cell under the same conditions as in the previous section.

The typical output energy is shown in Figure 6.13 against Stokes wavelength. Continuous tuning of the Stokes output from 2.08 μm to 2.93 μm was obtained with the dye laser tuned to this side of the $6s-7p_{3/2}$ transition. The maximum output energy of 22 μJ occurs around 2.7 μm and was generated from a dye laser energy of 0.7 mJ. Allowing for the Fresnel reflections of the heat-pipe windows and the focusing lens (f = 50 cm), the peak photon conversion efficiency was η = 20%.

An infrared Stokes output of greater than 1 μJ was obtained over the entire range 2.4 μm to 2.9 μm, a total of over 700 cm^{-1}. SERS on the 6s-7s transition using a Coumarin 2 dye laser is seen to offer a useful extension to the infrared output which can be generated from a 7D4MC dye laser. The wide continuous tuning makes this a practical source for spectroscopy and photochemistry in this wavelength region.

An extension of this tuning to shorter wavelengths may be expected with the application of a yet higher power dye laser. The effect of dimer ionization on the Raman gain is likely to be smaller at these wavelengths than at the long wavelength tuning limit. It is therefore, unlikely to be a restriction on the short wavelength limit.

6.4 The Use of the 6s-6d Transition to Measure Caesium Density

In Section 6.3 the problem of verifying that atomic Caesium is present throughout the length of the vapour cell became apparent. A method by which the integrated number density-length product of atomic Caesium can be measured using electric quadrupole (E2) transitions is now presented. This procedure has been used to ensure correct operation of the 1 m long superheated split wick vapour cell.

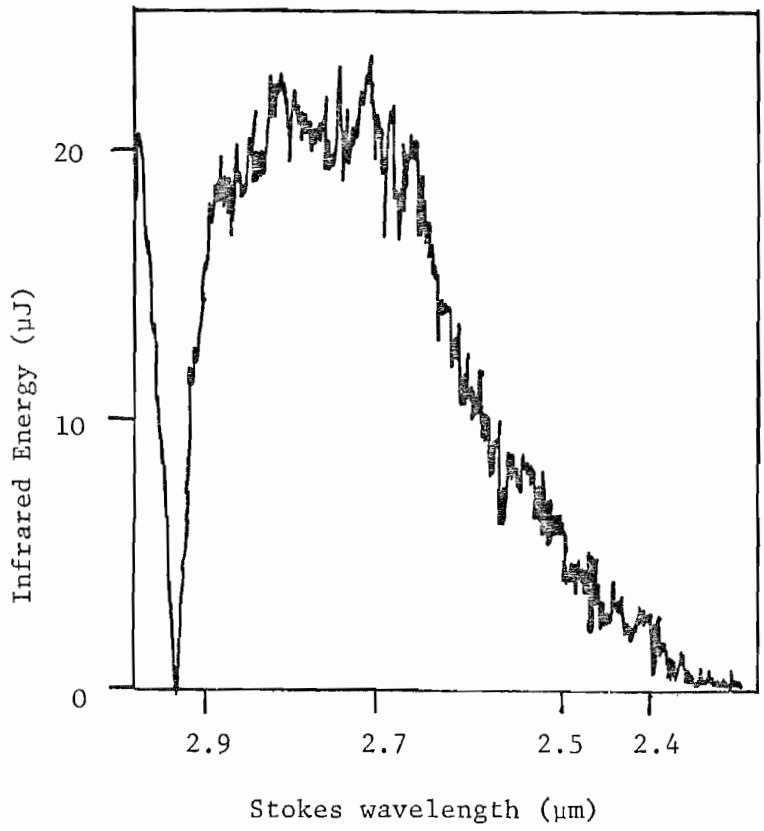

Figure 6.13 Short wavelength production on the 6s-7s transition

The weak electric quadrupole 6s-5d and 6s-6d transitions in Caesium have been considered experimentally as well as theoretically by several authors (see Sayer et al (1971) and references therein). Recently, values of the transition probabilities have been determined by Sayer et al (1971) and Glab and Nayfeh (1981), who both used optical methods. Their results agree well with both their theoretical predictions as well as those of Warner (1968). Using these values, the oscillator strengths of the transitions can be calculated, and are given in the following table

Lower State 1	Upper State 2	f_{12}
6s	$5d_{5/2}$	5.04×10^{-7}
6s	$5d_{3/2}$	3.28×10^{-7}
6s	$6d_{5/2}$	2.10×10^{-7}
6s	$6d_{3/2}$	1.41×10^{-7}

These oscillator strengths, taken in conjunction with the collision broadening coefficients measured for the 6s-6d transitions by Sayer et al, allow the absorption profile of a vapour column around these transitions to be determined. In their approximation this profile is a Lorentzian of linewidth $\Gamma_A = \gamma_c N_A$ as was discussed with relevance to SERS in Section 2.3. The transmission of the vapour column as a function of detuning Δ from line centre in this approximation will be given by

$$T(\Delta) = \exp[-\beta(\Delta)\ell] \tag{6.3}$$

where ℓ is the vapour column length and $\beta(\Delta)$ is the absorption per unit length at detuning Δ, given by

$$\beta(\Delta) = 2\pi^2 r_e c N f_{12} \cdot \frac{\Gamma_A}{\pi(\Gamma_A^2 + \Delta^2)} \tag{6.4}$$

N is the atomic number density and Γ_A is the convolution of the Doppler and collision broadened linewidths $(\Gamma_D^2 + \Gamma_c^2)^{\frac{1}{2}}$.

If, for simplicity, a Lorentzian laser spectrum is also assumed, and the peak of the laser profile is taken to be tuned to the peak of the absorption, the normalized laser spectrum will be given by

$$S(\Delta) = \frac{\Gamma_L}{\pi(\Gamma_L^2 + \Delta^2)} \tag{6.5}$$

where Γ_L is the laser linewidth (HWHM). The vapour transmission expected for the laser under these circumstances is

$$T = \int_{-\infty}^{\infty} S(\Delta)T(\Delta)d\Delta \tag{6.6}$$

i.e. the integrated fraction of the power input to the vapour which leaves it.

The integral of Equation 6.5 has been performed numerically for the $6s\text{-}6d_{5/2}$ transition. The linewidth substituted for Γ_L was 0.08 cm^{-1} (HWHM); namely that measured for the dye laser with an air-spaced Fabry-Perot interferometer. The collision broadening coefficient was taken as the mean value of those given by Sayer et al; viz 8×10^{-19} $cm^3 cm^{-1}$. The value of the calculated transmission is given in Figure 6.14 as a function of atomic number density. As can be seen the curve is quite steep at number densities of around 10^{17} cm^{-3}, making this a useful measure of the atomic number density for pressures of 1-100 torr. For comparison, curves of transmission are presented for two lengths of vapour column, namely 30 cm and 1 m, as well as for a 1 m cell with the laser tuned to the $6s\text{-}5d_{5/2}$ transition.

Absorption of light by excitation of ground state atoms to the 6d levels was observed using an attenuated blue Coumarin 2 dye laser. This laser was slowly tuned between 443 nm and 441 nm while monitoring the blue laser energy leaving the 1 m superheated vapour cell. Two narrow absorptions were observed as expected; the absorption spectrum is shown in Figure 6.15. Taking the transmission between the two narrow dips to be 100%, the on-resonance

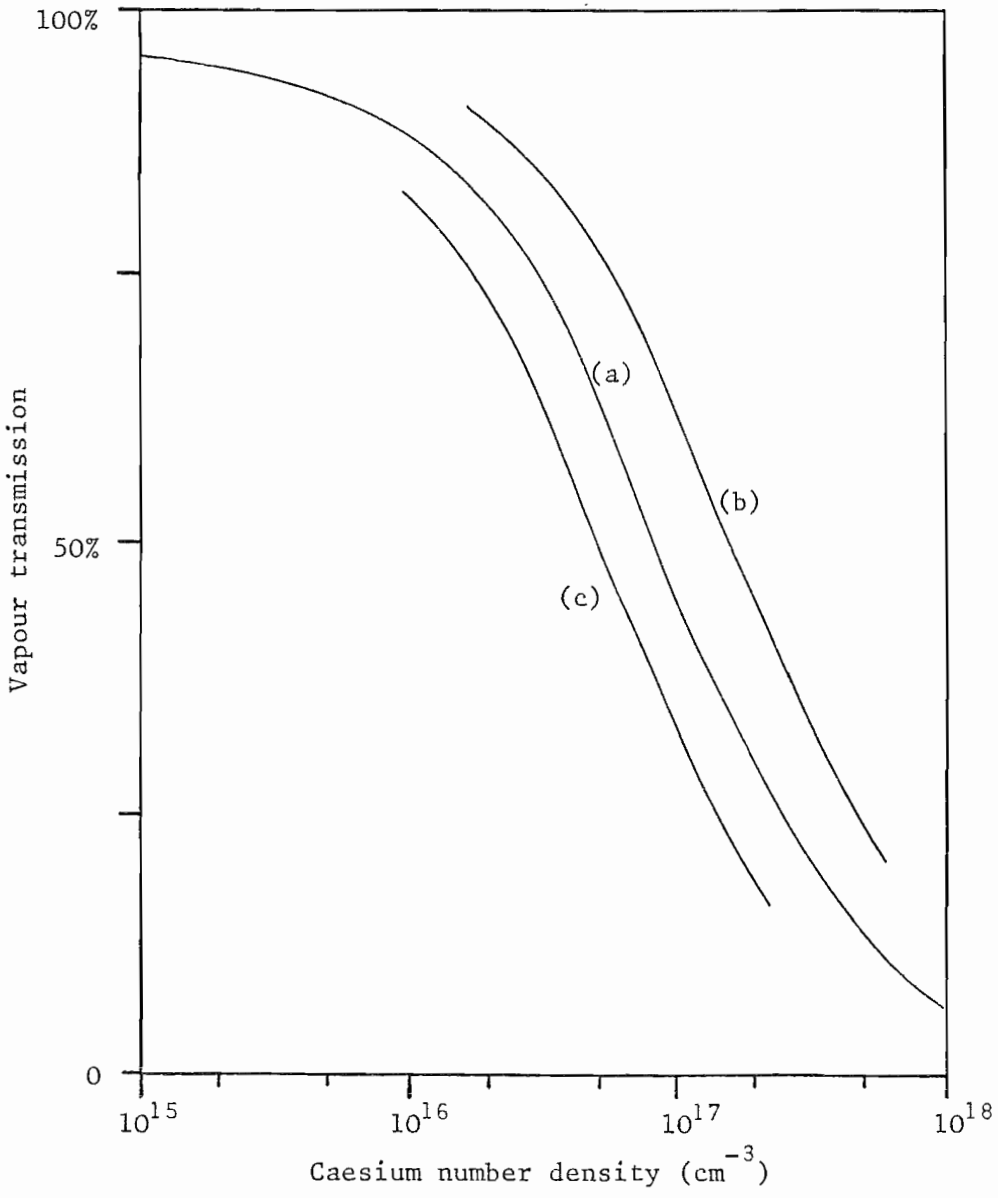

Figure 6.14 Transmission of laser tuned to electric quadrupole transitions in Caesium vapour.

(a) $6s\text{-}6d_{5/2}$; 100 cm vapour column

(b) $6s\text{-}6d_{5/2}$; 30 cm vapour column

(c) $6s\text{-}5d_{5/2}$: 100 cm vapour column

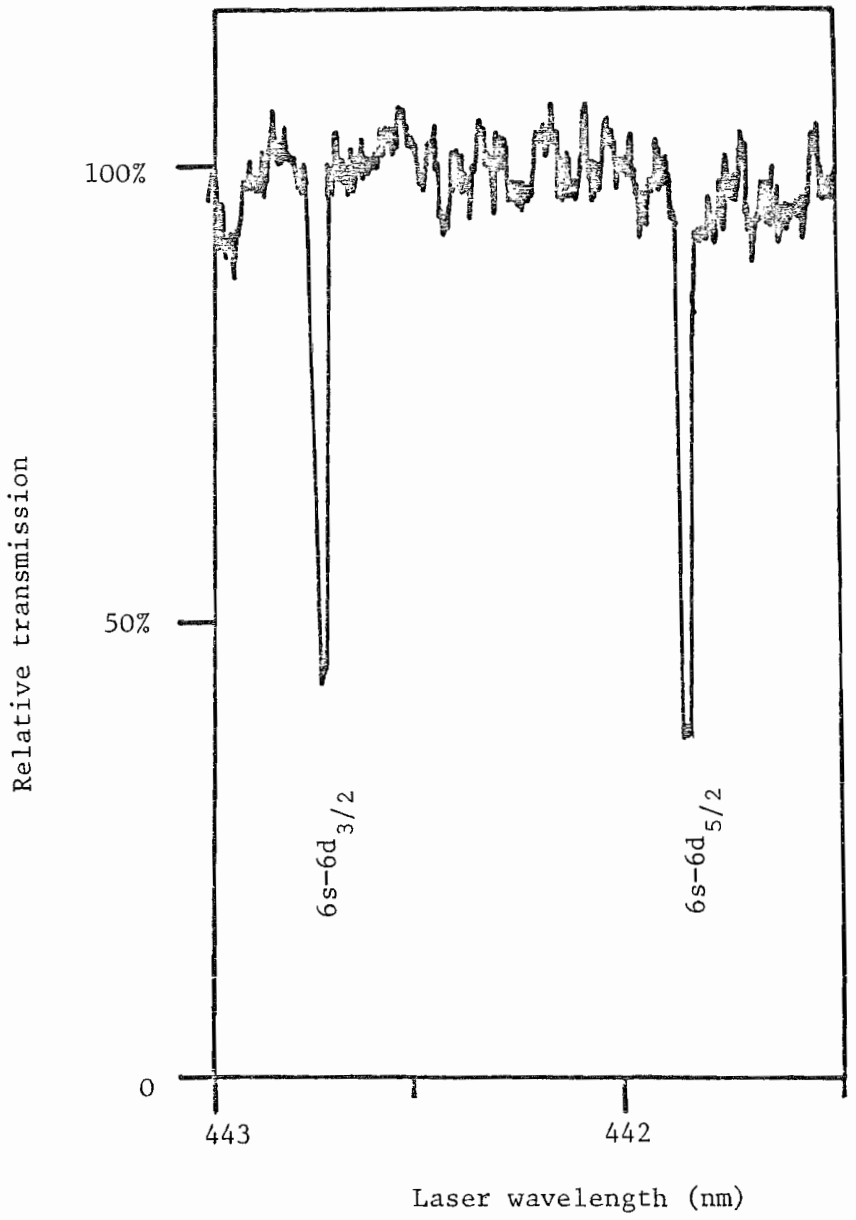

Figure 6.15 Transmission of Caesium vapour near 6s-6d electric quadrupole resonances (see text)

transmission of the $6s-6d_{5/2}$ transition is seen to be 35%. From Figure 6.14, this corresponds to an atomic number density of 1.6×10^{17} cm^{-3}. This can be compared to a number density of 1.57×10^{17} cm^{-3} calculated using the measured heat-pipe pressure of 20 torr and a superheated vapour temperature of 1230 K.

The agreement between the measured and predicted transmissions both of the atomic and molecular species verifies the assumption that the long superheated vapour cell is operating as expected. In principle, this technique can be used with all quadrupole transitions in the alkali metal vapours and therefore provides a method of verifying correct operation of vapour cells for all such materials. Care must be exercised in choosing the value of number density assumed for a superheated cell. This will depend on the superheated temperature as well as the operating pressure.

6.5 SERS on the $6s-5d_{5/2}$ Transition

The use of the 6s-5d Raman transition in Caesium to generate tunable infrared light is interesting for many reasons. The 5d level is the lowest lying state in the alkali atom which can be used as a final Raman level. Unlike the higher lying 6s-ns transitions (n = 7, 8, 9), which require a blue or ultraviolet pump laser, the 6s-5d transition offers the possibility of efficiently Raman shifting dye lasers which operate between 500 nm and 675 nm into the medium infrared (2-20 μm).

The energy level diagram (Figure 4.4) shows that lasers in the above wavelength range are not resonant with any single photon transitions. The Raman gain, therefore, will be rather small due to the lack of resonance enhancement. However, as will be seen in the next section, this means that it will be a slow function of the pump laser wavelength. It is to be expected that wide uninterrupted Stokes tuning will be obtained on this transition if threshold can be exceeded.

In the following sections the measurement of the Raman threshold for 532 nm light will be discussed. The result of this will be compared with the threshold predicted using the ideas of section 2.3

on collision broadening of the Raman linewidth. In earlier work this comparison was not made; (Wyatt (1976), Tuttlebee (1977)). A Raman linewidth, empirically determined as around 1 cm^{-1}, was previously used for calculating Raman gains and predicting threshold powers.

The viability of the 6s-5d scheme with a fixed frequency laser was first demonstrated by Hodgson (1979). Using a frequency doubled multimode Nd:YAG laser focused into a 1 m vapour column with a 1 m focal length lens, he measured a threshold energy of 2 mJ in a 10 ns pulse. The 532 nm light was found to undergo SERS at best for a broad range of Caesium pressures around 40 torr. A conversion efficiency of 7% from 532 nm to 2.38 μm was noted. The threshold was also found to remain essentially unchanged when the linewidth of the 532 nm light was changed from < 0.005 cm^{-1}, 0.5 cm^{-1} (HWHM).

Despite success with 532 nm light, Hodgson was unable to exceed Raman threshold with 7.5 mJ of 601 nm light from a Rhodamine B dye laser/amplifier combination. Unlike 532 nm, which lies in a minimum of the molecular absorption spectrum (see Figure 4.8), 601 nm is heavily absorbed by dimers. For the particular vapour cell length and focusing conditions chosen by Hodgson, it would be very difficult to bleach the dimer absorption as the number of illuminated dimers is roughly equal to the number of pump laser photons.

Wyatt and Cotter (1980) measured the Raman threshold for a range of pump wavelengths between 477 nm and 541 nm. Like Hodgson, they found a minimum threshold energy of 1.5 mJ in a 7.5 ns pulse at 531 nm, the wavelength at which the minimum of the dimer absorption occurs. The threshold energy was again found to be nearly constant for Caesium vapour pressures in the range 30-90 torr. The threshold was found, unlike Hodgson's results, not to remain constant with dye laser linewidth. A factor of over 3 increase in threshold, from 1.5 mJ to nearly 5 mJ was observed to occur when the laser linewidth was increased from 0.03 cm^{-1} ($\sim$ two longitudinal modes) to 4 cm^{-1}. In this work they also found that up to a seven fold reduction in threshold could be achieved for wavelengths at which molecular absorption is strong, by superheating the vapour.

The experiments described in the following sections were largely performed in a long superheated vapour cell. This was used as it allowed the advantages of loose focusing and low dimer concentration. It is hoped that future experiments in this type of cell will investigate the tuning behaviour of SERS on the 6s-5d transition.

6.5.1 Calculation of the Raman Threshold Pump Power

In this section, the evaluation of the Raman threshold for a pump laser of wavelength near 532 nm is discussed. The effect of collision broadening of the final Raman level is included. This makes the Raman gain, and therefore the Raman threshold, essentially independent of the atomic number density, as may be expected from the discussion of Section 2.3. Threshold powers for SERS have been calculated, making allowance for the diffraction loss and gain focusing of the Stokes light.

The Raman gain coefficient for SERS on the $6s\text{-}5d_{5/2}$ transition is given by Equation 2.4 . Using radial matrix element data taken from Eicher (1975) and transition frequencies from Moore (1958), the coefficient is readily calculated. For this work, the summation was performed over the first six atomic p states. For pressures above 1 torr, collision broadening dominates over the Doppler width and so N/Γ_R in Equation 2.4 may be replaced by the collision broadening coefficient, γ_c^{-1} (see Section 2.3). This coefficient is quite well known for 6s-5d absorption (Sayer et al (1971)) and it can be argued that the same coefficient may be used for 6s-5d SERS.

For confocal focusing, Equation 2.14 predicts the gain-length product which would be necessary for the Stokes wave to reach detector threshold. The threshold power has been calculated using the lower value of the limits placed on γ_c by Sayer et al and is shown in Figure 6.16 for a range of pump laser wavelengths between 500 nm and 650 nm. For a peak laser power of 750 kW, Figure 6.16 shows that continuous tuning from 2 to 10 μm should be obtained in the absence of competing effects, such as molecular absorption and multiphoton ionization of the atoms and molecules. Production

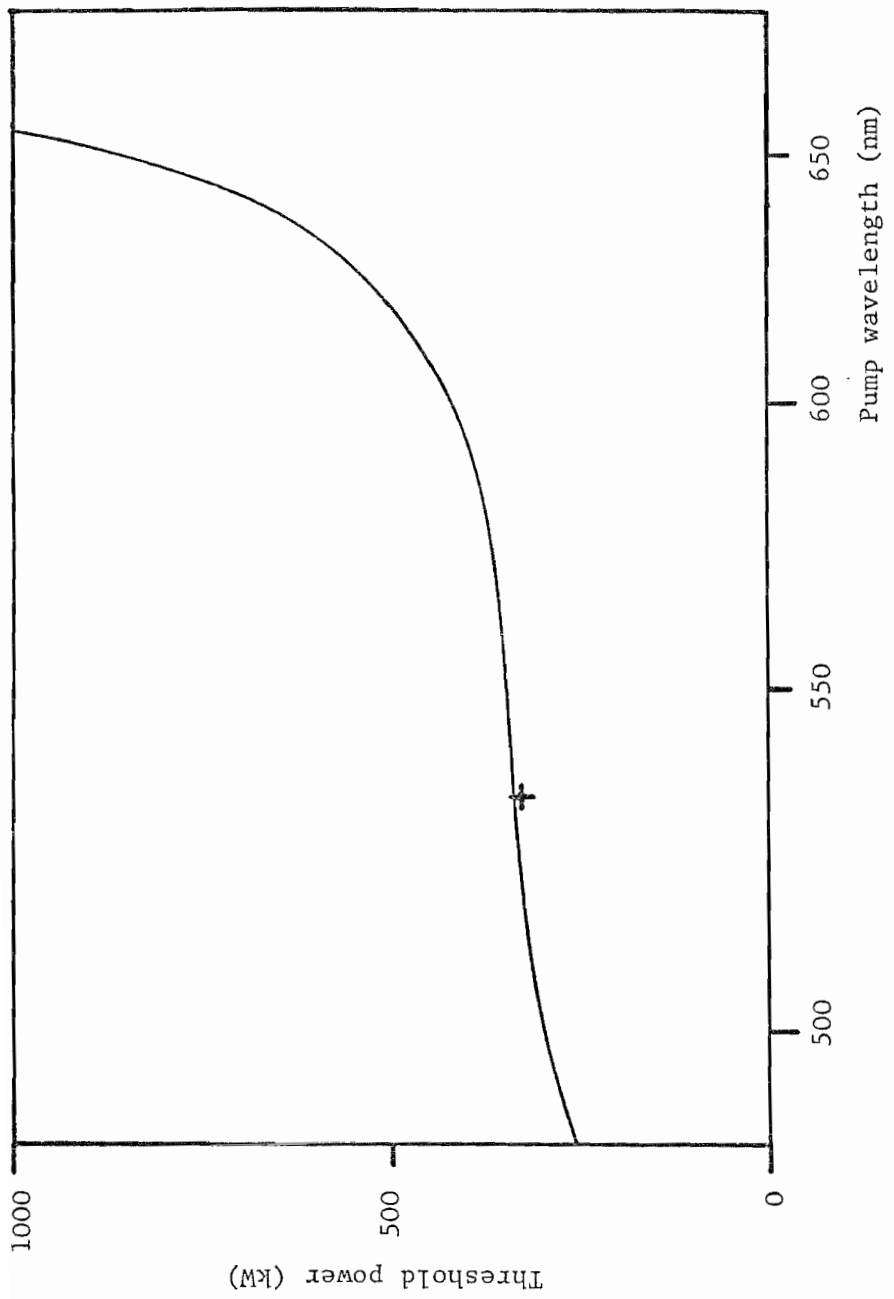

Figure 6.16 Calculated $6s-5d_{5/2}$ Raman threshold power for $\gamma_c = 6 \times 10^{-19}$ cm^3 cm^{-1}
(+ - this work; single mode result)

of light beyond 10 μm will be restricted by increasingly severe diffraction of the generated wave.

The work described here is limited to SERS of 532 nm light only. As this wavelength lies in a deep minimum of the molecular absorption, SERS of 532 nm will be largely unaffected by molecular effects. The use of this wavelength allows a comparison to be made between experimental Raman threshold and theoretical prediction. For such a pump laser g_R is expected to have a broadening limited value of 2.55×10^{-9} cm W^{-1}, and the threshold pump power is predicted to be 340 kW. For a laser pulse containing only a few laser modes, the Raman linewidth is much broader (typically 0.1 to 1 cm^{-1}) than the laser bandwidth of around 0.01 cm^{-1}, and so the medium is able to follow the field envelope of the laser pulse. Raman threshold will be exceeded if the peak power of the pulse exceeds the threshold power. For a 22 ns long single mode laser pulse, this peak power is equivalent to a total pulse energy of 8 mJ.

The Raman threshold at 532 nm has been investigated at several laser bandwidths. These measurements will be discussed in Section 6.5.3.

6.5.2 Single and Two Mode Operation and the Effect of Second Harmonic Generation

Before considering the experimental measurement of Raman threshold, it is apt to estimate the effect which laser mode beating will have on the value of measured threshold energy. This will allow some account to be made of the effect of using a multimode pump laser. In this section, the expected reduction in threshold when the laser operates on two longitudinal modes is calculated. Firstly, however, the relationship between single mode peak power and pulse energy will be established.

A single mode pulse from a frequency doubled Nd:YAG laser has a near Gaussian temporal profile. A typical 532 nm pulse from the slow Q-switched laser developed at Southampton University has a duration $\tau_{\frac{1}{2}}$ (FWHM) of 22 ns. The instantaneous power P(t)

at time t, may be written as

$$P(t) = P_o \exp\left[-4\ln 2 \frac{t^2}{\tau_{\frac{1}{2}}^2}\right] \tag{6.7}$$

where the peak power of the pulse P_o occurs at t = 0. By integrating the power P(t) over all time, the total pulse energy E_p is found to be

$$E_p = \frac{1}{2}\left[\frac{\pi}{\ln 2}\right]^{\frac{1}{2}} P_o \tau_{\frac{1}{2}} \tag{6.8}$$

Given the total single mode pulse energy measured in an experiment, the peak power of the pulse can be found using

$$P = 0.939 \frac{E_p}{\tau_{\frac{1}{2}}} \tag{6.9}$$

allowing direct comparison of measured energy with predicted threshold power.

The comparison of the experimental and expected thresholds for two mode operation of the laser is complicated by the semi-random behaviour of the mode powers. Fluctuations in the relative electric fields of two beating modes can lead to significant changes in the peak value of the pulse power. An attempt will now be made to predict the effect of this randomness on the measured value of Raman threshold and therefore the expected reduction in threshold for two mode operation.

When two consecutive laser modes with fields E_1 and E_2 beat together, they give rise to an average intensity proportional to $(E_1^2 + E_2^2)$. Superimposed upon this is an oscillating term, $2E_1E_2\cos\delta t$ where δ is the inter-mode spacing. The modulation depth arising from this second term can be expressed by a parameter k

$$k = \frac{2E_1E_2}{E_1^2 + E_2^2} = \frac{2\alpha}{1 + \alpha^2} \tag{6.10}$$

and is just the ratio of the modulation amplitude to the average intensity. The variable, α, introduced here is the ratio of the two (separate) mode fields; $\alpha = E_2/E_1$. The peak intensity present during the pulse will be greater than the single mode peak intensity by a factor 1 + k. Given a fixed value of k, the Raman threshold would be expected to be $(1 + k)^{-1}$ times the single mode threshold. However, the value of k depends on the relative electric fields of the two modes, which are semi-random. In order to deal with the pulse to pulse distribution of these two electric fields, the frequency selecting contributions of the laser components must be considered.

The effect of frequency selective elements in the Nd:YAG laser used has been studied by Hanna (private communications (1981)) and Sawyers (1981). For the case of a slow Q-switched laser with an internal etalon, they define a fractional selectivity per round trip of the laser cavity as

$$\varepsilon = 2\left[\frac{2\Delta_L F_E}{\Delta_E}\right]^2 \qquad (6.11)$$

where Δ_L is the free spectral range (FSR) of the laser and Δ_E and F_E are the FSR and finesse of the etalon. For small values of ε ($\varepsilon << 1$), the fraction of the output laser shots for which the beating of the mode fields is characterized by $\alpha > \alpha_o$ is given by

$$R = 1 - \frac{2\ln\alpha}{\varepsilon q} \qquad (6.12)$$

where q is the number of round trips over which the laser output builds up from noise to a detectable level. For a typical slow Q-switched laser q = 800. For the particular laser used here $\varepsilon = 8 \times 10^{-2}$ giving $\varepsilon q = 64$.

If the two mode shots are taken as those whose beating is greater than $\sim$1% of the average intensity, then 17% of the shots will be two mode. For a '1 shot in 3' threshold condition, two thirds of the two mode shots will be below threshold, and so only

5.5% of the total (one mode and two mode) shots will exceed threshold and generate an infrared output. From this, a new value of α may be determined at which the peak power in the pulse is the threshold power. The resulting value of k can then be used to find the expected reduction in threshold using the two mode laser. For R = 5.5%, a value of α = 5.98 is obtained. The reduction in threshold from Equation 6.10 is to $(1 + k)^{-1}$ i.e. 76% of the single mode value. This can be compared to the two-fold reduction that might be expected from pure two mode operation when the modes have equal fields.

To be able to compare experimental results with theoretical predictions, the effect which second harmonic generation has on the peak power of the pulse must also be considered. Most important is the relationship between the peak power incident on a doubling crystal and the generated peak power. Arguments valid for the fundamental power can be applied to the second harmonic if the frequency conversion process becomes linear in the applied power.

The behaviour of second harmonic generation is different in the small signal and large signal regimes. In the small signal case, the generated second harmonic intensity depends on the square of the fundamental intensity. However, in the very large signal case, depletion of the fundamental wave restricts the generated intensity to be proprotional to the applied intensity.

In terms of the small signal efficiency η_s the large signal conversion efficiency is given by

$$\eta_L = \tanh^2 \eta_s^{\frac{1}{2}} \qquad (6.13)$$

(Armstrong et al (1962)). For very large values of η_s the value of η_L tends to unity and the generated power becomes linear in the instantaneous applied power. As a criterion η_s = 1 can be taken to correspond to the level at which proportionality of input fundamental and output second harmonic powers can be assumed. The calculation of the input power corresponding to η_s = 1 is simple for the steady state plane wave case. Armstrong et al (1962) also dealt with the steady state conversion of Gaussian beams. For the

present work the time varying case of a single mode pulse laser was considered and the results of the required numerical integration are given by Sawyers (1981). It was found that, for the conditions of the present experiments, the generated power becomes linear in the applied power when more than 200 kW of 532 nm light is being produced. Here an 80 mJ Nd:YAG pulse having a spot-size of 0.35 mm was frequency doubled in a 2 cm long $CD^{*}A$ crystal.

As the predicted Raman threshold power of 340 kW is above 200 kW, arguments about the peak power of the fundamental are also applicable to the peak second harmonic power. The measured two mode threshold is therefore expected to be approximately 76% of the single mode power. The measurement of two mode threshold will of course be rather complicated by the fact that it is the 532 nm pulse energy and not power which is measured. A smaller contribution to this energy will be made by the light generated in the small signal, low power portions of the pulse.

6.5.3 Measurement of $6s\text{-}5d_{5/2}$ Raman Threshold

The experimental layout is detailed in Figure 6.17. A large volume TEM_{oo} mode Nd:YAG laser of the 'Hyperyag' type described by Sarkies (1980) and Hanna et al (1981), produced 82 mJ of 1.06 μm radiation in a single transverse mode from a 4" by $\frac{3}{8}$" Nd:YAG rod. Line narrowing of the laser was achieved by using a resonant reflector as an output coupler and by the inclusion of a 1 cm thick etalon of reflectivity 72% per surface in the cavity. When slow Q-switched, the laser gave reliable single longitudinal mode operation with an expected linewidth of $< 0.001\ cm^{-1}$ and a pulse energy of 80 mJ. When Q-switched in this manner, the output pulses had a near Gaussian temporal profile and were 32 ns long. The near field output from this laser was then frequency doubled in a 2 cm long Caesium Dideuterium Arsenate ($CD^{*}A$) crystal. In this way, 22 ns long 532 nm pulses of up to 15 mJ were produced, with a photon conversion efficiency of up to 19%.

After rejection of the unconverted fundamental 1.06 μm radiation by a dichroic beam splitter, the transmitted green light was focused using a f = 1 m silica lens to the centre of the

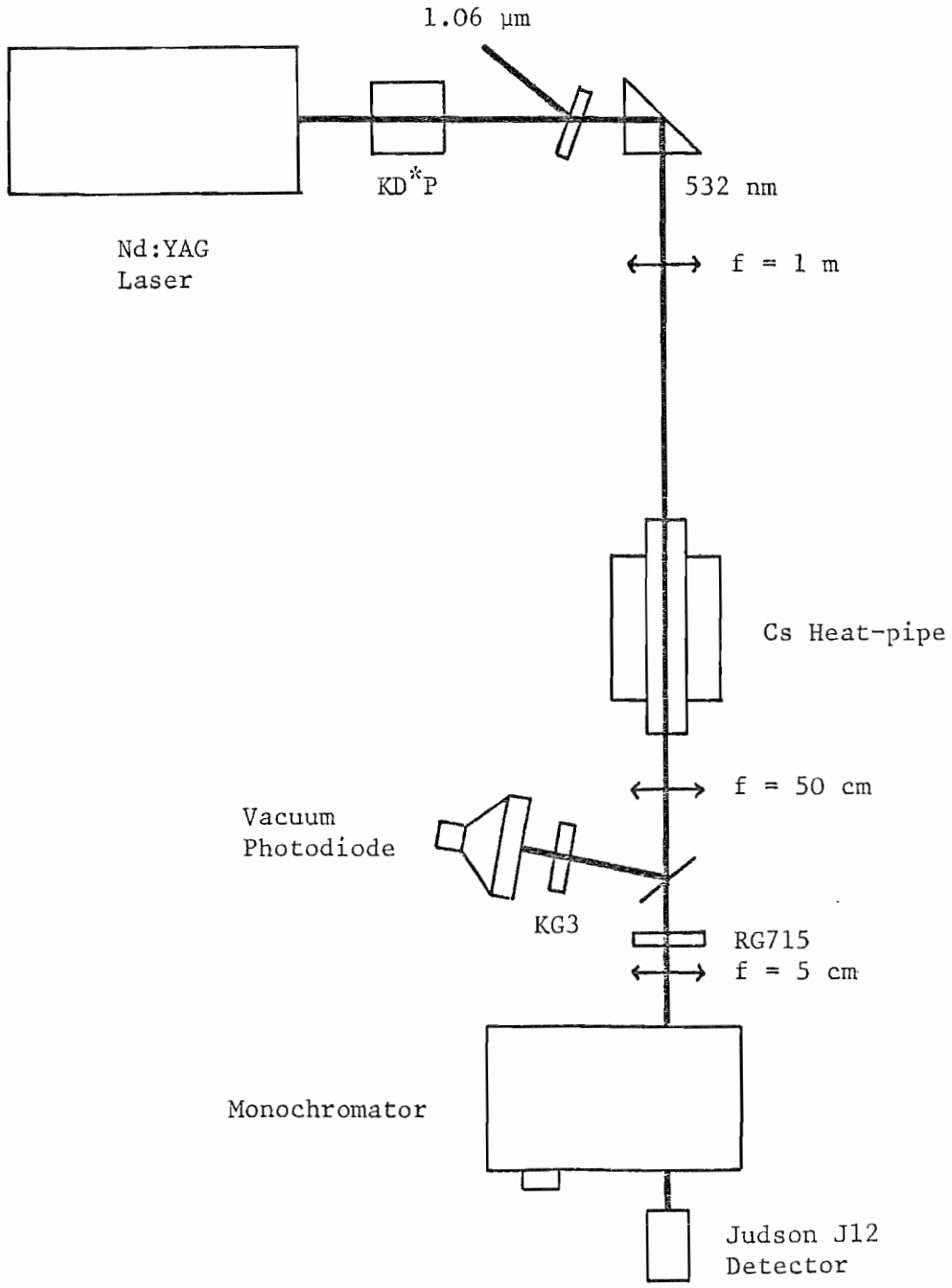

Figure 6.17 Experimental arrangement used to determine the Raman threshold on the 6s-5d transition.

1 m superheated split-wick vapour cell described in Chapter 4. The position of the lens and the optical distance from the laser output coupler to the centre of the vapour cell were chosen to ensure that the beam was focused confocally over the vapour column. The light leaving the vapour cell was filtered to remove the remaining green light and then passed through a Hilger-Watts D330 monochromator onto a room temperature photoconductive InAs detector (Judson J-12). The monochromator was set to transmit the Stokes wavelength of 2.38 μm. The signal from the detector was monitored on a Tektronix R7912 transient digitizer with a fast 50 Ω vertical amplifier plug-in (type 7A19).

Threshold measurements were performed with the laser having several bandwidths; this was achieved by altering the Q-switching arrangements. Slow Q-switched, the laser operated on one longitudinal mode, but by suitable misadjustment of the intracavity etalon, mainly two mode operation could be obtained for periods of up to 10 seconds. For larger bandwidths the laser was fast Q-switched, in which case the laser output consisted of 3-5 modes with the internal etalon and around 12 modes without the etalon (Sawyers, private communication (1981)). These larger bandwidth measurements are included as they represent the typical results that may be obtained with a multimode laser, such as that used by Hodgson (1979). However, these cannot be taken as very meaningful, as only a single mode threshold can be compared with theoretical predictions (see Section 2.4). Some feel for the relationship of the multimode to the single mode threshold can be obtained from the following considerations.

In principle, the peak intensity reached during a laser pulse can be as much as N times the single mode value, where N is the number of modes present in that pulse. This assumes that all modes can lase in phase with equal shares of the output energy, whereas in general this will not be the case. It is more realistic to say that, for example, one half of these modes have an appreciable power. As the phases of the modes are independent, the peak power is expected to be of the order of $(N/2)^{\frac{1}{2}}$ times the single mode peak. The reduction in threshold power is likely to be small and around 50% for a laser operating on 12 modes. This argument can be

extended to include the effect of second harmonic generation in producing the 532 nm pump light.

The vapour cell was run at a temperature of 980^{o} C and a heated pressure of 25 torr. This is below the optimum suggested by Hodgson (1979) and Wyatt and Cotter (1980), but was the maximum safe pressure which could be used with this cell. Higher pressures would require intolerably high wall temperatures. The present cell suffered from slight sagging at the temperature used, which soon reduced the available aperture. With a shorter cell this amount of sagging could be accepted.

The threshold measurements were performed by monitoring the generated infrared signal and tilting the SHG crystal slightly (and thus reducing the amount of 532 nm light generated) until a Stokes output was observed on around 1 in 3 of the laser shots. The average green pulse energy was then measured, together with the spread of these energies. The measured threshold energy was corrected for the transmission of the optical components which were present between the vapour and the point at which the energy was measured. To allow for the transmission of the vapour, all the absorption and scattering of the light was assumed to take place in 'plugs' of Caesium vapour in the heat-pipe regions of the vapour cell. (These occur in the regions of the cell containing wicks.) The measured 532 nm transmission of the column was 57% giving each of these regions a transmission of $(0.57)^{\frac{1}{2}}$ or 75%. The value of transmission was measured for both low input ($<<$ 100 μJ) and for high input (but less than the Raman threshold). Good agreement between these (54% and 57%) despite the possibility of substantial bleaching of molecular absorption suggests that the major loss mechanism is scattering of the 532 nm light by a particulate suspension of Caesium dust. This was observed in the Caesium to Argon transition regions in these experiments as well as being noted by Hodgson (1979). To reduce this effect, Hodgson used Helium as the buffer gas in his experiments.

The results obtained running the laser under the four conditions detailed earlier are presented in the following table

(corrected for the transmissions discussed):

Number of modes	Threshold energy (mJ)†	Threshold Power (kW)	Laser Linewidth (cm^{-1})
1	7.5 (±1%)	320	<0.002
2	6.3 (±10%)	270	0.01
3-5	6.4 (±3%)	275	0.02
12	6.2 (±3%)	265	0.06

The value of the threshold power, P_{th}, given here is that which was obtained by measuring the energy and duration of the laser pulse and calculating the equivalent peak power of a smooth (Gaussian) pulse, namely

$$P_{th} = \hat{P}_p = 0.939 \frac{E_p}{\tau_p} \qquad (6.14)$$

This is, of course, applicable for

(i) smooth structureless pulses, when the laser linewidth is much less than the Raman transition linewidth or

(ii) whenever the laser linewidth is much larger than the Raman linewidth (see Section 2.4).

In this work where the laser linewidth was much less than the collision broadened atomic width, only condition (i) was ever met. This occurred when the laser was operating on a single mode. For the other results P_{th} is presented as the value of power which might be calculated in lieu of more detailed information about the pulse structure.

---

† The bracketed figures are the shot to shot variations in 532 nm pulse energy with the Nd:YAG laser set up for each type of operation.

The measured single mode threshold agrees quite well with the predicted threshold power of 340 kW, calculated using the collision broadening coefficient due to Sayer et al (1971). It would seem from this that their value is applicable to 6s-5d SERS in Caesium. The results obtained with the laser running on more than one mode are seen to be less than the single mode threshold by 15-20% in qualitative agreement with the behaviour expected under these circumstances.

6.5.4 Measurements Performed in the Short Heat-pipe

The thresholds measured for the 1 m vapour column are in good quantitative agreement with those of Hodgson (1979), as well as the lowest of those of Wyatt and Cotter (1980). The latter used a 30 cm long heat-pipe, which, in the absence of competing effects, will given the same results for the same value of ℓ/b_p. However, as will be seen, this is not always true.

The 1 m long cell was replaced by an air-cooled heat-pipe having a 30 cm vapour column. The position and focal length of the lens were altered to focus the 532 nm light confocally over the shorter vapour. The Caesium pressure was set at 20 torr. Raman threshold for 22 ns long pulses could not be reached with 15 mJ of single mode 532 nm light. To increase the available green light, the laser was then fast Q-switched; this gave up to 25 mJ per pulse at 532 nm in the vapour. An occasional output Stokes pulse indicated that this was generally just insufficient to exceed Raman threshold. The experiment was repeated at a Caesium pressure of 50 torr but with the same qualitative results. This pressure was noted as near optimum by both Hodgson (1979) and Wyatt and Cotter (1980).

As the pulse energy was increased up to its maximum value, severe scattering of the green light was observed at both pressures. This became visually obvious for the 50 torr case at an input energy of 140 μJ and for high input energy was accompanied by various amplified spontaneous emissions. For a slow Q-switched frequency doubled input of 15 mJ, the output consisted of

$7s-6p_{3/2}$ ASE at 1.46 μm. With the extra pulse energy obtained when the laser was fast Q-switched, this output was joined by ASE on the $5d_{5/2} - 6p_{3/2}$ (3.5 μm) and $8s - 6p_{3/2}$ (796 nm) transitions. Emissions starting on high lying levels, such as the 8s level, suggests the occurrence of strong two photon ionization of the Caesium vapour, followed by ionic recombination and a subsequent electron cascade back to the ground state. The presence of a high degree of ionization will lead to a reduction in the Raman gain due to Stark broadening of the final (5d) level, as well as scattering of the pump laser light by the inhomogeneous refractive index generated by the plasma. The magnitude of the Raman gain under the influence of two photon ionization will be considered in the next section.

The scattering of single mode 532 nm light showed an interesting temporal behaviour. For low input power, the pulse shape remained unchanged. However, as the pump pulse energy was increased, defocusing of the latter part of the pulse ensued. The on-axis behaviour of the transmitted green light is shown in Figure 6.18 for several values of input energy. An aperture was used to select the part of the beam which was still within one beam radius of the axis. Also shown in the Figure is the off-axis behaviour corresponding to an input energy of 2 mJ. The light transmitted by the vapour is affected significantly by this effect; only for very low input powers is the peak of the laser pulse passed intact by the vapour. This will have a very detrimental effect on SERS and the ability to reach SERS threshold.

A possible cause of this defocusing effect is the presence of a high ion density in the vapour. This is created by two-photon ionization of atomic and molecular Caesium by the intense 532 nm radiation. The resulting plasma would be concentrated along the beam axis and, as the refractive index of the plasma would be less than that of neutral Caesium vapour, this would tend to defocus the light. Considered dynamically, this would lead to a lowering of the ionization rate. A slow smearing out of the ionic density would then follow. The refractive index profile would become slightly less severe and the beam will start to move back into its unperturbed path, and again the on-axis ionization rate will increase. In this

(a)

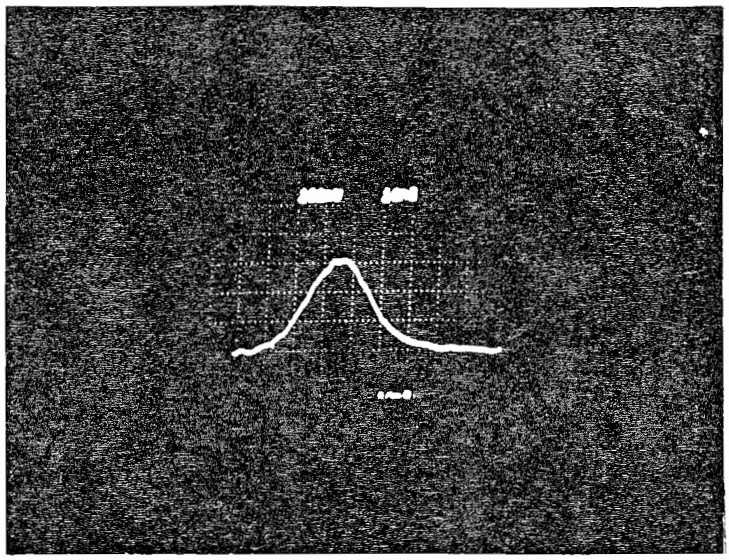

(b)

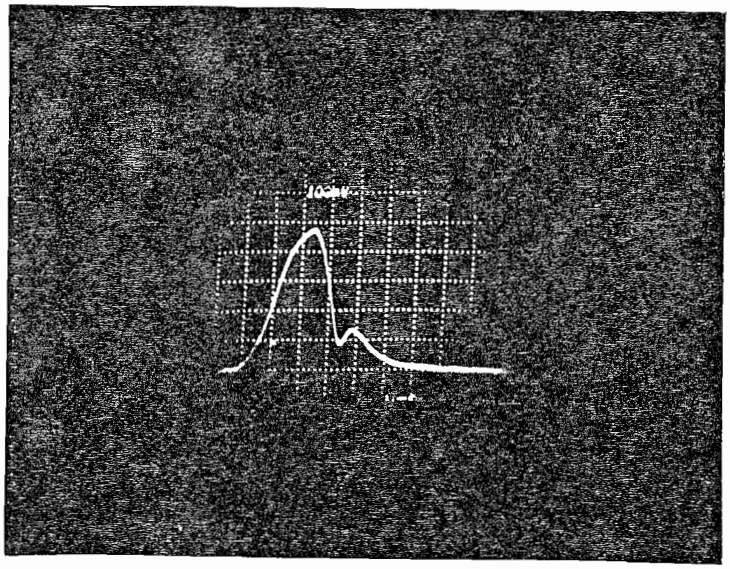

Figure 6.18a - Temporal behaviour of 532 nm light transmitted through a 30 cm Caesium vapour column

(a) 100 μJ input

(b) 140 μJ input

(Horizontal scale 10 ns/div, vertical scale 100 mV/div)

(c)

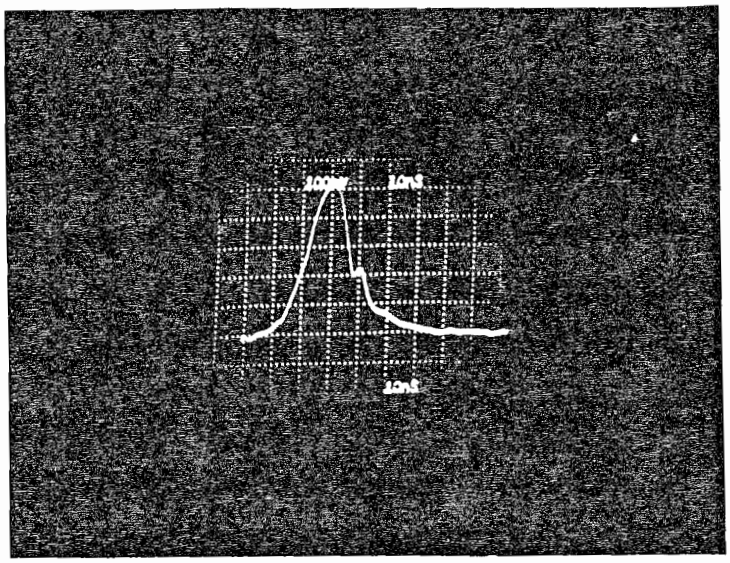

(d)

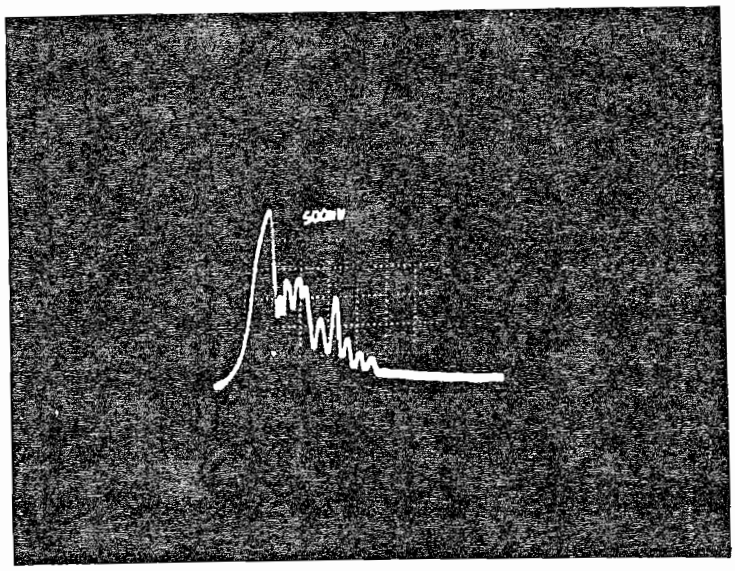

Figure 6.18b - Temporal behaviour of 532 nm light transmitted through a 30 cm Caesium vapour column

(c) 240 μJ input (vertical scale 100 mV/div)

(d) 2 mJ input (vertical scale 500 mV/div)

(Horizontal scale 10 ns/div)

(e)

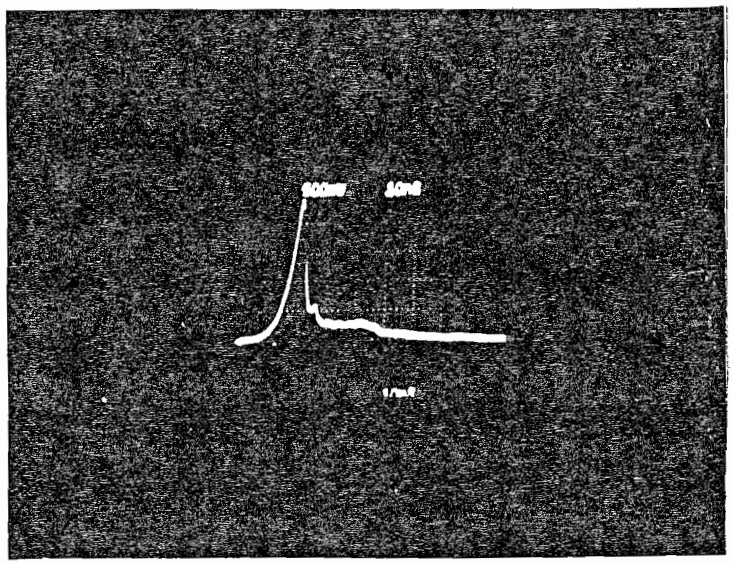

(f)

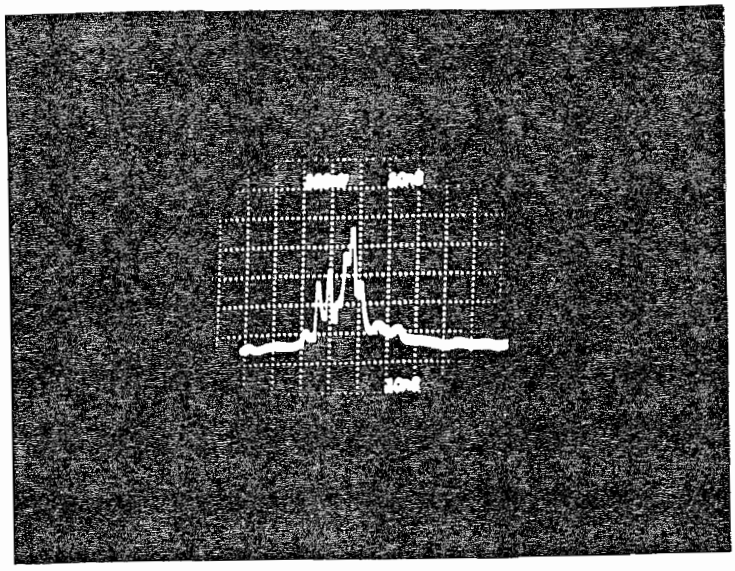

Figure 6.18c - Temporal behaviour of 532 nm light transmitted through a 30 cm Caesium vapour column

(e) 8.3 mJ (vertical scale 500 mV/div)

(f) off-axis light for 2 mJ input (vertical scale 100 mV/div)

(Horizontal scale 10 ns/div)

way oscillatory behaviour of the off-axis light may be expected. The results shown in Figure 6.18 are not inconsistent with this simple picture.

These results would appear contrary to the results of Wyatt and Cotter (1980), who could exceed threshold easily. However, two major differences exist between their experimental conditions and ours. Wyatt and Cotter used Helium as the buffer gas in their heat-pipe. In the experiments described here, Argon was used rather than Helium as the latter led to an unpredictable pressure increase as the vapour cell was heated. This was discussed in Section 4.2. Additionally, and perhaps more importantly, the laser pulse lengths used in this work (22 ns) were approximately three times those used by Wyatt and Cotter. The effect of this difference could cause a higher fractional ionization by the time the input pulse power reaches its peak value.

6.6 The Effect of Photo-ionization on the Raman Threshold

In this section the effect of atomic and molecular ionization on the Raman gain via Stark broadening of the Raman linewidth is considered. Raman threshold on the 6s-5d transition is seen to be critically dependent on the pump pulse length. The generation of ions and electrons in the illuminated region causes defocusing of the pump laser and its generated Stokes, adding to the effect of diffraction loss on Raman generation.

Stark broadening in the impact approximation has been considered by Hindmarsh (1974). In the presence of a number density N_e of electrons† of speed $\bar{v}$, the Stark broadened linewidth is given by

$$\Gamma_s = 11.4\left(\frac{C_4}{\hbar}\right)^{\frac{2}{3}}(\bar{v})^{\frac{1}{3}} N_e \qquad (6.15)$$

---

† During photoionization, most of the excess energy of the process is carried away by the kinetic energy of the electron. The ionic velocity is much smaller than the electronic; in Caesium, line-broadening due to electrons is nearly two orders of magnitude larger than that due to ions.

From this a broadening coefficient γ_s can be defined as $\gamma_s = \Gamma_s/N_e$ by comparison with the form of the collision broadening coefficient γ_c of Section 2.3.

The parameter C_4 arises from the expression for the quadratic Stark shift of an atomic level due to an electron at distance R from the atom:

$$\Delta E = C_4 R^{-4} \tag{6.16}$$

and is given for the 5d states by

$$C_4 = \left(\frac{e^2 a_o}{4\pi\varepsilon_o}\right)^2 \sum_{np} \frac{|\langle 5d|z|np\rangle|^2}{\hbar\Omega_{5d-np}} \tag{6.17}$$

Here $\hbar\Omega_{5d-np}$ is the energy difference between the $|5d\rangle$ states and the state $|np\rangle$. The z matrix elements are in atomic units.

The value of C_4 can easily be found since, as the major contribution to the summation comes from the $|6p\rangle$ state, it converges rapidly. Using the matrix element data of Eicher (1975) and the transition frequencies of Moore (1958), the value of C_4 is found to be 1.63×10^{-56} Jm^4, giving γ_s as 9.01×10^{-17} cm^3 cm^{-1}.

As the Lorentzian linewidth contributions of collision and Stark broadening are dominant for Caesium pressures over 1 torr, the Raman linewidth will be given approximately by the sum of the two. Expressing the atomic and electron number densities N_A and N_e explicitly, the Raman linewidth is

$$\Gamma_R = \gamma_c N_A + \gamma_s N_e \tag{6.18}$$

Substituting values of γ_c and γ_s, Stark broadening of the 6s-5d transition is dominant when the ionization exceeds 0.7%.

In order to see the effect that ionization has on the measured Raman threshold, attention is now turned to calculating the

fractional ionization as a function of time into the pump pulse. Near threshold only the peak of the pulse can give sufficient gain to the Stokes wave to cause a detectable output. On the other hand, the earlier part of the pulse is still capable of causing two photon ionization in the vapour, which will accumulate and reduce the Raman gain.

Two photon ionization of the alkalis was considered by Bebb (1966); for Caesium a cross-section of $\sigma_2 = 6.5 \times 10^{-50}$ cm^4 s^{-1} at 532 nm was calculated using perturbation theory. This value has been measured expèrimentally by Morellec et al (1980). For Caesium dimer molecules, the cross-section can be extrapolated from the values measured by Granneman et al (1976) as $\sim 3 \times 10^{-44}$ cm^4 s^{-1}. In terms of the photon flux F, the ionization rate is given by

$$W^{(2)} = \sigma_2 F^2 \tag{6.19}$$

For a laser pulse having a Gaussian temporal intensity profile of length $\tau_{\frac{1}{2}}$ (FWHM), this rate varies in time as

$$W^{(2)}(t) = \frac{\sigma_2 I_o^2}{\hbar^2 \omega_p^2} \exp\left[-8\ln 2 \frac{t^2}{\tau_{\frac{1}{2}}^2}\right] \tag{6.20}$$

where I_o is the on-axis intensity. The peak of the pulse occurs at time t = 0. This rate may be integrated to give the fraction of the atoms or molecules which have been ionized before the peak of the pulse

$$\frac{N_e}{N_A} = \int_{-\infty}^{o} W^{(2)}(t)dt \tag{6.21}$$

This of course neglects ion-electron recombination. However, by monitoring the transmission of microwave radiation through Caesium vapour after ionisation by a blue dye laser pulse, Leslie et al (1977)

determined the free electron lifetime to be 15-20 μs. This is much larger than a typical Q-switched laser pulse of a few tens of nanoseconds.

After substituting the peak power of the pulse P_p into Equation 6.20, the on-axis, focal fractional ionization is given by

$$\frac{N_e}{N_A} = \frac{2\sigma_2 P_p^2 \tau_{\frac{1}{2}}}{\hbar^2 \pi^2 c^2 b^2} \left[\frac{\pi}{2\ln 2}\right]^{\frac{1}{2}} \tag{6.22}$$

where b is the confocal parameter of the focused beam. As the peak power is increased so does the fractional ionization.

The Raman linewidth of Equation 6.18 can now be re-expressed as

$$\Gamma_R = \gamma_c N_A \left[1 + \frac{\gamma_s}{\gamma_c} \cdot \frac{2\sigma_2 P_p^2 \tau_{\frac{1}{2}}}{\hbar^2 \pi^2 c^2 b^2} \left(\frac{\pi}{2\ln 2}\right)^{\frac{1}{2}}\right] \tag{6.23}$$

For large ionization ($\gamma_s N_e >> \gamma_c N_A$) the linewidth increases as the square of the pump laser power. To see the effect of this on the Raman threshold, the threshold condition (Equation 2.14) can now be written in terms of the ionization broadened linewidth.

The Raman gain coefficient in this approximation becomes

$$g_R = g_{Ro} \left[1 + \frac{\gamma_s N_e}{\gamma_c N_A}\right]^{-1} \tag{6.24}$$

where g_{Ro} is the usual collision dominated value of g_R. The effect of the non-uniformity of N_e/N_A is difficult to solve and so the value of N_e/N_A will be assumed to be constant throughout the medium and to have one half of the on-axis focal value given by Equation 6.22. This will be justified later.

N_e/N_A can be replaced using Equation 6.22,

$$g_R = g_{Ro}\left[1 + aP^2\right]^{-1} \tag{6.25}$$

where a has been introduced for convenience. The intensity I_p in the threshold condition $gI_p\ell \simeq 30$ can be expressed in terms of the pump power P_p by $I_p = 4P_p/b\lambda$ and so

$$'gI_p\ell' = \frac{4g_{Ro}\hat{P}_p\ell}{b\lambda}\left[1 + aP^2\right]^{-1} \tag{6.26}$$

The maximum value of $'gI_p\ell'$ occurs when $P^2 = a^{-1}$, and is one half of the ionization free value. Thus an optimum power P_{opt} can be defined as

$$P_{opt} = \left[\frac{\gamma_c}{\gamma_s} \cdot \frac{\hbar^2\pi^2c^2b^2}{\sigma\,\tau_{\frac{1}{2}}} \left(\frac{21n2}{\pi}\right)^{\frac{1}{2}}\right]^{\frac{1}{2}} \tag{6.27}$$

This maximizes the overall gain, and gives it the value

$$'gI_p\ell'_{max} = \frac{g_{Ro}P_{opt}\ell}{b\lambda} \tag{6.28}$$

Substituting values relevant to 6s–5d scattering into the fractional ionization formula,but including only atomic ionization as it makes the larger contribution, P_{opt} is found from Equation 6.27 to be

$$P_{opt} = 2.46\,\frac{b}{\sqrt{\tau_{\frac{1}{2}}}} \tag{6.29}$$

From this the maximum available Stokes gain for a given laser pulse duration and vapour column length can be found as

$$'gI_p\ell'_{max} = 1.18 \times 10^{-4}\,\frac{\ell}{\sqrt{\tau_{\frac{1}{2}}}} \tag{6.30}$$

Table 6.1 gives the magnitude of this for the 532 nm experiments described here as well as those of Wyatt and Cotter (1980) and Hodgson (1979). Even with this simple model, it is seen to be unlikely that threshold could be exceeded in a 30 cm heat-pipe with pulse lengths as great as 22 ns.

Returning to the effect of non-uniformity of N_e/N_A mentioned earlier, some justification of the assumption that N_e/N_A can be taken as constant is necessary. The integrated on-axis Stokes gain for a pump beam focused confocally over a vapour column is compared in Figure 6.19 to the value calculated assuming the axial intensity to remain constant at one half the focal value. As can be seen, the curves in this Figure indicate the validity of this assumption.

6.6.1 Discussion

Having put forward a picture of the effect that focusing and pump laser pulse length may have on SERS, it is apt to consider how the model could be verified. Although the discussion of Section 6.5.4 exposes the fact that some catastrophic effect occurs for the particular circumstances of that experiment, the measurement only indirectly hints at the cause. Two lines of attack are immediately apparent; the ionization could be measured directly or the Raman gain monitored as the intensity is increased.

Determining the Raman gain is notoriously difficult in atomic media. Threshold can be measured, but as the pump intensity is increased the gain $g_R I_p$ is usually assumed to rise linearly with pump intensity. In fact, it is only at threshold that the Raman gain can be known, as saturation and other competing effects become dominant in determining the output Stokes energy above this level. However, if the model developed in the last section is valid there will be two values of laser power at which the overall Stokes gain is just sufficient for threshold. As the gain eventually falls rapidly with increasing power the process will fall below threshold. In principle this 'second threshold' could be measured and the model validated. In practice plasma generation, high densities of excited states, self focusing or defocusing and a assortment of other effects would make this measurement impossible.

	Cell length	$\frac{\ell}{b}$	Pulse length	$'gI_p\ell'_{max}$
Hodgson (1979)	1 m	?	10 ns	80
Wyatt and Cotter (1980)	30 cm	0.64	7.5 ns	42
This work	1 m	1	22 ns	118
This work	30 cm	1	22 ns	23

Table 6.1 Ionization limited Raman gain on the $6s\text{-}5d_{5/2}$ transition (see text)

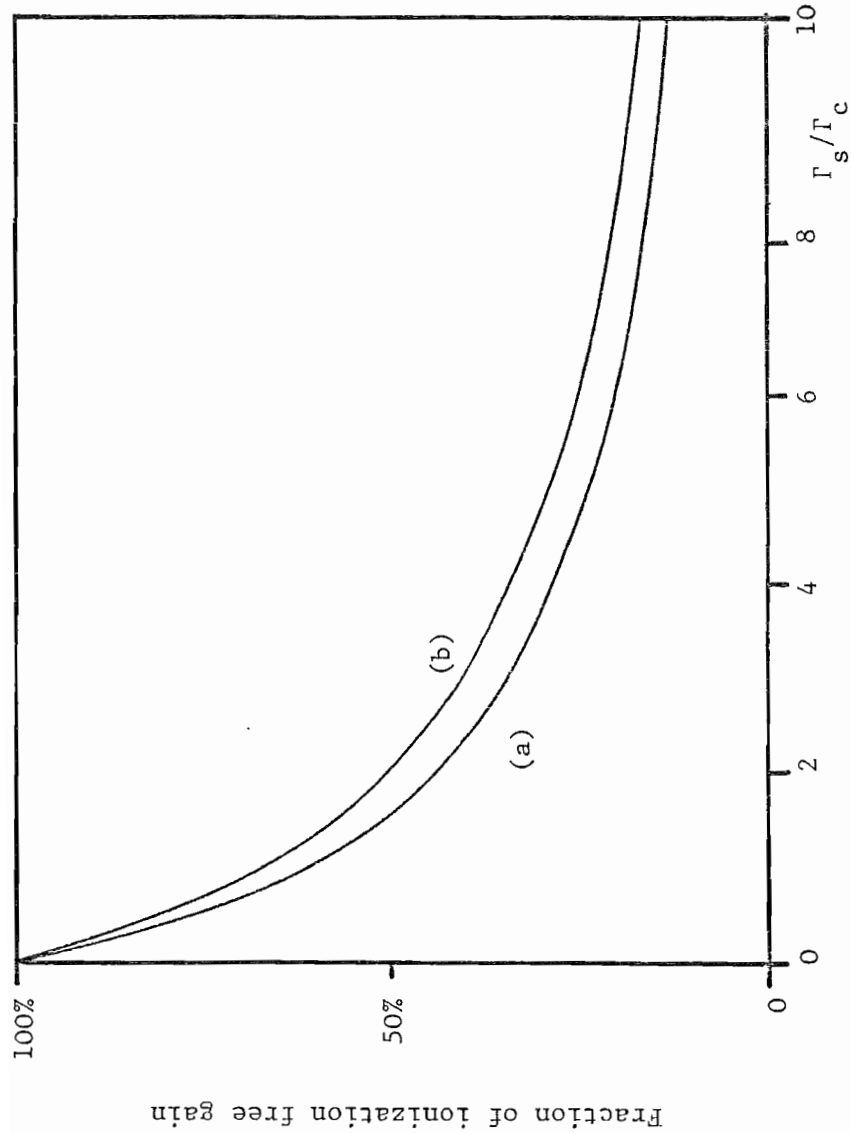

Figure 6.19 Reduction of the Raman gain by Stark broadening
(a) Full integrated solution
(b) Approximation used in text

Turning to the direct measurement of ion and electron densities, yet another difficulty arises. The Caesium vapour pressure which is used for SERS experiments is typically between 3 and 100 torr. At such a high pressure and with the high ionic density predicted by Equation 6.22, the mean free path of the charged particles will be small and the Coulomb attraction between them large. It would be impractical to collect the charge and so some other property of the generated ions must be observed. The large pumping geometry of Leslie et al (1977) allowed them to measure the relative microwave transmission before and after a blue dye laser pulse in their work on super-elastic collisions between Caesium atoms. As only a focused pencil of light was used in the SERS experiments described earlier, this technique is not likely to be particularly useful for absolute measurements. Another method employed by Lucatorto and McIlrath (1980) to monitor highly ionized Lithium vapour, entails the measurement of the vacuum ultraviolet absorption due to Lithium ions. Their method could also be utilized for measuring Caesium ion density. To be able to interpret the results of such an investigation an accurate knowledge of the Caesium ion transition oscillator strengths would be required. However, a measurement of this type is not within the scope of the equipment currently available in this laboratory.

6.7 Conclusions

In this chapter some techniques which allow the reduction of molecular concentration and absorption in alkali vapours have been described. They have been used to enhance 6s-7s SERS in Caesium vapour. This SERS process has, historically, been used to generate infrared light in the range 2.5 μm to 3.5 μm. A reduction in dimer concentration has allowed a useful extension to this tuning range and good agreement between the limits of this tuning and those predicted for SERS on the 6s-7s transition has been obtained.

The use of a collisionally broadened linewidth for the 6s-5d transition has proved consistent with the measured threshold. The tuning range obtainable from this transition for a given power dye laser, can now be calculated without assuming a value for the

Raman linewidth. In a superheated cell, or one in which the concentration of molecules has otherwise been reduced, this can be performed with some confidence. In a standard heat-pipe, absorption and ionization are likely to have a large detrimental effect on the process. It is hoped that future work will look at the tuning behaviour of 6s-5d SERS in a superheated vapour cell.

CHAPTER 7

Concluding Remarks

In this thesis the related processes of stimulated electronic Raman scattering and biharmonic pumping have been investigated in atomic vapours of Barium and Caesium. These processes have been used to efficiently generate widely tunable infrared radiation.

In Barium vapour, SERS processes involving the harmonics of a Nd:YAG laser were studied. It was found that the second harmonic at 532 nm was unable to exceed Raman threshold. This occurred despite theoretical predictions that threshold would be easily reached under the conditions of the experiment. This negative result is in line with those obtained in Strontium by Wynne and Sorokin (1977) as well as by Tuttlebee (1977). Single photon absorption of the pump laser was found to limit the process in Strontium. In Barium, on the other hand, absorption was seen not to be the factor preventing SERS. No alternative competing mechanism has yet been found to explain the discrepancy.

The third harmonic of a Nd:YAG laser at 355 nm exceeded threshold with ease. The measured threshold power of 700 W is in good agreement with a power calculated on the basis of a Doppler broadened Raman linewidth. Conversion of this ultraviolet light into its Stokes counterpart at 596 nm was found to peak at over 30%. The low threshold of this process offers the possibility of obtaining quasi-continuous operation. With an Ar-ion laser running on its 351.1 nm line, the detuning from intermediate resonance with the $5d6p\ ^1P_1$ level is an order of magnitude smaller than that of the Nd:YAG third harmonic, and so the Raman gain coefficient is around 100 times greater. In addition, the good results of Djeu and Burnham (1977), who used a XeF laser, indicate that pump absorption on this transition is not severe. From these considerations, a threshold power near 10 W is predicted. Atomic saturation will occur as the SERS process promotes atoms to the metastable excited $6s6p\ ^1D_2$ state. However this will be to some extent overcome by atomic diffusion and a chopped laser beam is likely to exceed Raman threshold.

The strong 355 nm to 596 nm Raman process was found to allow parametric generation of infrared light from the Nd:YAG second harmonic at 532 nm. This represents the first observation of biharmonic pumping or 'coherent Raman mixing' in an atomic vapour. The use of the biharmonic pumping process was extended to produce tunable infrared from a Coumarin 522 dye laser. This proved an effective method of overcoming the problems associated with the use of the principle line transition for enhancement. Conversion of light into the range 1.16 to 1.5 μm was achieved with an efficiency nearly an order of magnitude larger than previously reported for comparable processes in atomic vapours.

Previous work in Caesium on the 6s-7s Raman transition had not realized the full predicted tuning. It was believed that the presence of a significant concentration of dimer molecules in the vapour led to absorption and other competing processes which curtailed the tuning capability. Experiments to remove the effect of these molecules were conducted. Use was made of a bleaching technique in which molecules were excited and dissociated by Nd:YAG laser light; a method which had been tried unsuccessfully by Hodgson (1979). In addition, a superheating technique demonstrated by Wyatt and Cotter (1980) was used to reduce their equilibrium concentration. Both methods were found to allow an extension of the Raman tuning range although the results obtained indicated that the presence of dimer molecules was not the only cause of limited tuning. The work of Sayer et al (1971), suggested the possibility of strong collision broadening of the Raman transition. It is this broadening which is now believed responsible for the discrepancy between the observed behaviour and predictions based on the use of a Doppler limited Raman gain.

A knowledge of the broadening coefficient for 6s-5d electric quadrupole transitions allowed a prediction of the Raman gain for 6s-5d SERS to be made. A careful measurement of the threshold of this process was made at 532 nm and was found to concur with the prediction. This measurement is important as it is a step on the way to a study of tunable generation on the same transition. In the absence of competing effects, efficient generation of light between 2 μm and 10 μm is likely from a 750 kW dye laser. Dimer effects can be reduced by the use of a superheated vapour cell.

In the 6s-5d work, the transmitted 532 nm light exhibited an interesting temporal behaviour. This led to the consideration of photoionization and the effect this will have on Raman threshold and infrared generation. Account must be made of this competing effect when considering Stokes generation on a low gain transition such as the 6s-5d transition considered here. Improved SERS characteristics were obtained by using a long vapour cell.

A major limitation to Raman processes in atomic vapours is atomic saturation. The infrared pulse energies produced in this way are generally of the order of 10^{-8} J to 10^{-6} J and so applications of the generated light are likely to be of a spectroscopic nature. Given this limitation, the most promising avenues for future work are in the generation of tunable infrared on the $6s\text{-}5d_{5/2}$ transition in Caesium and in a general reappraisal of the alkaline earth materials as nonlinear media. The use of high energy, large area light beams in biharmonic pumping should allow the extension of the process to produce far greater infrared outputs. In addition, the design of high temperature vapour cells for the alkaline earth metals will alleviate the problem of atomic saturation. These developments, coupled with the narrow linewidths expected from the alkaline earths, offer the possibility of infrared sources of high spectral brightness. In the present work, parametric generation of light between 1.16 μm and 1.5 μm was observed. The use of biharmonic pumping on the singlet-triplet $6s^2\ {}^1S_o$ - $6s5d\ {}^3D_1$ and ${}^3D_2$ transitions could allow efficient generation beyond 3 μm; outside the range presently available from SERS in Barium.

In conclusion, Raman type processes in atomic vapours have been studied and have been found to allow widely tunable generation of infrared light. The main advantage of these processes in that they are simple and require little maintenance or adjustment. Unlike other schemes for producing infrared light they do not require a resonant cavity and so are devoid of complicated alignment procedures. Although most of the experiments performed here used carefully aligned single transverse mode lasers, this is not a stringent requirement; simple compact commercially available laser systems can be utilized.

REFERENCES

AKHMANOV, S. A., D'YAKOV, Yu. E. and PAVLOV, L. I. (1974)
"Statistical phenomena in Raman scattering stimulated by a broadband pump". Sov. Phys. JETP 39(2), pp. 249-256 (1974).

ARMSTRONG, J. A., BLOEMBERGEN, N., DUCUING, J., and PERSHAN, P.S. (1962)
"Interactions between light waves in a nonlinear dielectric". Phys. Rev. 127, pp. 1918-1939, (1962).

BAUMGARTNER, G., DEMTRODER, W., and STOCK, M. (1970)
"Lifetime measurements of alkali-molecules excited by different laser lines". Z. Phys. 232, pp. 462-472, (1970).

BEBB, H. B. (1966)
"Quantitative theory of the two-photon ionization of the alkali atoms". Phys. Rev. 149, pp. 25-32, (1966).

BENEDICT, R. P., DRUMMOND, D. L. and SCHLIE, L. A. (1977)
"Absorption spectra of the Cs_2 molecule". J. Chem. Phys. 66 pp. 4600-4607, (1977).

BLOEMBERGEN, N. and YABLONOVITCH, E. (1979)
"Collisionless multiphoton dissociation of SF_6: A statistical thermodynamic process". In 'Laser Spectroscopy III', Springer series in optical sciences, Eds. Hall, J. L. and Carlsten J. L., Springer-Verlag, (1977).

BURNHAM, R., and DJEU, N. (1978)
"Efficient Raman conversion of XeCl laser radiation in metal vapours". Optics Letters 3, pp. 215-217, (1978).

BYER, R. L. and HERBST (1977)
"Parametric oscillation and mixing in nonlinear infrared generation". In 'Nonlinear Infrared Generation', Springer Verlag Topics in applied physics. Vol 16, Ed. Shen, Y. R., (1977).

CARLSTEN, J. L., and DUNN, P. C. (1975)
"Stimulated Stokes emission with a dye laser : intense tunable radiation in the infrared". Optics Commun. 14, pp. 8-12, (1975).

CARMEN, T. W. and DYER, P. E. (1979)
"Continuous tuning characteristics of a small high pressure UV preionized CO_2 laser". Opt. Commun. 29, pp. 218-222 (1979).

COTTER, D. (1976)
"Tunable stimulated electronic Raman scattering in alkali metal vapours". Ph.D. Thesis, The University of Southampton (1976).

COTTER, D. and HANNA, D. C. (1976).
"Effects of spin-orbit coupling on resonant enhancement of stimulated electronic Raman scattering". J. Phys. B: Atom. Molec. Phys 9, pp. 2165-2171, (1976).

COTTER, D. and HANNA D. C. (1978)
"Saturation and tuning behaviour of stimulated electronic Raman scattering". IEEE J. Quant. Electron. QE-14, pp. 184-191 (1978).

COTTER, D. and HANNA, D. C. (1977)
"Stimulated electronic Raman scattering in Cs vapour, a simple tunable laser system for the 2.7 to 3.5 μm region". Opt. and Quantum Electronics 9, pp. 509-518, (1977).

COTTER, D., HANNA, D. C. and WYATT, R. (1975)
"Infrared stimulated Raman generation: effects of gain focussing on threshold and tuning behaviour". Appl. Phys. 8, pp. 333-340 (1975).

COTTER, D. and ZAPKA, W. (1978)
"Efficient Raman conversion of XeCl excimer laser radiation in Ba vapour". Opt. Commun. 26, pp. 251-255, (1978).

DJEU, N. and BURNHAM, R. (1977).
"Efficient Raman conversion of XeF laser output in Ba vapour". Appl. Phys. Letts, 30, pp. 473-475, (1977).

EICHER, H. (1975)
"Third-order susceptibility of alkali metal vapours". IEEE J. Quant. Electron. QE-11, pp. 121-130, (1975).

FREY, R. and PRADERE, F. (1976)
"Tunable infrared generation by stimulated Raman scattering". Infrared Physics 16, pp. 117-120, (1976).

FRIEDRICH, H. and TREFFTZ, E. (1969)
"Configuration mixing and oscillator strengths for some two-electron spectra (Ca I, Ba I, and others)". J. Quant. Spectrosc. Radiat. Transfer 9, pp.333-359, (1969).

GLAB, W. and NAYFEH, M. H. (1981)
"Measurement of the oscillator strength of the E2 transition Cs(6s-5D)". Opt. Commun. 38, pp. 262-264, (1981).

GRANNEMAN, E. H. A., KLEWER, M., NYGAARD, K. J. and VAN DER WIEL, M. J. (1976)
"Two-photon ionization of Cs_2, Rb_2 and RbCs using an Ar-ion laser". J. Phys. B : Atom. Molec. Phys. 9, pp.865-873, (1976).

GUPTA, R., HAPPER, W., WAGNER, J. and WENNMYR, E. (1978)
"Absorption studies of Cs_2 and Rb_2 molecular bands in the visible and near visible". J. Chem. Phys. 68, pp. 799-803, (1978).

HANNA, D. C., LUTHER-DAVIES, B. and SMITH, R. C. (1972)
"Active Q-switching technique for producing high laser power in a single longitudinal mode". Electron. Letts. 8, pp. 369-370, (1972).

HANNA, D. C., LUTHER-DAVIES, B. and SMITH, R. C. (1972)
"Single longitudinal mode selection of high power actively Q-switched lasers". Opto-Electronics 4, pp. 249-256, (1972).

HANNA, D. C., SAWYERS, C. G. and YURATICH, M. A. (1981)
"Large volume TEM_{oo} mode operation of Nd:YAG lasers". Opt. Commun 37, pp. 359-362, (1981).

HANNA, D. C., YURATICH, M. A. and COTTER, D. (1979)
"Nonlinear optics of free atoms and molecules". Springer series on optical sciences, Vol. 17, Springer Verlag (1979).

HEARN, D. B., TUTTLEBEE, W. H. W., SAYWERS, C. G., YURATICH, M. A. and HANNA, D. C. (1979)
"Efficient near-infrared generation by four wave mixing in Barium vapour". Proc. Fourth National Quantum Electronics Conference, (1979). Pub. J. Wiley and Sons (1980).

HINKLEY, E. D., KU, R. T. and KELLEY, P. L. (1976)
"Techniques for detection of molecular pollutants by absorption of laser radiation". In 'Laser monitoring of the Atmosphere', Springer topics in applied physics, Vol. 14, Ed. E. D. Hinkley, Springer-Verlag (1976).

HINDMARSH, W. R. (1974)
"Linewidth and Line broadening". In Atoms, Molecules and Lasers, Lectures presented at International Winter College, Trieste, January-April 1973. IAEA, Vienna (1974).

HODGSON, R. T. (1979)
"Stimulated electronic Raman scattering from the 6s $^2S_{\frac{1}{2}}$ *to the 5d* $^2D_{5/2}$ *state of Caesium"*. Appl. Phys. Letts 34, pp. 58-60, (1979).

KAISER, W. and LAUBEREAU, A. (1979)
"Ultrafast vibrational relaxation of polyatomic molecules". in 'Laser-induced processes in molecules', Springer series in chemical physics, Vol. 6, Eds. Kompa, K. L. and Smith S. D., Springer Verlag (1979).

KARKKAINEN, P. A. (1977)
"Two-photon resonant parametric generation in alkali metal vapours". Appl. Phys. 13, pp. 159-163, (1977).

KARMYSHIN, Yu. V., TOTSKII, E. E., and SHPIL'RAIN, E. E. (1974)
"Experimental study of the saturated vapour pressure of Barium". High Temperature (USA) 12, pp. 445-449, (1974).

KATO, H. and YOSHIHARA, K. (1979)
"Laser induced fluorescence, energy transfer, and dissociation of Cs_2*"*. J. Chem. Phys. 71, pp. 1585-1592, (1979).

LAPP, M., and HARRIS, L. P. (1966)
"Absorption cross-section of alkali-vapour molecules 1. Cs_2 *in the visible; 2.* K_2 *in the red"*. J. Quant. Spectrosc. Radiat. Transfer. 6, pp. 169-179, (1966).

LAYCOCK, L. C. (1978),
"Development of lasers for coherent anti-Stokes Raman spectroscopy". Ph.D. Thesis, The University of Southampton (1978).

LESLIE, S. G., VERDEYEN, J. T. and MILLAR W. S. (1977)
"Excitation of highly excited states by collisions of two excited Caesium atoms". J. Appl. Phys. 48, pp. 4444-4448, (1977).

LITTMAN, M. G. and METCALF, H. J. (1979)
"Spectrally narrow pulsed dye laser without beam expander".
Appl. Opt. 17, pp. 2224-2227, (1979).

LUCATORTO, T. B. and McILRATH, T. J. (1976)
"Efficient laser production of a Na^+ ground-state plasma column : Absorption spectroscopy and photoionization measurement of Na^+".
Phys. Rev. Letts. 37, pp. 428-431, (1976)

LUCATORTO, T. B. and McILRATH, T. J. (1980)
"Laser excitation and ionization of dense atomic vapours".
Applied Optics 19, pp. 3948-3956, (1980).

MELTON, L. A. and WINE, P. H. (1980)
"Operation of near ideal spectroscopic heat-pipes".
J. Appl. Phys. 51, pp. 4059-4069 (1980).

MILES, B. M. and WIESE, W. L. (1970)
"Bibliography on atomic transition probabilities". NBS Special publication no. 320, US Department of Commerce (1970).
Also Supplement 1 to the above, Fuhr, J. R. and Wiese W. L. (1971).

MOORE, C. E. (1958)
"Atomic energy levels". NBS circular no. 467, Vol. 1 (1949), Vol. 2 (1952), Vol. 3 (1958), US Department of Commerce.

MORELLEC, J., NORMAND, D., MAINFRAY, G. and MANUS, C. (1980)
"First experimental evidence of destructive interference effects in two photon ionization of Cs atoms". Phys. Rev. Lett. 44 pp. 1394-1397, (1980).

MOULTON, P. and MOORADIAN, A. (1979)
"Broadly tunable CW operation of $Ni:MgF_2$ and $Co:MgF_2$ lasers".
Appl. Phys. Lett. 35, pp. 838-840, (1979).

PENZKOFER, A., LAUBEREAU, A. and KAISER, W. (1979)
"High intensity Raman interactions". Prog. in Quant. Electron 6, pp. 55-140, (1979).

RABSON, T. A., RUIZ, H. J., SHAH, P. L. and TITTEL, F. K. (1972)
"Stimulated parametric fluorescence induced by picosecond pump pulses". Appl. Phys. Letts. 21, pp. 129-131, (1972).

ROKNI, M. and YATSIV, S. (1967)
"Resonance Raman effect in free atoms of Potassium".
Phys. Letts. 24A, pp. 277-278, (1967).

SARKIES, P. H. (1979)
"A stable YAG resonator yielding a beam of very low divergence and high output energy". Opt. Commun. 31, pp. 189-191, (1979).

SAYER, B., WANG, R., JEANNET, J. C. and SASSI, M. (1971)
"Absorption measurements of quadrupole transition probabilities 6S-nD in Caesium vapour". J. Phys. B : Atom. Molec. Phys. 4, L20-23, (1972).

SAWYERS, C. G. (1981)
"Development of a high power single-mode laser for nonlinear optics applications". Ph.D. Thesis, The University of Southampton (1981).

SCHINS, H. E. J., VAN WIJK, R. W. M. and DORPEMA, B. (1971)
"The heat-pipe boiling point method and the vapour pressure of twelve metallic elements in the range 10-10^{4} torr". Z. Metallkde. Bd. 62. H.4. pp. 330-336, (1971).

SCHNEIDER, I. and MARQUARDT, C. L. (1981)
"Broadly tunable laser action beyond 3 μm from $(F_2^+)_A$ centres in lithium doped KI". Optics Letters 6, pp. 627-628 (1981).

SHARMA, A., BHASKAR, N. D., LU, Y. Q. and HAPPER, W. (1981)
"Continuous-wave mirrorless lasing in optically pumped atomic Cs and Rb vapours". Appl. Phys. Lett 39, 209-211, (1981).

SHOSHAN, I., DANON, N. N. and OPPENHEIM, U. P. (1977)
"Narrowband operation of a pulsed dye laser without intracavity beam expansion". J. Appl. Phys. 48, pp. 4495-4497, (1977).

SMITH, G. C. (1982)
"The generation of widely tunable infrared radiation by SERS in a split-wick heat-pipe Caesium vapour oven". Minithesis, The University of Southampton, (1982).

SOROKIN, P. P. and LANKARD J. R. (1971)
"Infrared lasers resulting from giant pulse laser excitation of alkali metal molecules". J. Chem. Phys. 54, pp. 2184-2190 (1971).

SOROKIN, P. P., SHIREN, N. S., LANKARD, J. R., HAMMOND, E. C. and KAZYALEA, T. B. (1967)
"Stimulated electronic Raman scattering". Appl. Phys. Letts. 10, pp. 44-46, (1967).

TRUTNA, W. R. Jnr., PARK, Y. K. and BYER, R. L. (1979)
"The dependence of Raman gain on pump laser bandwidth". IEEE, J. Quantum. Electron., QE-15, pp. 648-655, (1979).

TUTTLEBEE, W. H. W. (1977)
"Stimulated Raman processes in metal vapours". Ph.D Thesis, The University of Southampton (1977).

TYLER, I. L., ALEXANDER, R. W. and BELL, R. J. (1975)
"Saturation effects in a tunable coherent near-infrared source". Appl. Phys. Letts. 27, pp. 346-347 (1975).

VENKIN, G. V., KROCHIK, G. M., KULYUK, L. L., MALEEV, D. I. and KHRONOPULO, YU. G. (1976)
"Effect of four-wave parametric processes on the dynamics of the Stokes components of stimulated Raman scattering". Sov. Phys. JETP 43, pp. 873-879, (1976).

VIDAL, C. R., COOPER. J. (1969)
"Heat-pipe oven : A new, well defined metal vapour device for spectroscopic measurements". J. Appl. Phys. 40, pp. 3370-3374, (1969).

VREHEN, Q. H. F., and HIKSPOORS, H. M. J. (1977)
"Two-photon induced stimulated Raman scattering in Caesium vapour". Optics. Commun. 21, pp. 127-131, (1977).

WALLING, J. C., PETERSON, O. G., JENSSEN, H. P., MORRIS R. C. and O'DELL, E. W. (1980)
"Tunable Alexandrite lasers". IEEE, J. Quantum. Electron. QE-16, pp. 1302-1315, (1980).

WARNER, B. (1968)
"Atomic oscillator strengths - III, Alkali-like spectra". Mon. Not. R. Astr. Soc.139, pp. 115-128 (1968).

WYATT, R. (1976)
"Generation of tunable infrared radiation by stimulated electronic Raman scattering". Ph.D Thesis, The University of Southampton (1976).

WYATT, R. and COTTER D. (1981)
"A tunable picosecond IR laser generating multi-megawatt pulses in the range 3-8 μm". Opt. Commun. 37, pp. 421-425, (1981).

WYATT, R. and COTTER, D. (1980)
"Tunable infrared generation using the 6s-5d Raman transition in Caesium vapour". Appl. Phys. 21, pp. 199-204, (1980).

WYATT, R., TURNER, A. J. and SMITH R. C. (1977)
"Performance characteristics and applications of a Lithium Niobate optical parametric oscillator". In 'Lasers in Chemistry', London, May-June 1977, Conference digest (1977). Ed. West, M. (1977).

YARIV, A. (1975)
"Quantum Electronics". John Wiley and Sons (1975).

YURATICH, M. A. and HANNA, D. C. (1976)
"Nonlinear atomic susceptibilities". J. Phys. B : Atom. Molec. Phys. 9, pp. 729-749, (1976).

ZOUBOULIS, E., BHASKAR, N. D., McCLELLAND, T. and HAPPER, W. (1980)
"New infrared absorption bands of Caesium vapour". J. Chem. Phys. 72, 2356-2363, (1980).

ZARE, R. N. (1979)
"Laser-induced chemical processes : Reactions with oriented reagents". In 'Laser-induced Processes in Molecules', Springer series in chemical physics, Vol. 6, Eds. Kompa, K. L. and Smith S. D., Springer-Verlag (1979).

ACKNOWLEDGEMENTS

I should like to thank my supervisors, Dr. Mike Yuratich and Dr. David Hanna, for the interest and encouragement they have given me during the course of this work, and for help with funding during the final six months.

I am also indebted to many past and present members of the Laser and Nonlinear Optics Group. I would like to thank Wally Tuttlebee for his collaboration in the early Barium work. In addition, I am very grateful to Craig Sawyers and Graham Smith for their help at various stages of the Caesium experiments, in particular for the late night sessions toward the end of this work.

My love to Tina for the long hours spent typing this thesis and for being a good friend.